To the Graduate Council:

I am submitting herewith a thesis written by Amy Luckstead DeMint entitled "The Microstructure of the Arispe Meteorite." I have examined the final copy of this thesis for form and content and recommend that it be accepted in partial fulfillment of the requirements for the degree of Master of Science, with a major in Metallurgical Engineering.

Charlie R. Brooks

Charlie R. Brooks, Major Professor

We have read this thesis and recommend its acceptance:

Lawrence A. Taylor

Dan T. Oliver

E. E. Stansbury

Harry G. McDaniel

Accepted for the Council:

Lew Minkel

Vice Provost and
Dean of the Graduate School

STATEMENT OF PERMISSION TO USE

In presenting this thesis in partial fulfillment of the requirements for a Master's degree at The University of Tennessee, Knoxville, I agree that the Library shall make it available to borrowers under rules of the Library. Brief quotations from this thesis are allowable without special permission, provided that accurate acknowledgment of source is made.

Permission for extensive quotation from or reproduction of this thesis may be granted by my major professor, or in his absence, by the Head of Interlibrary Services when, in the opinion of either, the proposed use of the material is for scholarly purposes. Any copying or use of the material in this thesis for financial gain shall not be allowed without my written permission.

Signature Amy R. DeWitt

Date December 1985

THE MICROSTRUCTURE OF THE ARISPE METEORITE

A Thesis

Presented for the

Master of Science

Degree

The University of Tennessee, Knoxville

Amy Luckstead DeMint

December 1985

ACKNOWLEDGMENTS

The author wishes to acknowledge Patrick Walker for doing preliminary metallographic work, major professor Charlie R. Brooks for his help guiding the research, and committee members Ben F. Oliver, Eugene E. Stansbury, Lawrence A. Taylor, and Harry Y. McSween for their helpful corrections and suggestions. Thanks are also extended to H. B. Thompson and Doug Fielden of the Machine Shop for their services.

ABSTRACT

The microstructure of the Arispe iron meteorite, a coarse octahedrite with anomalous structure (IC-An), was studied using optical and scanning electron microscopy, with emphasis placed on the various morphologies of plessite seen in this meteorite: pearlitic, spheroidial, and martensitic structures, as well as microwidmanstatten plessite and comb plessite.

The pearlitic and spheroidal plessites were generally associated with each other and were found only in the vicinity of the large ($\sim$ 1 cm) cohenite ($(Fe,Ni)_3C$) "nests," while the microwidmanstatten and comb plessites were seldom seen in intimate contact with the cohenite.

Schreibersite and rhabdite (both $(Fe,Ni)_3P$) and Neumann bands were also observed. Rhabdite was present throughout the kamacite, although it was more prolific in some grains than others. Schreibersite occurred as both large ($\sim$ 1 cm long) inclusions and as small ($\sim$ 50 μm) inclusions in plessite and cohenite. The Neumann bands seen were either of a constant width, or were pinched and segmented (perhaps indicating reheating). They were seen to be very orientation sensitive, appearing very densely in some grains, and being virtually absent in others.

No simple or clear-cut mechanism for the formation of these complex structures could be deduced.

TABLE OF CONTENTS

CHAPTER PAGE

LIST OF FIGURES

FIGURE PAGE

FIGURE PAGE

FIGURE PAGE

FIGURE PAGE

CHAPTER I

INTRODUCTION

Meteorites have long been a source of fascination to man. They were the first contact man made with the universe beyond the earth. The idea that meteorites were in fact of extraterrestrial origin was at first considered absurd, but later people grew to accept this fact. Obviously, an understanding of the structure of meteorites and their origins can provide important clues to the origin of the universe. On a smaller scale, we will learn how our own Earth formed and more clearly see how it continues to evolve.

Meteorites cool extremely slowly (e.g., 10-100°C/million years), indicating that they were nearly in equilibrium during their entire cooling process (something that man can never achieve in the lab). For this reason, iron meteorites (being essentially iron-nickel alloys with small amounts of phosphorus) are quite useful for the determination and verification of the Fe-Ni and Fe-Ni-P phase diagrams; if the structure of a meteorite is different than that predicted by the phase diagrams, then the phase diagrams must be in error.

Also due to their slow cooling rates, one can observe with the naked eye features on meteorites that would require high powered microscopes in man-made alloys.

The structures and minerals present in individual meteorites tell of different environments and cooling histories. The Arispe meteorite, the subject of this study, contains some anomalous features

making it not structurally like any other known meteorite. For this reason, as well as to gain insight into several recently discovered features, the Arispe meteorite is most beneficial to study.

CHAPTER II

DEFINITIONS AND TERMINOLOGY

Familiarity with the terminology of meteorites is essential to the understanding of the subject, so I shall begin by briefly defining the more important words.

I. METEOROIDS, METEORS, AND METEORITES

Chunks of metal or stone from outer space, called meteoroids, are occasionally caught by the earth's gravitational field and are pulled down to its surface. As the chunk falls toward the earth, friction with the atmosphere causes it to burn and glow. During this stage, the chunk is called a meteor (or falling or shooting star). Meteors are quite common and are easily seen if one is out looking at the stars on a clear night.

Tiny, dust sized particles will be slowed so much by air resistance that they will drift to the earth's surface with little heating by friction. Small, quickly moving meteors will most likely be completely vaporized in the fall and will never reach the earth's surface. When the meteorite is larger (from fist sized up to several tons), only a thin layer on the surface will burn in the fall, and due to the extremely short time spent falling through the atmosphere the body will not be heated through, so the interior will remain unaffected by the sudden surface heating (in fact, most recovered immediately after they fall are only warm, or sometimes even cold, to the touch) [1]. Those meteors that do reach the surface are

called meteorites. Many meteorites break up in the atmosphere and scatter fragments over an area of several miles [2].

It has been calculated that meteors larger than several tons will vaporize on impact with the earth's surface because of the tremendous amount of kinetic energy they have. As an example, a meteor weighing 100 tons, moving through the atmosphere at a rate of 10-20 km/sec, will not be slowed appreciably by friction with air; and at impact its kinetic energy will be roughly 20,000 joules/gram. This is enough to cause the meteor to explode by vaporization with as much force as a nuclear bomb, and cause a large explosion crater [3].

Tektites are glasses formed when silicates are impacted by a meteorite and melted, then refrozen. Although they are not of extra-terrestrial origin, they are evidence that a meteorite has fallen in the area [4].

II. STONES, STONY IRONS, AND IRONS

Meteorites are divided into three groups: stones, stony irons, and irons.

The stones (aerolites, to geologists) are made up of at least 75% silicates, generally with some Fe-Ni metal and FeS. Their group consists of [5]:

enstatite chondrites,

olivine-bronzite chondrites,

olivine-hypersthene chondrites,

olivine-pigeonite chondrites,

carbonaceous chondrites,

enstatite achondrites (aubrites),

hypersthene achondrites (diogenites),

olivine achondrites (chassignites),

olivine-pigeonite achondrites (ureilites),

diopside-olivine achondrites (nakhlites),

augite achondrites (angrites), and

pyroxene-plagioclase achondrites.

Chondrites are meteorites containing chondrules: "spherical grains about 1 mm in diameter composed of olivine ($(Mg,Fe)_2SiO_4$) and pyroxene ($(Mg,Fe)SiO_3$) silicates" [6]. Achondrites are stony meteorites that do not contain chondrules. Achondrites also contain no Fe-Ni metal and no FeS [2].

The stony irons (siderolites) consist of about half Fe-Ni metal and about half silicates. They are broken down into four subgroups [5]:

lodranites and

siderophyres (both of which only one example exists of each),

pallasites, and

mesosiderites.

Pallasites are made up of grains of olivine in a Fe-Ni metal matrix, while mesosiderites contain roughly equal amounts of metal and silicate (generally hypersthene and plagioclase) in which the metal does not form a continuous network.

The irons (siderites) consist mainly of Fe and Ni, but also contain FeS and other nonmetallic inclusions. The irons are broken down into six subgroups depending on their macroscopic structures [5]:

nickel-rich ataxites,

octahedrites,

hexahedrites,

nickel-poor ataxites,

metabolites, and

brecciated octahedrites.

Most iron meteorites are octahedrites: α has precipitated as plates along the octahedral ({111}) planes of the γ as the meteorite cooled leaving a Widmanstatten pattern. Octahedrites usually have between 7 and 11% Ni [5].

Hexahedrites have Ni contents less than about 7%. Like the octahedrites, upon cooling, the meteorite enters the $\alpha + \gamma$ field and α begins to precipitate on the octahedral planes of the γ. As the temperature continues to drop, the meteorite enters the α field, so there is no longer any γ separating the α plates. Should the α crystals become so large that the individual plates cannot be distinguished, the meteorite is classified as a hexahedrite. (If the plates can still be resolved, then the meteorite is still classified as an octahedrite.) [7]

Nickel-poor ataxites are just like hexahedrites, but they do not display Neumann bands, a feature which hexahedrites always show [8]. As this distinction is somewhat minor, hereafter both Ni-poor

ataxites and hexahedrites will be called "hexahedrites," and Ni-rich ataxites will be simply referred to as "ataxites."

Ataxites are rich in Ni, generally containing more than 12% [5]. Ataxites do not display the Widmanstatten pattern; instead they consist of plessite and some scattered α [9]. Ataxites containing more than roughly 27% Ni are all γ [8].

Metabolites are meteorites with 7-11% Ni that do not show the Widmanstatten pattern; either they never developed the pattern, or they have somehow lost it.

In brecciated octahedrites the Widmanstatten pattern changes its orientation every couple of inches, as opposed to retaining the same orientation throughout the entire mass (which can be up to several feet) [5].

While at first glance the irons may appear to be more numerous than stones and stony irons (as they make more interesting museum pieces), the reverse is actually true as shown by the following [2]:

	Falls	Finds	Total
Irons	42	503	545
Stony Irons	12	55	67
Stones	628	304	932

"Falls" are meteorites that were recovered after someone has actually seen them falling, while "finds" are meteorites that people have found that nobody has seen fall. The number of falls is more indicative of the actual relative amounts of meteorites, because irons stand out due to their high densities, while stones and stony irons look like many terrestrial rocks, and tend to go unnoticed.

We will be concerned only with the iron meteorites in this research.

III. PHASES PRESENT IN IRON METEORITES

There are many phases present in iron meteorites; a few are metallic, and many are nonmetallic.

A. Metallic Phases

Meteorites contain principally two metallic phases: an FCC Ni-rich iron phase, and a BCC Ni-poor iron phase. As the study of meteorites was originally carried out by geologists, the names given to the phases do not correspond to those that are familiar to most metallurgists. The Ni-rich phase (roughly equivalent to austenite in the iron-carbon system) is called taenite (γ), and the Ni-poor phase (equivalent to ferrite in steels) is called kamacite (α). Sometimes, the two phases are mixed together in a eutectoid-like structure called plessite. An ordered structure, FeNi (tetrataenite), has also been observed, and will be discussed later.

Metakamacite (α_2) is formed by a martensitic transformation. Like the martensite in steels, metakamacite has a distorted BCC (body-centered tetragonal) crystal structure. α_2 is either lath or lenticular (acicular) in morphology, depending on Ni content: lenticular martensite forms in areas with more than about 20% Ni [10].

B. Nonmetallic Phases

There are many nonmetallic inclusions in meteorites; the most common are phosphides, carbide, and troilite. Some meteorites also contain large silicates, but these will not be discussed here.

Phosphide inclusions, $(Fe, Ni)_3P$, are called either schreibersite or rhabdite depending on morphology: schreibersite is massive, while rhabdite has a regular rhombic shape. Rhabdite can be identified by its rhombic cross section in a meteoritic slice, but actually it grows as needles throughout the bulk of the meteorite [11]. Also, rhabdite is microscopic, while schreibersite need not be. Rhabdite is found mostly in hexahedrites and other meteorites with low Ni contents [12]. Reed [11] has found that the smallest schreibersite inclusions have the highest Ni contents, and tend to be found in taenite grains. Medium sized schreibersite inclusions are found in kamacite lamellae, while the largest inclusions may occur anywhere and are surrounded by "swathing kamacite." Most schreibersite tends to nucleate at kamacite/taenite interfaces. As the meteorite cools then, the schreibersite is many times enveloped in swathing kamacite [12].

Meteoritic carbide, $(Fe,Ni)_3C$, is called cohenite. Cohenite has been observed only in irons with less than 7% Ni. This carbide grows within kamacite and contains up to 3% Ni in solution [13]. Cohenite is not easily distinguished optically from schreibersite, so it may be more widespread than the older literature indicates [13]. Neither cohenite nor schreibersite have been found in terrestrial rocks.

Troilite, FeS, occurs as large brown inclusions easily observable to the naked eye. Moore [2] states that troilite is insoluble in molten Fe-Ni, but the phase diagram does not substantiate this.

Other nonmetallic phases which are frequently seen include olivine and orthopyroxene (both silicates), and daubreelite, $FeCr_2S_4$. Daubreelite is most common in hexahedrites and is generally associated with FeS [14].

IV. CLASSIFICATION OF IRON METEORITES

Many people have tried to categorize iron meteorites. One of the oldest schemes is based on structure (kamacite bandwidth), while another is based on chemical composition (more specifically, amounts of various trace elements present).

A. Classification with Respect to Structure (Bandwidth)

Meteorites are classified according to bandwidth or texture (generally width of the kamacite plates). The abbreviations Og, Om, and Of stand for coarse, medium, and fine octahedrites, respectively. Ogg designates a coarsest octahedrite, and Off a finest octahedrite. Opl indicates a plessitic octahedrite. Ataxites are given the symbol D, and hexahedrites are given the symbol H.

B. Classification with Respect to Trace Element Concentration

Many scientists have tried to divide meteorites into groups according to the amounts of certain trace elements, with the feeling

that meteorites with similar contents of these elements originated in the same parent body. The elements most often used for this purpose are germanium and gallium, but iridium is also used. Early work showed that most of the meteorites appeared to fall into four groups (I, II, III, and IV); but in more recent work, the previous groups have been broken down to create 12 new groups (IAB, IC, IIAB, IIC, IID, IIE, IIIAB, IIICD, IIIE, IIIF, IVA, and IVB). Some irons do not fit into any of the groups and are termed "anomalous"; others are put into groups into which they don't fit very well, and along with their group designation the suffix "-An" for anomalous is added. For example, the Arispe meteorite is classified as IC-An.

Group IC meteorites "are chemically very similar," but "display a bewildering variety of structures" (bandwidths) [15, p. 531]. The Arispe meteorite is anomalous within this group at least partly because of its Ir content; it has 9.7 ppm Ir, while aside from the Nocoleche meteorite (with 8.2 ppm Ir), the Ir contents in group IC range from 0.068 to 2.1 ppm.

From Table 1, which shows relative abundances of minerals in the various groups, group IC meteorites tend to have the following minerals and features: troilite nodules, daubreelite, schreibersite and rhabdite, cohenite macroprecipitates (> 1 cm in length), carlsbergite (CrN), chromite ($FeCr_2O_4$), sphalerite (ZnS), and shock melted troilite [15].

Table 1. Relative Abundances of the More Common Minerals in the Iron Meteorite Groups

Group	Sulfides: Troilite FeS	Sulfides: Daubreelite $FeCr_2S_4$	Phosphide: Schreibersite $(Fe,Ni)_3P$	Carbides: Cohenite Fe_3C	Carbides: Haxonite $(Fe,Ni)_{23}C_6$	Graphite C	Nitride Carlsbergite CrN	Silicates	Shock Signs: Melted Troilite	Shock Signs: Hatched Kamacite	Others
IA	2,N	1	2,M,rh	3,M	2	2,(M)	1	1-3,M[a]	1-2	1	ch,ph,sp
IB	2,N	0	2,(M)	1	1-2	2,(M)	0	1-3,M[a]	1	0	(ch),ph,sp
IC	2,N	1-2	2,(M),rh	1-3,M	0	dc	1-2	0	1-2	0	ch,sp
IIA	1	2	2,rh	1-2	1	dc	1	0[b]	2-3	0	(ch)
IIB	1,(N)	0-1	2 → 3,rh	1	1	dc	0	0[b]	1	1	(ch)
IIC	1-2,(N)	0-1	2	0	0	0	0	0	1-2	0	(ph)
IID	1-2,(N)	0-1	2 → 3,M	0	1	0-1	0	0-1	2	1	(ch)
IIE	1-2	0	1-2,(rh)	0	0	0	0	0-3,M	1-2	0	ch,ph
IIIA	1-2,N	2	1 → 2,rh	1	0	0-1	3 0	0	2	3	(ch),(ph),sp
IIIB	2-3,N	1	2 → 3,M	0	0	0	0	0	1-2	3	(ch),ph
IIIC	1,(N)	0	2,M	0	2	0	0	0	0	0	sp
IIID	1	0	2,M	1	2	1,(M)	0	0-1	1	0	ph,sp
IIIE	1-2	2	1-2,rh	0	2-3	dc	1-2	0	1-2	0-1	(sp)
IIIF	1	2-3	1-2	0	0	0	0	0	1	0	(ch)
IVA	2,(N)	3 → 2	0 → 1	0	0	0	0	0-1	2-3	2	(ch)
IVB	1	1-2	1 → 2	0	0	0	0	0	1-2	0	(ch)

[a]Bulk silicate composition close to chondritic values.

Key to abundances: 0, not observed; 1, sparsely distributed; 2, common; 3, ubiquitous.

Key to abbreviations: parentheses, infrequently observed; arrow, change in abundance with increasing bulk Ni content; N, nodules >1 cm in diameter; M, macroprecipitates ≥1 cm in length; rh, rhabdites; dc, graphite from decomposing carbide only; ch, chromite ($FeCr_2O_4$); ph, phosphates; sp, sphalerite (ZnS).

Source: Edward R. D. Scott and John T. Wasson, Classification and properties of iron meteorites, Reviews of Geophysics and Space Physics 13:527-546 (1975).

CHAPTER III

THEORIES ON THE ORIGIN OF METEORITES

There are many theories on the origin of meteorites, regarding both the parent body and where the parent body came from.

I. WHERE METEOROIDS COME FROM

Most meteoroids are believed to come from the asteroid belt between Mars and Jupiter, or from comets. The asteroids range in size from fine dust to 1000 km in diameter (the asteroid Ceres) [16]. Photographic recording networks have been set up to monitor meteorites as they fall; from the photographs, one can determine the orbits of these bodies. A few meteorites have been monitored in this way, and calculations indicate that they probably originated in the asteroid belt [17].

Using cooling rate calculations (see Section III of the Literature Search), it has been determined that most parental bodies must have been 10-800 km in diameter: asteroidal size [18]. Also, shock structures evident in some meteorites (high pressure minerals such as coesite and diamond, Neumann bands, etc.) indicate that the parent body underwent a catastrophic collision [18].

Asteroids were once thought to be the remains of a tenth planet which was shattered. There are, however, several problems with this theory. Asteroids are thought to travel at about 5 km/sec [16], and if two asteroids were to collide at this speed, the pieces would be

sent into space, not held together by gravity [16]. Also, the total mass of all the asteroids combined is not large enough to have been a planet. The combined mass of these asteroids is .02% of the mass of the earth [16].

On the other hand, most of the particles from the shattered bodies could have fallen toward other planets or could have been hurled into odd orbits around the sun (similar to the orbits of comets). In this case, the number of bodies remaining in the original orbit would be small compared to the size of the parent bodies.

It is conceivable that periodically one of these asteroids could leave its orbit, get caught by the earth's gravitational pull, and fall to the surface of the earth. This is a logical theory also from the standpoint that meteorites are thought to have originated from only a few "parent bodies." If indeed the asteroids came from only a few larger bodies that collided and shattered, then this could account for the compositional and structural similarities that exist between many meteorites.

It has been shown [16] that the asteroids are presently in very stable orbits, so it is unlikely that any would go out of orbit and come towards the earth. However, Hartmann says that asteroids and other small bodies could be knocked out of their orbits by "Jupiter's perturbations" [19, pp. 156 and 159]. This is also consistent with the theory that meteorites do not come from the asteroid belt, but rather from bodies drifting around the sun in odd orbits.

II. MAKE-UP OF THEORETICAL BODY

Two different theories have been proposed to explain the make-up of the parent body (or bodies) from which meteorites are presumed to come. The first model, proposed by Fish, Goles, and Anders [20], has been referred to as the "core model," and assumes that iron meteorites made up the metallic core of an asteroid or planet. The outside of the body is assumed to be largely silicate material. It was thought that originally the body was homogeneous, but that eventually the denser iron and nickel were pulled towards the center creating the source of iron meteorites, while the lighter silicate material rose to the surface to create the chrondrites. Where the metal was in contact with the silicate, the stony irons were created.

The second model was proposed by Urey [21] and has been called the "raisin bread" model by Goldstein and Short [22]. This model says that iron-nickel metal is scattered throughout a silicate body in blobs just like raisins in raisin bread. Urey's model states that the metallic areas were molten, while Levin (1965) (as discussed by Goldstein and Short [22]), who also believes in the raisin bread structure, says that these areas were never molten.

Wasson [23] says that meteorites with silicate inclusions must be of nonigneous origin. If the mixture were ever melted, he says, the light silicate material would rise to the surface, even under a very weak gravitational field, and so the silicates would never freeze as inclusions in the metal.

After studying Group III meteorites, Buchwald has determined that they must have solidified directionally because the troilite inclusions are roughly sausage shaped, and are all elongated in the same direction. Also, these troilite inclusions have trapped other minerals, and the trapped minerals have always been swept down to the same end. This indicates that a gravitational field must have existed at the time of solidification [18].

CHAPTER IV

LITERATURE SEARCH

A review of the literature available on meteorites reveals that they captured the interest of many famous early scientists, including geologists and metallurgists.

I. FAMOUS EARLY SCIENTISTS

Literature on meteorites goes back over 100 years and includes several well known names.

In 1808 in Austria, Alois von Widmanstatten, director of the Imperial Porcelain Works [1], was the first to etch an iron meteorite and reveal its octahedral structure. Almost simultaneously, G. Thomson, an Englishman, also discovered the structure. Thomson, in fact, even published an article about this discovery in 1808. (In contrast, Widmanstatten's work was not published until 1820, and then only in a pamphlet by Schreibers.) Widmanstatten, however, did considerable work on meteorites, so as a result, the octahedral pattern characteristic of many iron meteorites, as well as the related octahedral markings in steels and other alloys, now bears his name [24].

In 1849, Henry Clifton Sorby, a brilliant scientist, first used an optical microscope to look at a thin section of rock to see the minerals that comprised it. This worked well, so in the 1860's,

Sorby began to study chrondrites using this new method [3]. For his ingenuity, Sorby has been hailed as "the Father of Optical Petrography" as well as "the Father of Metallography." Later, in 1877 in a lecture on the origins of meteorites, Sorby pointed out that meteorites must surely be of igneous origin, and that slow cooling was required to produce the Widmanstatten pattern [25]. This was not as obvious to scientists of that age as it is to today's metallurgists. As late as 1923, Belaiew [26] said that cooling ought to be rapid through the taenite-kamacite transformation region for formation of the Widmanstatten pattern in meteorites.

In 1863, James P. Joule used velocity estimates of a meteorite to determine the temperature it achieved while falling, stating that "The meteorite of a foot section might have 1/5 of a grain of its surface" heated to 3000°C [27].

Also in the mid 1800's, Neumann first noticed a strange pattern of straight lines in meteoritic kamacite. These lines were later named after him, and they are now called Neumann bands.

II. THE FORMATION OF THE WIDMANSTATTEN PATTERN

As microscopes became more sophisticated and metallographic techniques progressed, scientists began to unravel the mystery surrounding meteorites. They learned that the Widmanstatten structure was formed upon slow cooling of the taenite phase, not by cooling rapidly, as Belaiew suggested.

In the 1920's Young, using x-ray analysis, determined the orientation relationships between kamacite and taenite: {111} γ is parallel to {110} α, and <110> γ is parallel to <111> α [28]. From this, people realized that the meteorite had to start out as single phase taenite, from which kamacite precipitated.

Eventually, agreement on how the pattern was formed became universal. Scientists realized that as the meteorite slowly cooled, it went from the single phase taenite region on the phase diagram to the kamacite + taenite region. When this happened, kamacite began to precipitate on the close-packed octahedral {111} planes. Slow cooling allowed the kamacite plates to grow very large.

As the kamacite precipitated, the surrounding taenite was enriched in nickel. The diffusion rate of nickel in kamacite is greater than that in taenite, so the Ni atoms built up along the edges of the taenite, while the concentration of Ni in kamacite stayed fairly constant. As the temperature decreased, the maximum solubility of Ni in kamacite first increased, then decreased. This caused still more Ni to build up on the taenite side of the kamacite/taenite interface, and also caused a depletion of Ni on the kamacite side of the interface. This depletion is known as the Agrell effect [29].

As the concentration gradients within the taenite became more pronounced, the low Ni areas of the taenite became unstable and broke down into plessite.

The concentration gradient can be seen using an electron microprobe. It was found that the concentration of Ni varies in the

shape of an "M" when a pass is made across a region of plessite and the surrounding kamacite. This is referred to as an M-profile, and it can be used in determination of cooling rates.

III. COOLING RATE CALCULATIONS

In 1964, Wood [29] used M-profiles to determine cooling rates for several meteorites. He programmed a computer to trace out compositional profiles using diffusion data and information from the phase diagram. Goldstein and Short [30] did basically the same thing soon thereafter, although in 1967 [22], they revised their model to take into account undercooling, impingement of plates, and pressure. The cooling rates calculated for iron meteorites using this method are generally between 1 and 10 °C/million years [22].

Randich and Goldstein [31] also developed a model to determine cooling rates of hexahedrites using computer generated curves and phosphide size and shape.

Recently, Rasmussen [32] devised a new way to calculate cooling rates of meteorites. While Wood, Short, Goldstein, and Randich assumed an undercooling of up to 190°C, this new model does not. Instead, it assumes that the kamacite nucleated in a piecewise fashion, and that the bulk Ni content of the taenite was thus continuously increasing. From this method one can simulate more accurate M-profiles than with the previous methods.

More recently still, Narayan and Goldstein [33] experimented with cooling Fe-Ni-P alloys and found that the Widmanstatten pattern

could be generated by cooling rates as fast as 5°C/day. This is because as the taenite cools, phosphides (schreibersite) nucleate first; these phosphides then become sites for kamacite to nucleate and grow. Using this new cooling rate, Narayan and Goldstein estimate that the cooling rates of most meteorites are 150-6000°C/million years, instead of 1-10. If this is true, the parent bodies can be as small as only a few kilometers in diameter.

IV. THE HIGH PRESSURE THEORY

Early theories speculated that the parent body had to be very large and that the meteorite must have cooled under very high pressure. The high pressure theory came about partly because scientists trying to recreate meteoritic structures were puzzled by the presence of the carbide cohenite.

Ringwood [13] said that Ni should increase the rate of decomposition of cohenite, as Ni_3C is less stable than Fe_3C. Upon slow cooling, he reasoned, the meteorite should be in equilibrium and so the cohenite should graphitize. Since the cohenite has not graphitized in most meteorites, this led to the conclusion that it had to be a stable phase as the meteorite cooled. For cohenite to be thermodynamically stable, it was theorized that the meteorite cooled under high pressure—above 25,000 atm, according to a paper from 1960 by Ringwood [13]. Ringwood and Kaufman [9] later calculated phase diagrams for pressures of 50 and 100 kbars, and observed that the 50 kbar diagram seemed to portray the situation most accurately. (Cohenite was later found to be formed at only modest pressures [34].)

Also contributing to the idea of high pressure was the presence of diamonds in the Canyon Diablo meteorite (later found to be formed by shock pressure from impact) [34].

Uhlig [8] also states that meteorites must have formed under high pressure. He speculates that in the case of ataxites, the meteorite remained all taenite under pressure until the pressure was suddenly released (as for example when the large parent body was broken apart). Upon release of this pressure, the taenite spontaneously transformed to metakamacite, which subsequently transformed to plessite.

Goldstein and Ogilvie [35] later determined that meteorites had to be formed at lower pressures (less than 12 kbar) because above this pressure, the kamacite plates cannot obtain the width we see in meteorites today.

V. COMMON FEATURES OF METEORITES

Aside from the Widmanstatten pattern, there are several other features common to meteorites. Among them are: Neumann bands, veining, and plessite.

A. Neumann Bands

Neumann bands have been found in many meteorites. A form of mechanical twinning, Neumann bands indicate that the meteorite has been shocked. Neumann bands are found generally only in kamacite (preferably in large, clear grains) parallel to (112) α planes, and their formation seems to be aided by phosphorus (as P makes slip

more difficult) [34]. These Neumann bands are generally not formed by the meteorite's impact with the earth, but rather from a more powerful shock, such as the breakup of the parent body [37] or the fragmentation that sometimes occurs as meteorites fall through the earth's atmosphere [6].

Should a meteorite be shocked at a pressure above 130 kbar, the kamacite will take on a martensitic appearance ("hatched kamacite"). This is caused by a pressure induced transformation from α to the dense ε-iron (hcp), then back to α. This causes the α to be distorted. Below 130 kbar, only Neumann bands are formed [18].

B. Veining

Uhlig (1954) describes a phenomenon of meteorites called "veining." Veining occurs in kamacite grains and has the appearance of grain boundaries, but is observed on a much smaller scale. The veined network is not continuous from one kamacite plate to the next.

The creation of subgrains causes the sample to take on a veined appearance upon etching and is thought to be the result of a congregation of defects (such as dislocations) in an effort to make the subgrains more perfect [8]. Buchwald states that veining is caused by dislocations, which have been instigated by mild hot working, running through the crystal [18].

C. Plessite

Plessite is a feature common to most meteorites. Many scientists have tried to recreate meteoritic structures in the

laboratory, but early attempts failed because nobody could create plessite (then thought to be merely a eutectoid structure).

In 1954, Uhlig [8] proposed two theories on the formation of plessite which still serve as the best basis for discussion of its formation. One says that as the kamacite plates thickened, the edges of the taenite became Ni rich while the center remained Ni poor in comparison, so the center decomposed to plessite. The second theory says that these taenite regions remained as supercooled taenite until the parent body was broken apart, and the sudden release of pressure prompted the taenite to transform to α_2, which subsequently decomposed to plessite [8]. Thus plessite can be formed by one of two reactions: (a) $\gamma \rightarrow \alpha + \gamma$, or (b) $\gamma \rightarrow \alpha_2 \rightarrow \alpha + \gamma$. The first reaction produces "type I plessite." Type I plessite has a microwidmanstatten pattern of kamacite and taenite. The second reaction produces "type II plessite" as an intermediate product, followed by plessite like that produced in the first reaction. Type II plessite is called meta-kamacite (martensite), and is much like the lath and plate martensite found in steel. It was discovered that plessite could be formed artifically by cooling taenite quickly to form metakamacite, and then reheating to allow the metakamacite to decompose into kamacite and taenite. Plessite formed by the decomposition of metakamacite is termed "type III plessite" [38].

As a compositional profile is made across a region of plessite, several distinct regions are observed. Optically, this creates a zoned look upon etching.

Figure 1 shows a profile that was made across the Carlton fine octahedrite. The region marked 1 is "clear taenite" or original taenite that has been retained instead of being broken down. The nickel content of the taenite in this region is over 40%. Region 2 has been termed "the cloudy zone," and is present in all meteorites unless they have been reheated [39]. The cloudy zone, so-called because it appears brown upon etching, was once thought to be made up of a honeycomb network of kamacite with rods of taenite running through it [39]. It is also called "type IV plessite." According to Lin et al. [38], this is the type of structure formed when α_2 decomposes. Region 3 is again clear, retained taenite, but this time with only 25-30% Ni. Region 4 is called "black plessite" or martensite and consists of type II or III plessite. Region 5 is a duplex mixture of kamacite and taenite and consists of type I or III plessite [38].

VI. CLEARING THE MIST SURROUNDING CLOUDY TAENITE: ORDERED STRUCTURES

Taenite is zoned just as plessitic regions are zoned, and for the same reason. Shown in Figure 2 is a concentration profile made across a band of taenite. As in the plessite profile, region I is clear; region II is cloudy taenite, and region III is again clear [40].

In recent years, researchers using Mossbauer spectroscopy have found that the "cloudy zone" actually consists of two phases: an

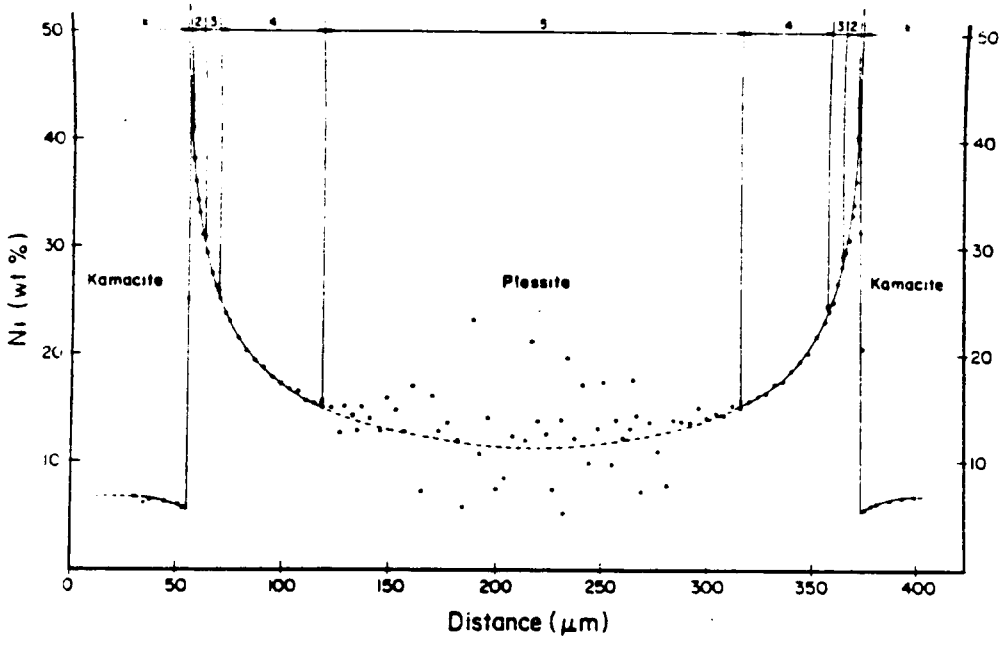

Figure 1. An M-profile made across the Carlton octahedrite.

Source: L. S. Lin, J. I. Goldstein and D. B. Williams, "Analytical electron microscopy study of the plessite structure in the Carlton iron meteorite," Geochimica et Cosmochimica Acta 41:1861-1874 (1977).

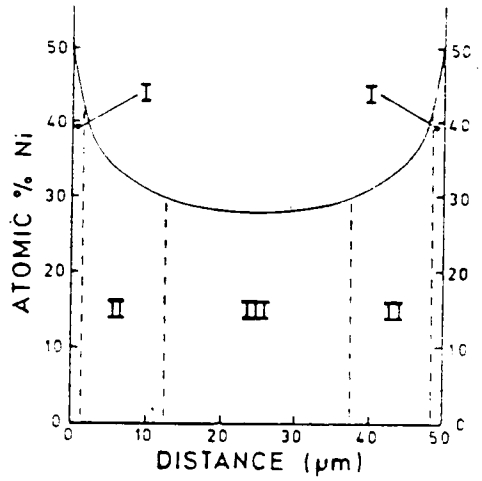

Figure 2. An M-profile made across a taenite band in the Toluca meteorite.

Source: J. F. Albertsen, G. B. Jensen, J. M. Knudsen, J. Danon, "On superstructure in meteoritical taenite," Meteoritics 13: 379-383 (1978).

ordered FeNi phase called tetrataenite [41], and a disordered iron-nickel phase.

Clear taenite with over 40% Ni (region I in Figure 2) is mostly ordered, tetragonal FeNi, formed from taenite [42], [43]. In very recent work, Albertsen et al. [44] have found that this clear zone is actually made up of two zones: the outer zone is "monomineralic" tetrataenite, while the inner zone (bordering the cloudy zone) is a "delicate duplex" structure comprised of tetrataenite and disordered taenite (see Figure 3). The cloudy zone (region II in Figure 2) has a lower concentration of FeNi. It consists of a "coarse duplex" structure of rounded cells (these are the "rods of taenite" that Scott [39] saw) in a disordered taenite matrix (Scott's "kamacite matrix" [39]). These cells are themselves duplex and have the same structure as the inner region of the clear zone (delicate duplex). The FeNi in the cells consists of 3-10 antiphase domains having the same c-axis orientation [44]. The disordered taenite matrix may falsely appear to be kamacite because the surface may transform to α_2 upon polishing [44]. Region III in Figure 2 also contains small amounts of FeNi [42].

The disordered taenite is optically isotropic [45], has an FCC structure, is paramagnetic, and contains less than 25% Ni.

The ordered FeNi phase, on the other hand, is optically anisotropic [45], is tetragonal with the $L1_0$ structure (AuCu structure) [42], and is ferromagnetic [40]. The ordering temperature for a 50 Ni-50 Fe alloy is 320°C [46]. Tetrataenite

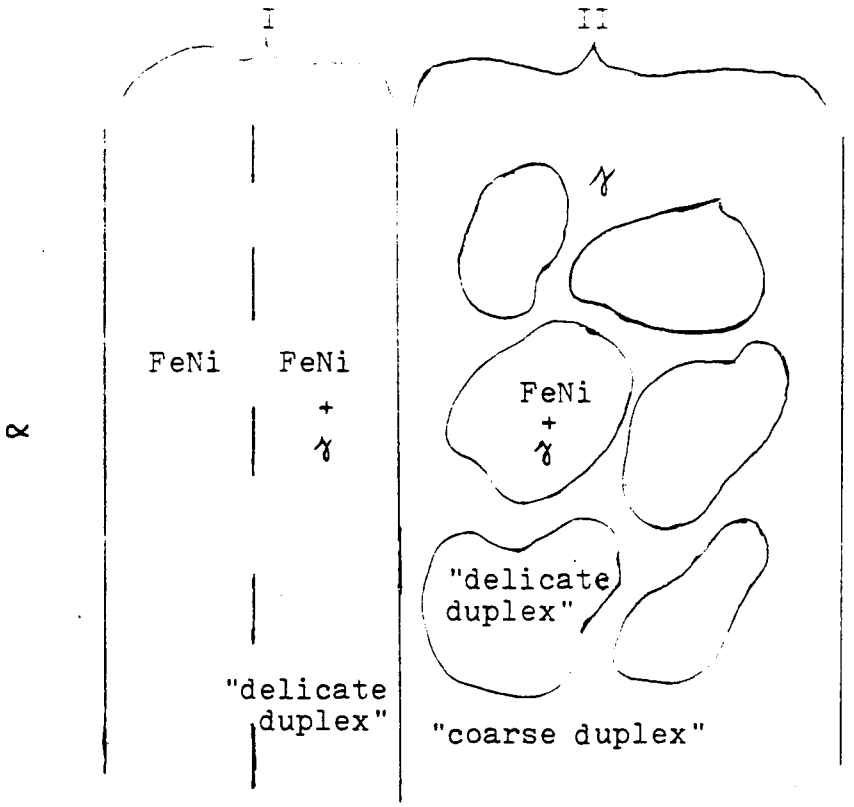

FeNi = ordered tetrataenite
γ = disordered taenite, < 25% Ni
α = kamacite

Figure 3. Schematic of zones I and II from Figure 2.

in meteorites contains 46-50% Ni [44]. As the amount of Ni decreases, the ordering temperature drops [40]. The FeNi structure is tetragonal, although only slightly: a = 3.5761 ± .0005 A, and c = 3.5890 ± .0005A. c/a then = 1.0036 ± .0002 [47].

The lattice parameter for the ordered phase is quite close to the cell parameter of the disordered phase: 3.596 ± .001 A [46]. In fact, the two phases have the same Bravais lattice and form a "pseudo monocrystal, whose axes are those of the original high temperature FCC crystal" [40].

The FeNi superstructure tends to be disordered by shock [46]. Also, it can be formed artificially in Fe-Ni alloys by irradiating disordered taenite with either electrons or high energy neutrons [42].

The terrestrial mineral josephinite (an Fe-Ni alloy) contains an intergrowth of $FeNi_3$ (awaruite) and FeNi superstructure; but as of the present, awaruite has not been found in any meteorites [42], even though it can be easily formed using conventional heat treatments.

A third meteoritic "taenite" exists in addition to the tetrataenite and the disordered taenite; this is the taenite that is found when taenite (either ordered or disordered) has undergone rapid heating and cooling (such as in heat affected rim zones). This third type of taenite is paramagnetic, disordered, unequilibrated, and contains 30-50% Ni [44].

VII. THE IRON-NICKEL PHASE DIAGRAM

The Fe-Ni phase diagram is not known with much certainty in the low temperature portion. It appears to be a fairly complex system

with three ordered phases: FeNi (with superstructure $L1_0$), Ni_3Fe (with superstructure $L1_2$), and Fe_3Ni. Of these, only the FeNi phase has been observed in meteorites.

A recent version of the Fe-Ni phase diagram is shown in Figure 4. It predicts that γ (Fe, Ni) decomposes into FeNi superstructure and Fe_3Ni (probably also ordered). However, Fe_3Ni has not been detected in meteorites. Meteorites seem to indicate that γ (Fe, Ni) (high temperature form) decomposes to ordered FeNi and disordered γ (Fe, Ni) (low temperature form) [48]. Goldstein and Williams [49] and Albertsen, Nielsen, and Buchwald [44] have revised part of the Fe-Ni phase diagram to more accurately portray this reaction.

VIII. THE P-Fe-Ni AND C-Fe-Ni PHASE DIAGRAMS

Phosphorus is present in large enough quantities in iron meteorites to make a look at the Fe-Ni-P phase diagram worthwhile. Phosphorus has been found to decrease the size of the kamacite + taenite region by increasing the maximum solubility of P in kamacite [50]. Isotherms of 300, 400, 500, 600, and 700 °C have been determined by Romig and Goldstein [50]. Reed shows the entire iron-rich corner in an older paper [11].

For meteorites with high carbon concentrations, the Fe-Ni-C diagram may be of interest. Romig and Goldstein have determined isotherms for this system at 500, 600, 650, and 730 °C [51].

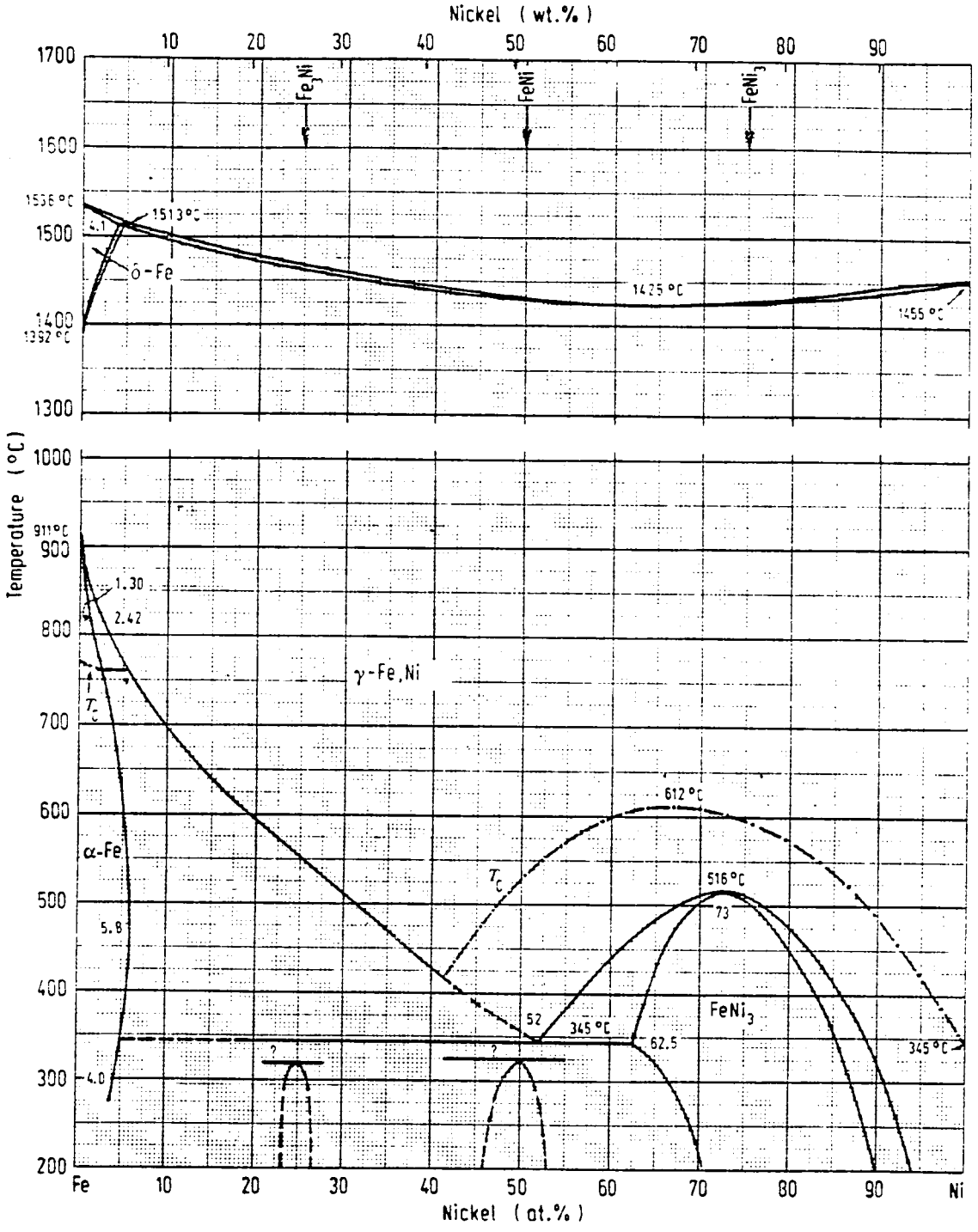

Figure 4. The Fe-Ni phase diagram. (From [43].)

CHAPTER V

THE ARISPE METEORITE

The Arispe meteorite is a coarse or coarsest octahedrite. Its composition is shown in Table 2 [52]. Scott and Wasson [15] have classified Arispe as Group IC-An. Group I meteorites are noted for their abundant inclusions.

The Arispe meteorite was part of a fall consisting of at least 16 meteorites which were all found near Sonora, Mexico. The first two masses were found in 1896, and a larger mass (124 Kg or 272 lb) was found in 1898. The accumulated mass of all the known meteorites belonging to this shower is 683 Kg [52].

Few people have studied the microstructure of the Arispe meteorite in depth. Previous investigations of the meteorite by Brooks [53] have revealed that our slice of the Arispe meteorite is polycrystalline (it originally had three taenite grains) and has large areas of inclusions. Retained taenite can be easily seen between the kamacite plates (although it is not abundant, as the Ni content is low). Much of this taenite has decomposed revealing plessitic structures, in which ordered FeNi is probably present. Spheroidized and pearlitic areas have also been seen and have been examined more closely in this research.

Studies of the Arispe meteorite by Buchwald have revealed that the Arispe has cohenite "nests"—growths of cohenite looking somewhat like bird's nests. (This feature has not been found in other

Table 2. Selected Chemical Analyses of the Arispe Meteorite

	Percentage			ppm								
	Ni	Co	P	C	S	Cr	Cu	Zn	Ga	Ge	Ir	Pt
Hawley in Buddhue 1950	6.80	0.45	0.31	140	200		200				15.8*	
Goldberg et al. 1951	6.97	0.49							55.6			
Lovering et al. 1957		0.48				46	110		51	233		
Nichiporuk & Brown 1965											7.6	17.2
Smales et al. 1967						14	112	7.3	51	229		
Moore 1968, pers. comm.	6.69	0.46	0.31									
Wasson 1968, pers. comm.	6.54								50.8	260	9	

*The value is from Hawley (1939) and includes all platinum metals.

meteorites.) The Arispe meteorite is reported to have some small (1 x 5 micrometers) inclusions of carlsbergite within the kamacite, as well as Neumann bands which are indistinct and possibly decorated with precipitates. Areas of heat-affected metakamacite with rhabdite that has been melted have been observed on some pieces., as well as a dendritic iron fusion crust [52].

Axon [54] states the Arispe's polycrystallinity indicates that it was hot worked while still in the taenite state, which subsequently caused it to recrystallize.

CHAPTER VI

EXPERIMENTAL PROCEDURE

I. HISTORY OF THE SAMPLE

The meteorite piece used for this experiment is a 1 cm thick slice (Figure 5), apparently from piece A of the Arispe meteorite (meteorite A was the largest of the fragments found). It is thought to originally have belonged to the Geology Department at The University of Tennessee, and the Chemical and Metallurgical Engineering Department acquired it from them. As nobody could recall how the University acquired the slice or from which meteorite it came, it was sent to Arizona State University's Center for Meteorite Studies for identification. There, Dr. Charles F. Lewis, Associate Curator of the Center, identified it as a slice of the Arispe iron.

II. SAMPLE PREPARATION

A triangular section (about 3 cm on each side and 1 cm thick) was cut out of the edge of this slice of the meteorite with a band saw (sample "A"). This sample was mounted in epoxy and polished using standard metallographic procedures, then heavily etched in Nital. Extremely heavy etching was required to adequately bring out the Neumann bands.

Later, a second sample was cut out of the center of the slice. This sample was removed to allow us to distinguish between structures

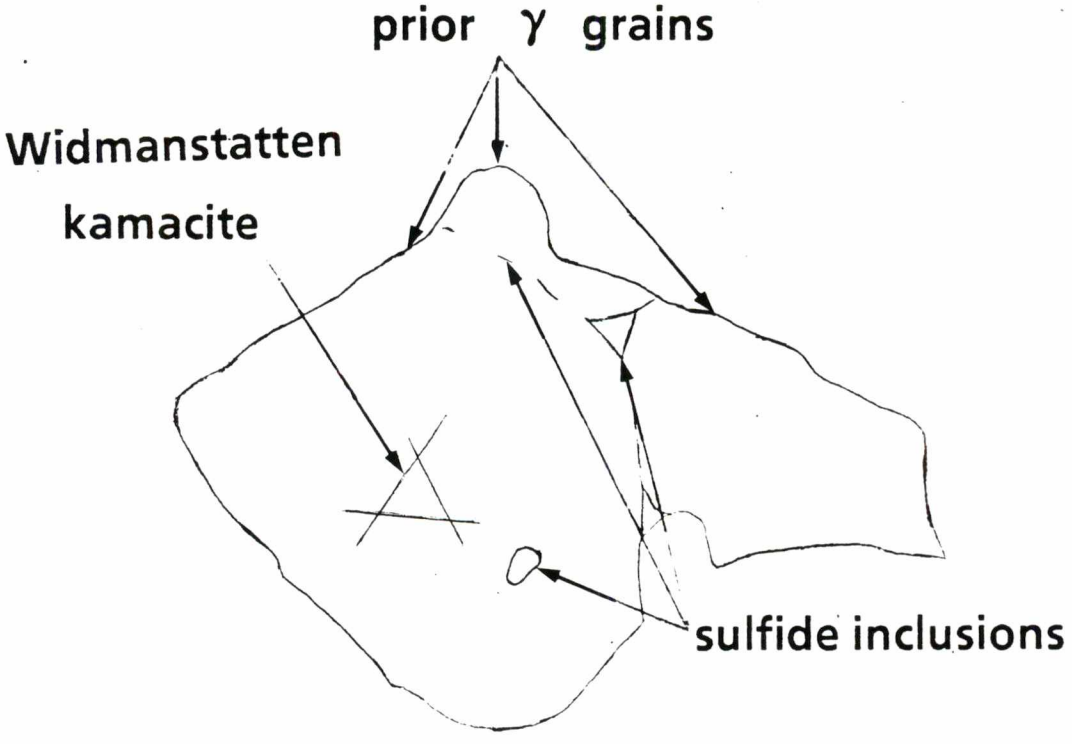

Figure 5. The slice of the Arispe meteorite owned by The University of Tennessee. Notice the three prior taenite grains, separated by inclusions, and the coarse Widmanstatten kamacite.

that were affected by heating during passage through the earth's atmosphere, and those present in the meteorite before it reached the earth's atmosphere. This center sample was then further subdivided into three pieces: B, C, and D (Figure 6). All were mounted and polished through 1 micron diamond, then etched for about 30 seconds in 2% Nital. Sample B contains a large cohenite nest, sample C features a large, shiny inclusion, and sample D contains only plessite in Widmanstatten kamacite.

Piece D was then cut once more, this time through the plessite, and the new cut face (D') was polished using the previous method. This allowed us to get a sort of three-dimensional view of these stringers by observing these two faces which had been cut at 90° to each other.

On the figures, OM denotes an optical micrograph and SEM denotes a scanning electron micrograph.

III. EDS PROCEDURE AND LIMITATIONS

The EDS (Energy Dispersive Spectrometer) unit on the scanning electron microscope provides merely a qualitative idea of what major elements are present in a sample; it does not detect trace elements. The EDS was used mainly to analyze small (1 micron in diameter or smaller) particles to give an indication of what minerals we might be looking at; but it was also used to distinguish the metallic phases (taenite and kamacite) from each other. When analyzing small particles even at high magnifications using small beam sizes, the surrounding matrix phase was occasionally excited and would

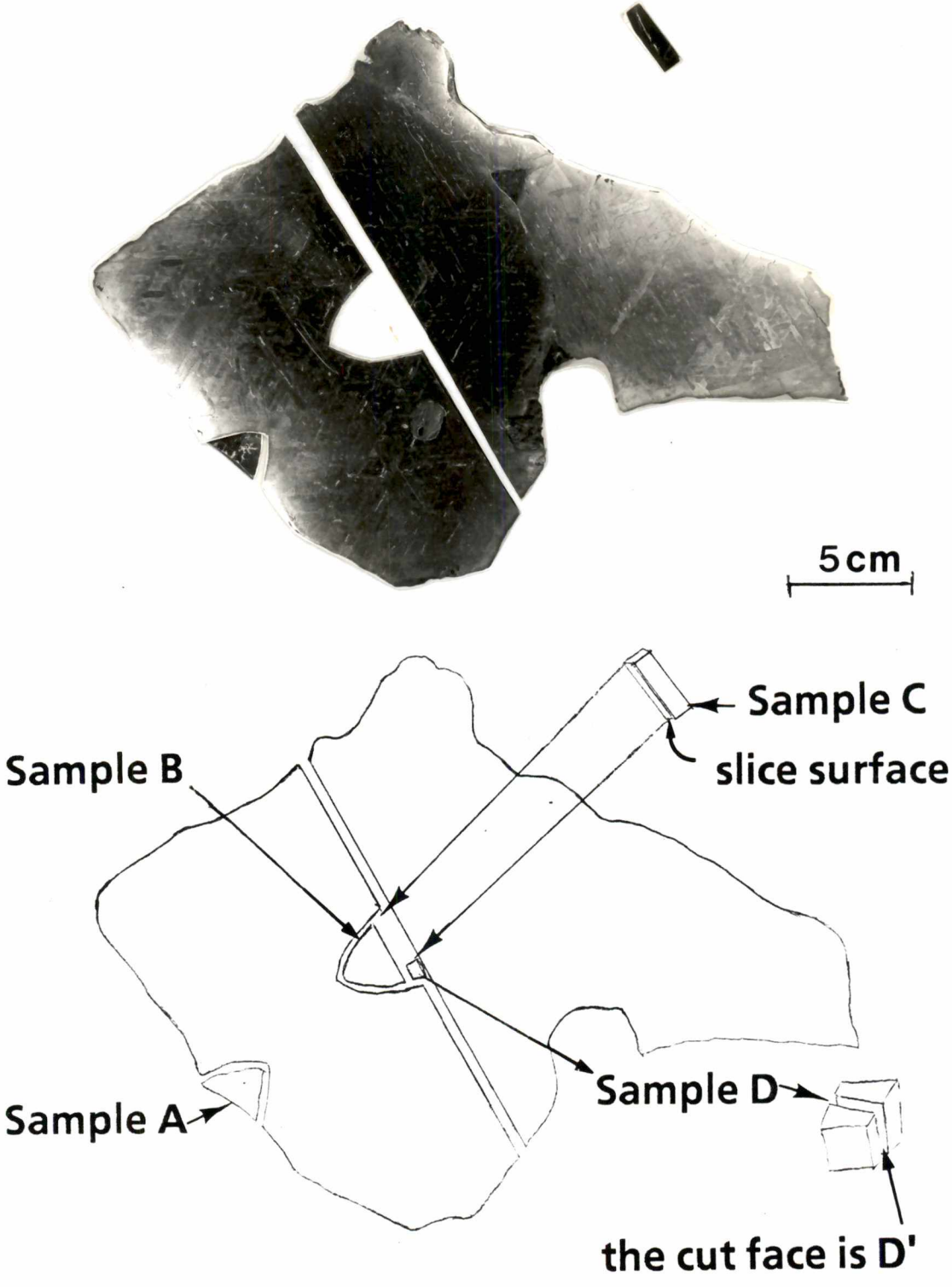

Figure 6. Photograph of the meteorite slice showing the metallographic samples that were cut from it.

give off x-rays, thus making it unclear whether all observed peaks were actually due to the phase being analyzed, or whether some were due merely to contributions from the matrix.

The EDS used cannot detect any element with an atomic number lower than 11 (sodium), so it was impossible to detect important light elements such as oxygen, carbon, and nitrogen.

All EDS analyses will be given in terms of ratio of K_α peaks to the iron K_α peak.

IV. ARTIFACTS

Several artifacts were encountered during this study which confused proper identification of the microstructure at times.

A. The Inclusion

A puzzling inclusion was found on sample B (Figure 7). It had the large, spherical shape of a troilite inclusion, but EDS readings showed no S present. The entire EDS analysis was very weak in fact, leading one to suspect that this inclusion had been pulled out and that we were just seeing a hole. Under the optical microscope, however, polishing scratches on the inclusion's surface could be seen. Curiously, we found that we could focus not only on the surface of the "inclusion," but also on the bottom of the "hole." After some thought, we realized that the inclusion had long since been pulled out, and the hole had been filled with clear epoxy during mounting.

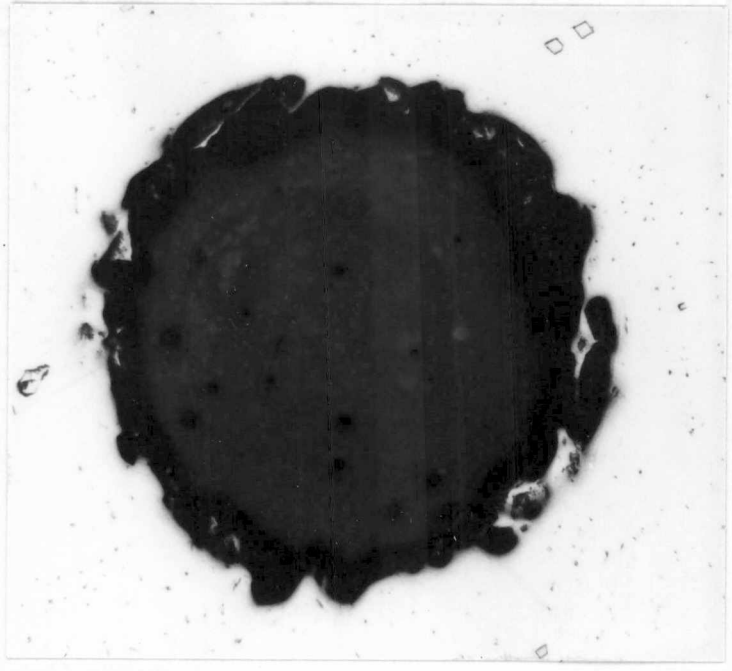

Figure 7. Epoxy-filled inclusion hole found on sample B.

B. Corrosion

All samples were kept in a vacuum dessicator, but corrosion products would appear nonetheless. In all samples, the taenite would take on a fuzzy, oxidized appearance (Figure 8) after a few weeks which would have to be polished off. The kamacite was apparently unaffected. This corrosion was especially troublesome during Tennessee's humid summer months.

C. Cloudy Products

Around certain phosphides on D', a dendritic appearing product developed on the kamacite (Figure 9). Macroscopically, these areas appeared cloudy. This product could be easily polished off. EDS measurements showed no difference compositionally between these phosphides and neighboring unaffected phosphides (Figure 10), but the phosphides showing this behavior all had large cracks, and it is supposed that this problem was due to etchant seeping back out of these cracks.

A similar appearing product also showed up on sample C, but no cracks around the schreibersite were evident (Figure 11).

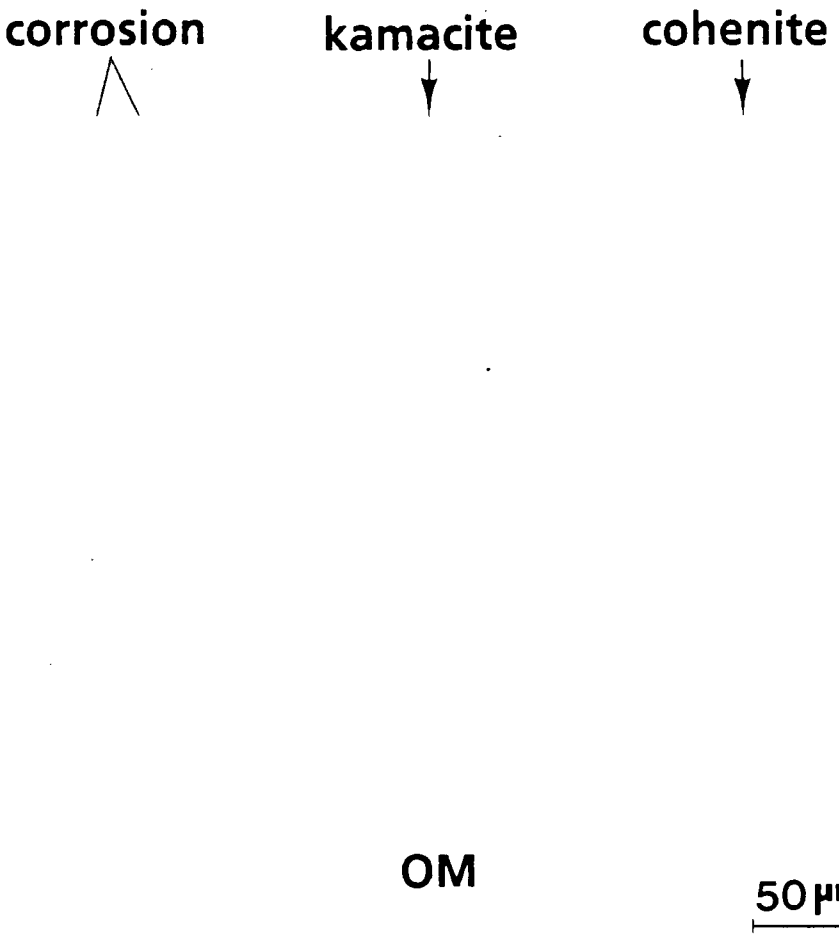

Figure 8. Fuzzy appearing corrosion frequently found on taenite can be seen on the corner of this stringer of sample A.

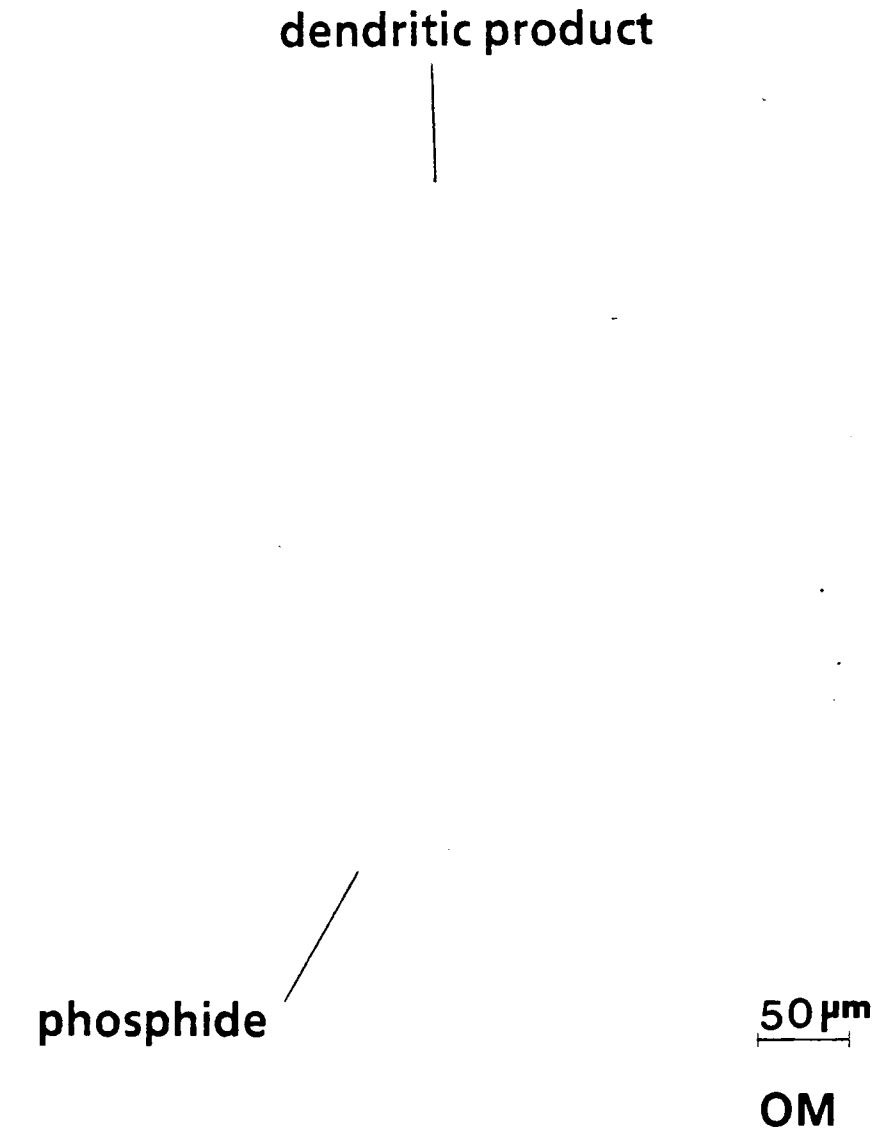

Figure 9. Dendritic product around phosphide on sample D'.

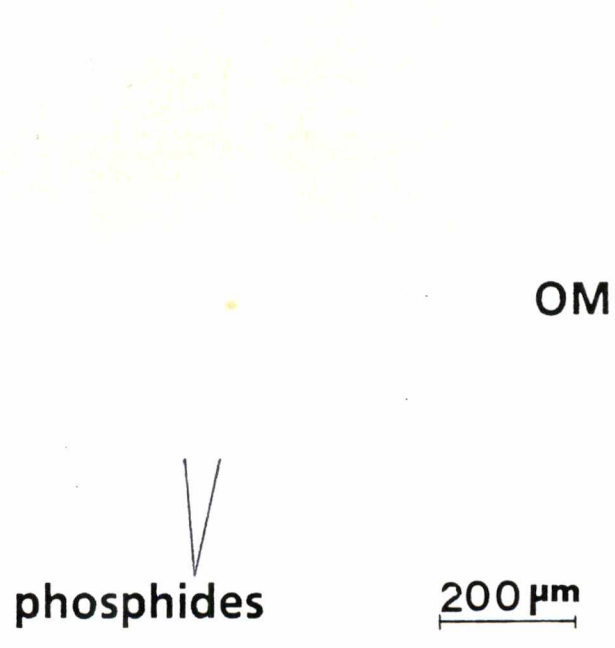

Figure 10. Two neighboring phosphides on sample D', one unaffected by the dendritic product, and the other completely surrounded by it.

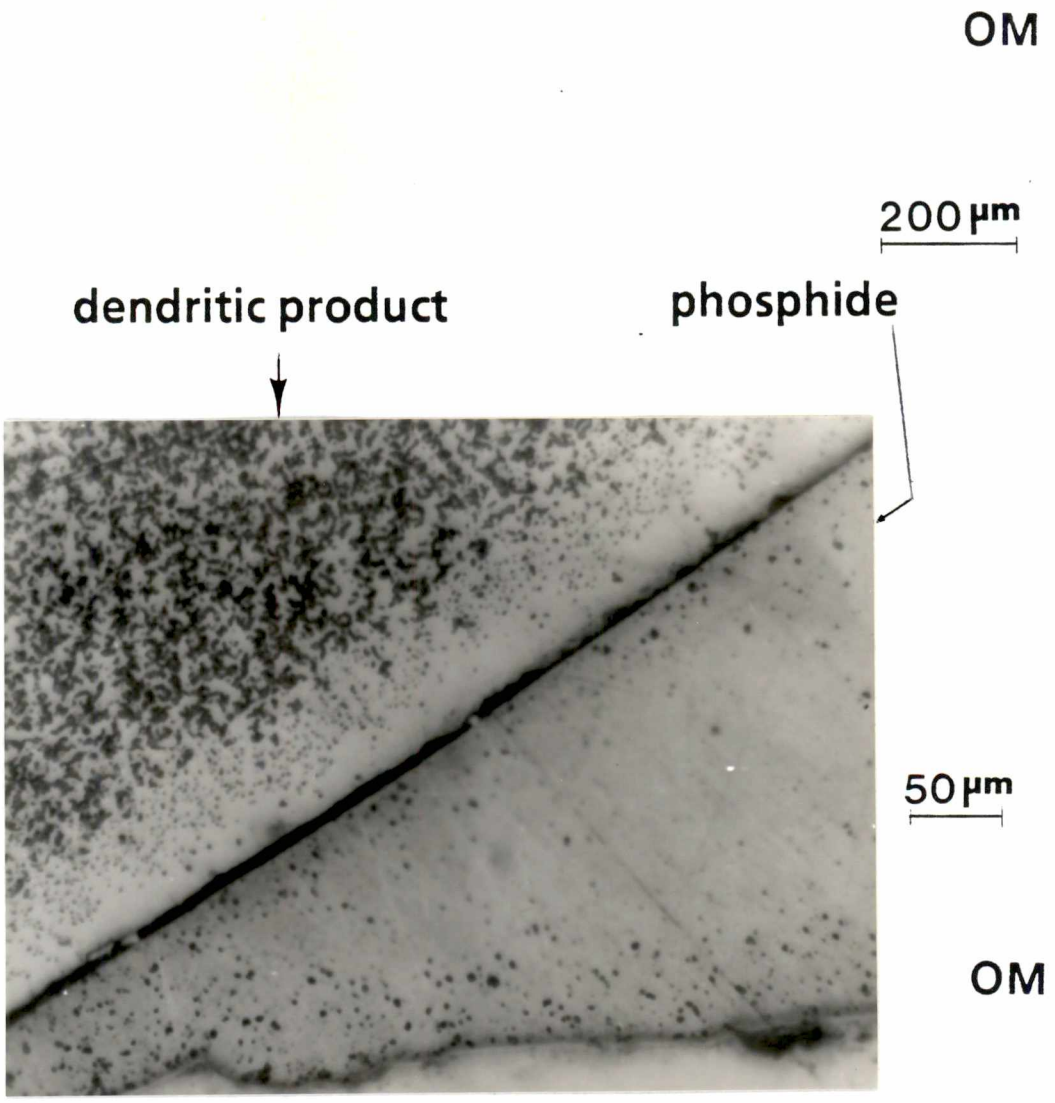

Figure 11. A phosphide on sample C displaying a dendritic product.

CHAPTER VII

RESULTS

I. MACROSTRUCTURE

The most important macrostructural features in the Arispe meteorite are Widmanstatten kamacite, the appearance of the outer crust, and nonmetallic inclusions.

A. Widmanstatten Kamacite

The slice observed here consists of over 95% Widmanstatten kamacite. The kamacite is present as coarse (2.9 mm) [18] plates oriented in the characteristic Widmanstatten directions (see Figure 5, p. 37). The kamacite is littered with inclusions, mostly rhabdite, and displays a high density of Neumann bands in places.

The polycrystalline nature of this meteorite can also be seen in Figure 5: one large taenite grain and two small ones were originally present (see sketch in Figure 5). Nonmetallic inclusions (probably sulfides) fill the grain boundaries.

B. Outer Crust

The outer crust appears brown and somewhat glassy macroscopically. The expected α_2 layer along the slice edge is not obvious; perhaps it is not even present on this sample. The dendritic iron fusion crust seen by Buchwald [52] was not observed in this study.

Upon cutting the slice in half, rust could be seen in cracks between the kamacite plates, extending in 1-2 inches from the crust Figure 12).

C. Nonmetallic Inclusions

The two obvious nonmetallic inclusions present on a macroscopic scale are cohenite and sulfides—probably troilite. Some schreibersite inclusions can also be seen.

1. Cohenite

The cohenite is present as nests (Figure 13); six of these nests can be easily seen on the polished surface of the slice. A few cohenite nests can also be seen on the rusty back side of the slice, where they have been preferentially corroded away. The nests are relatively active under polarized light in the polished condition, and may tarnish to a golden color after long exposure to the air.

The composition of these nests has not been verified in this study, although some EDS analyses have been done, revealing iron with only a trace of Ni (Ni/Fe = .02). As carbon cannot be detected with our instruments, I am assuming these inclusions are cohenite strictly from Buchwald's picture and description in his section about the Arispe meteorite [52].

2. Sulfides

The sulfides are present as a brown rim along the former taenite grain boundaries, and also as a large inclusion in the largest of the

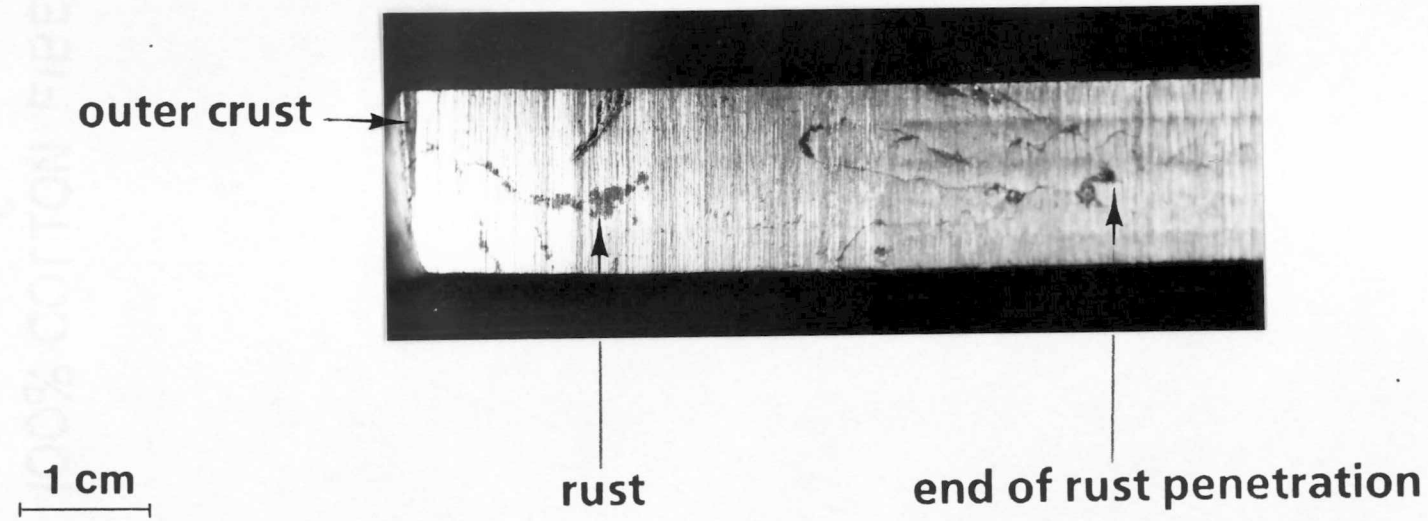

Figure 12. Photograph of slice center after being cut by bandsaw, showing penetration of rust along kamacite grain boundaries.

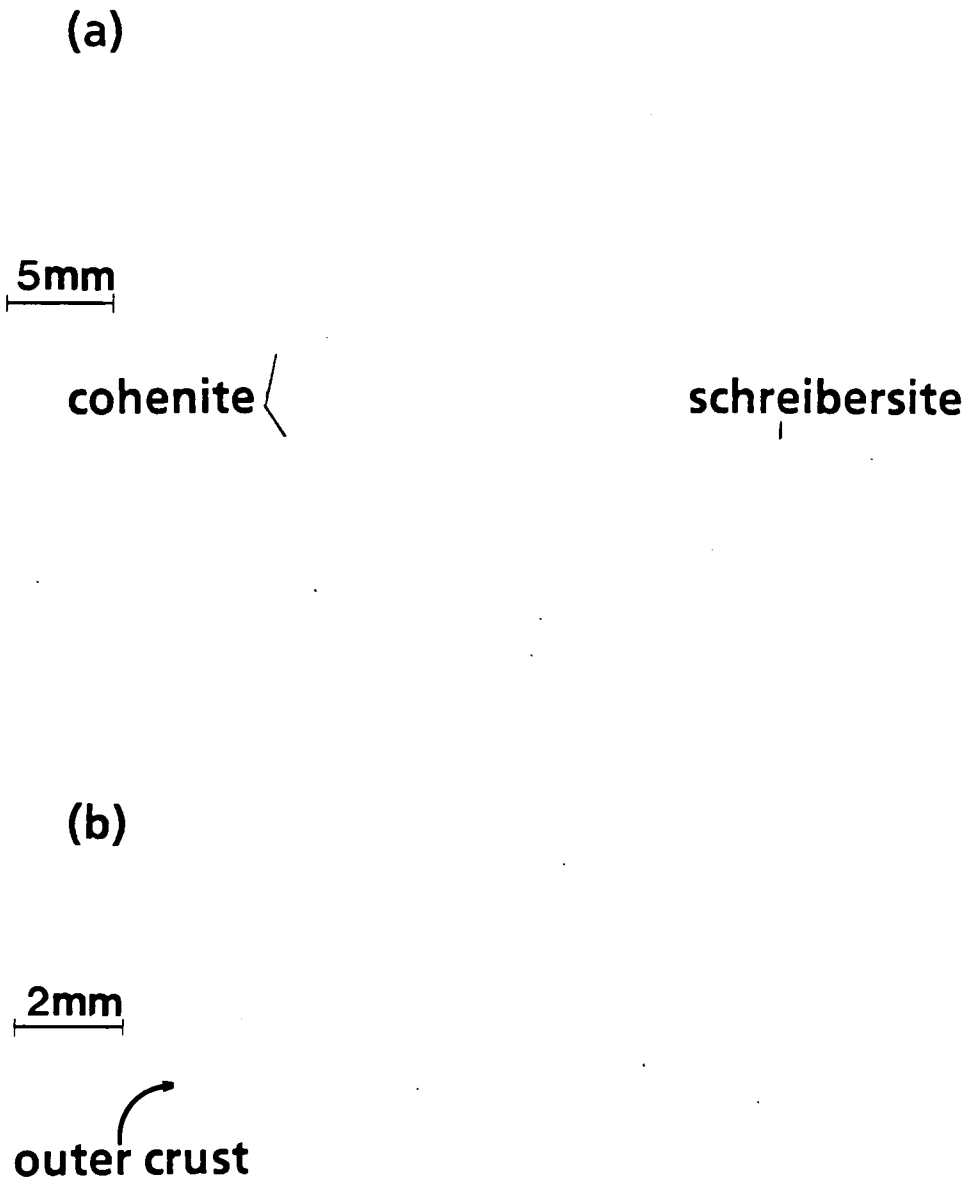

Figure 13. Cohenite nests in (a) bulk of slice and (b) on sample A.

three grains (see Figure 5, p. 37). No analyses were performed on these inclusions, but they are assumed to be troilite from Buchwald's description [52]. Also, these inclusions can be dissolved by the etchant (2% Nital) used, and upon etching gave off a H_2S odor and left yellow stains where the solute-rich etchant evaporated on the meteorite's surface.

3. Schreibersite

Some especially large schreibersite grains could be seen macroscopically; these grains appeared as small shiny inclusions on the surface of the slice and on cut faces. These inclusions will be discussed further in the next section.

II. MICROSTRUCTURE

There are many interesting microstructural features in the Arispe meteorite. Among them are the many inclusions—phosphides, oxides, and Cr-bearing particles; Neumann bands; and the many structures of plessite.

A. Phosphides

Both schreibersite and rhabdite are common in the Arispe. Schreibersite can occur as very large (Figures 14 and 15) or as relatively small (Figure 16) discrete inclusions, or it can be included in the branches of the cohenite nests (Figure 17).

Rhabdite only occurs on a microscopic scale and is found throughout the meteorite (Figure 18), except in areas where especially

5mm

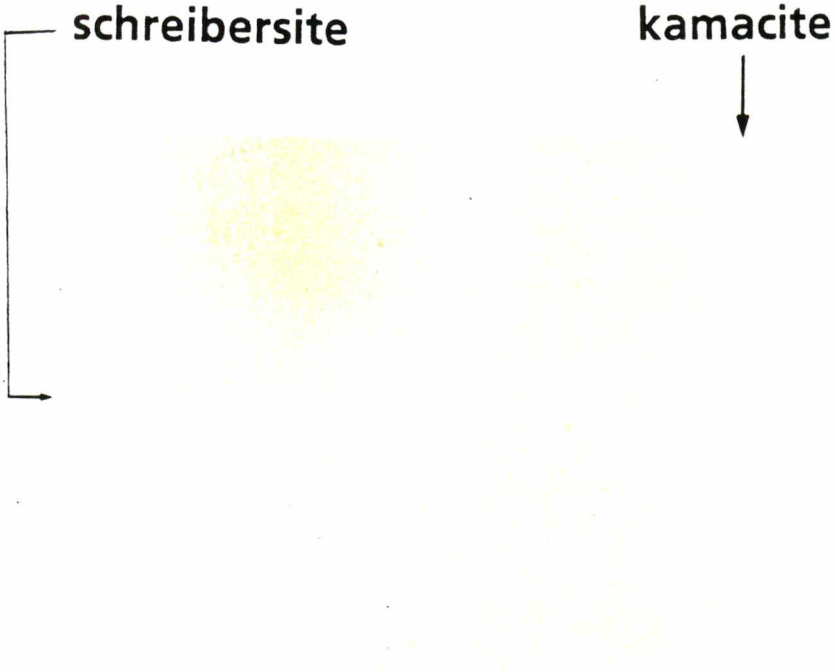

OM

Figure 14. Large schreibersite grains in sample C (top). Higher magnification view of this schreibersite (bottom).

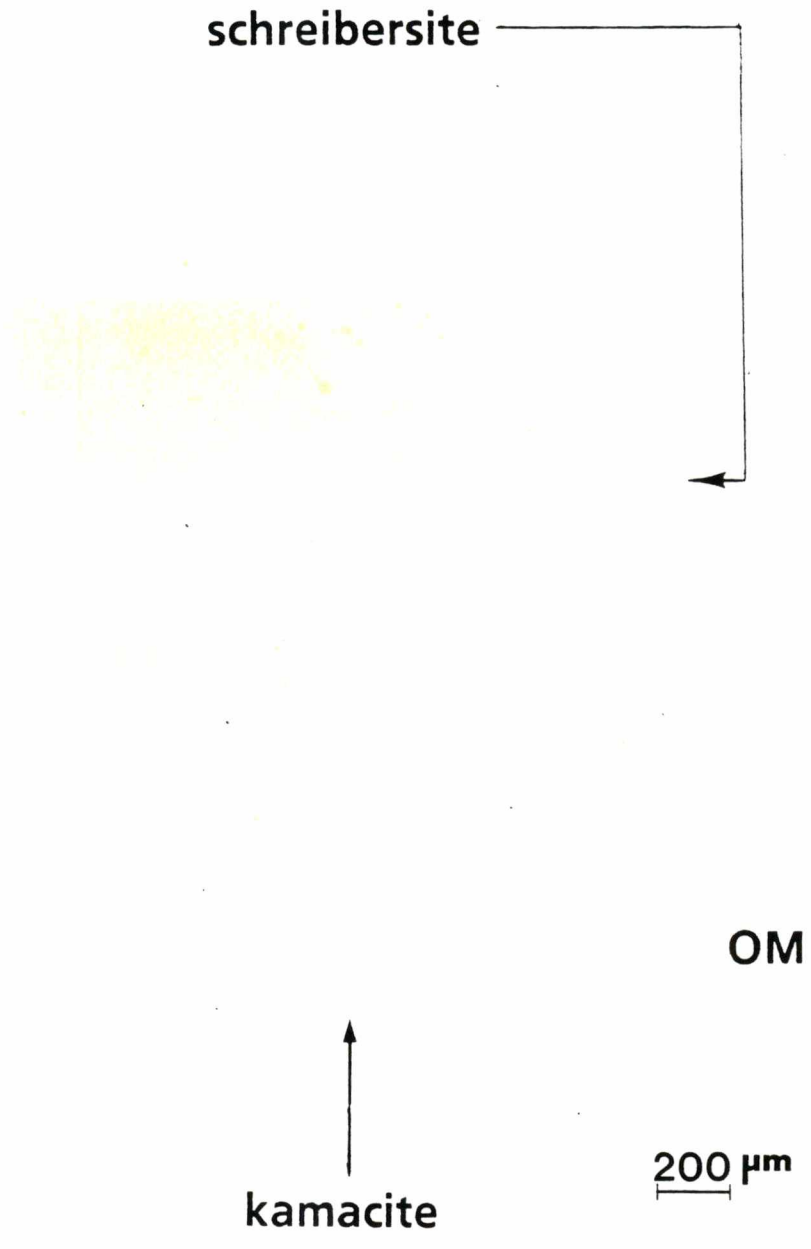

Figure 15. Large schreibersite grain in sample A. This grain can also be seen on Figure 13b.

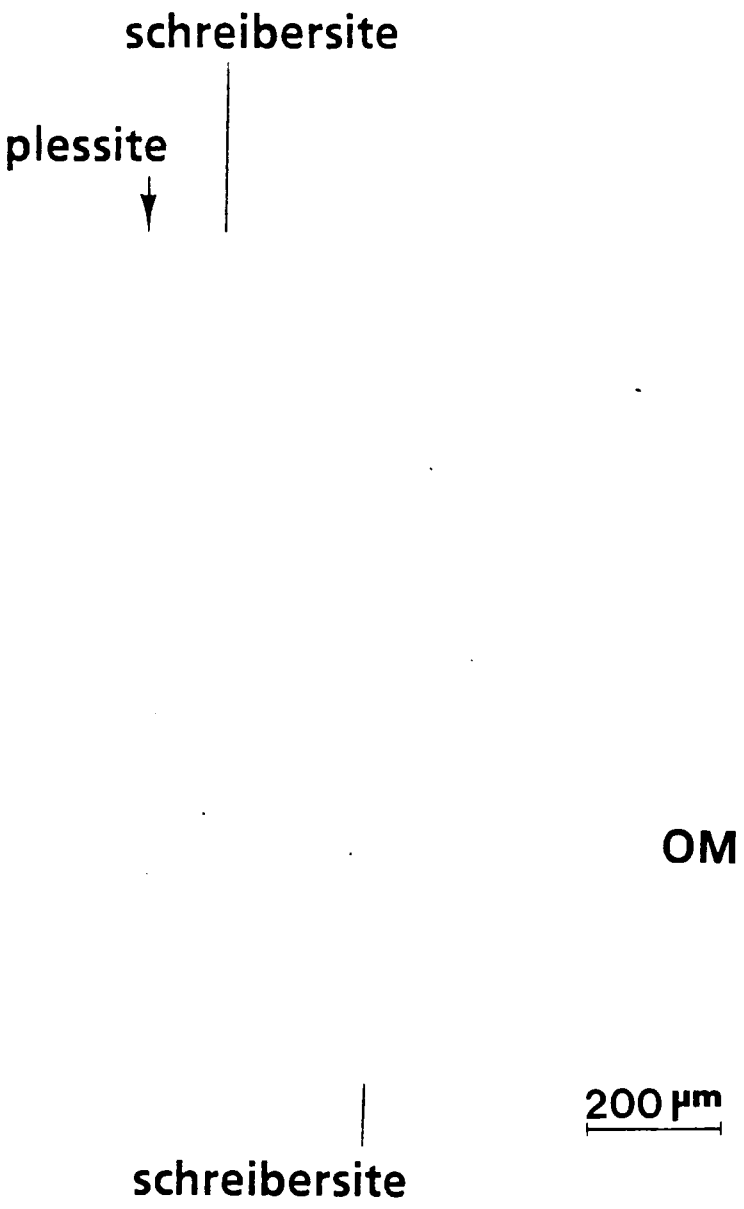

Figure 16. Small schreibersite grains around plessite.

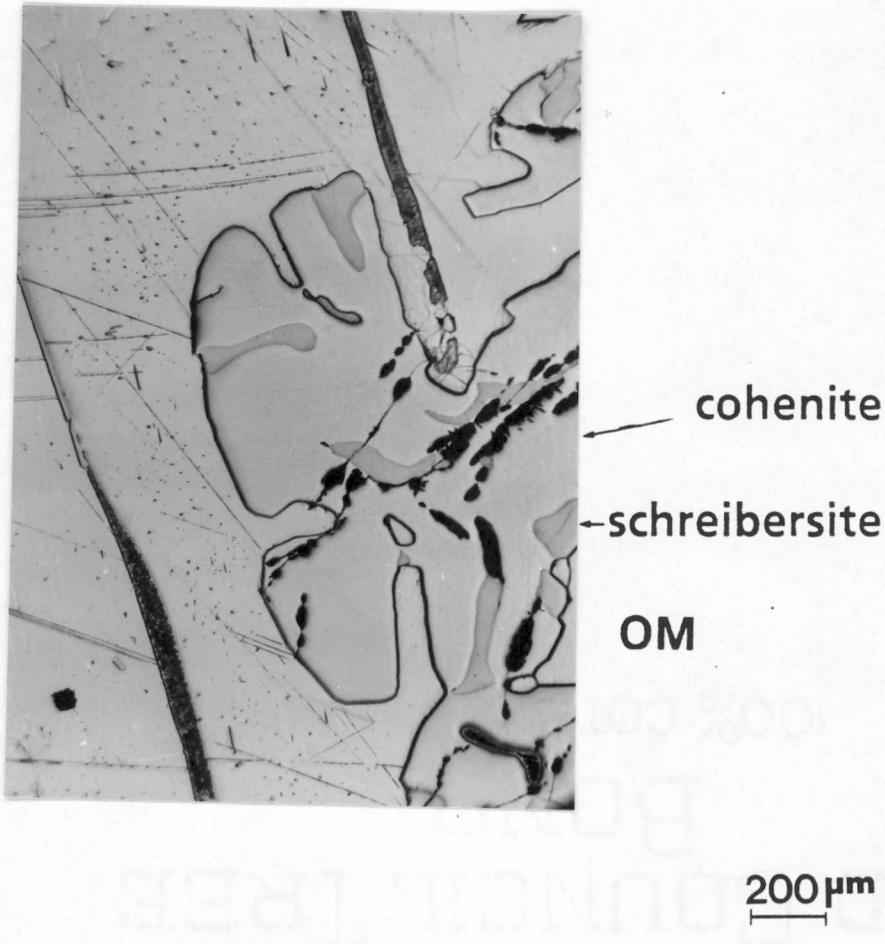

Figure 17. Schreibersite inclusions in cohenite.

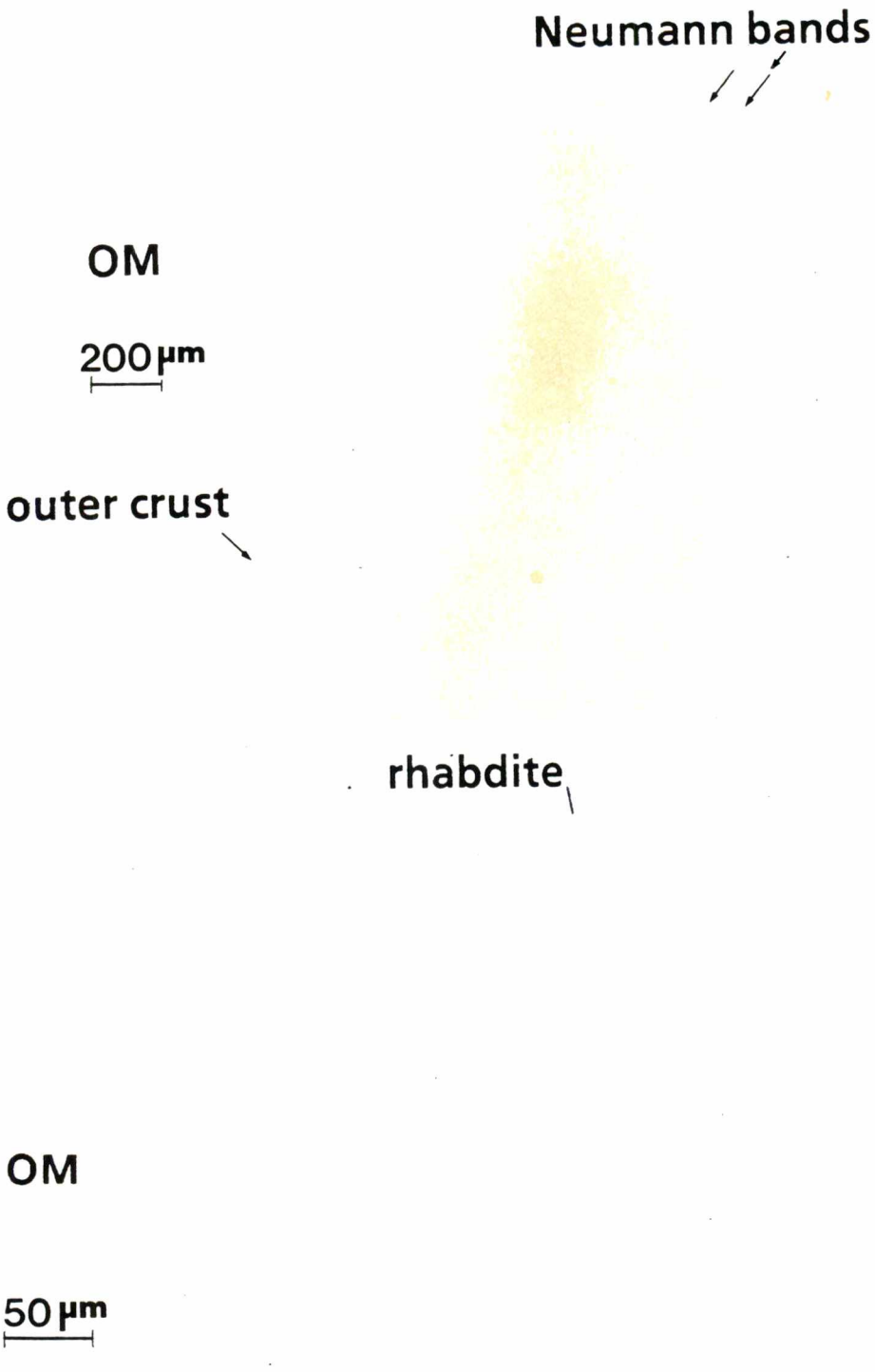

Figure 18. Scattered rhabdite crystals in sample A.

large schreibersite crystals have depleted the area of P (Figure 19). Notice in Figure 20 that the density of rhabdite is heavier in some kamacite grains than in others.

B. Grey Corrosion Products

A grey phase, presumed to be an iron oxide or oxyhydrate of terrestrial origin, composes the outer crust (Figure 21), and is also found along cracks leading in from the edge (Figure 22). These cracks may extend up to 1-2 cm. Cracks in the center of the meteorites were also filled with a grey phase (Figure 23). Using the EDS on the SEM, only iron was detected when analyzing this phase; no Ni was detected.

C. Other Nonmetallic Phases

Several different nonmetallic inclusions were found which could not be identified.

1. Pale Crystals

On sample D', pale colored rhombic inclusions were observed. These inclusions, resembling rhabdite in shape, were all arranged along a line (Figure 24). EDS analyses show the composition of these particles to be identical to that of the surrounding kamacite.

2. Cr-Bearing Particles

Cr-bearing inclusions were also found (see Figure 25). These particles were so small that an EDS analysis inevitably picked up x-rays from the metal matrix as well as the particles, thus making it

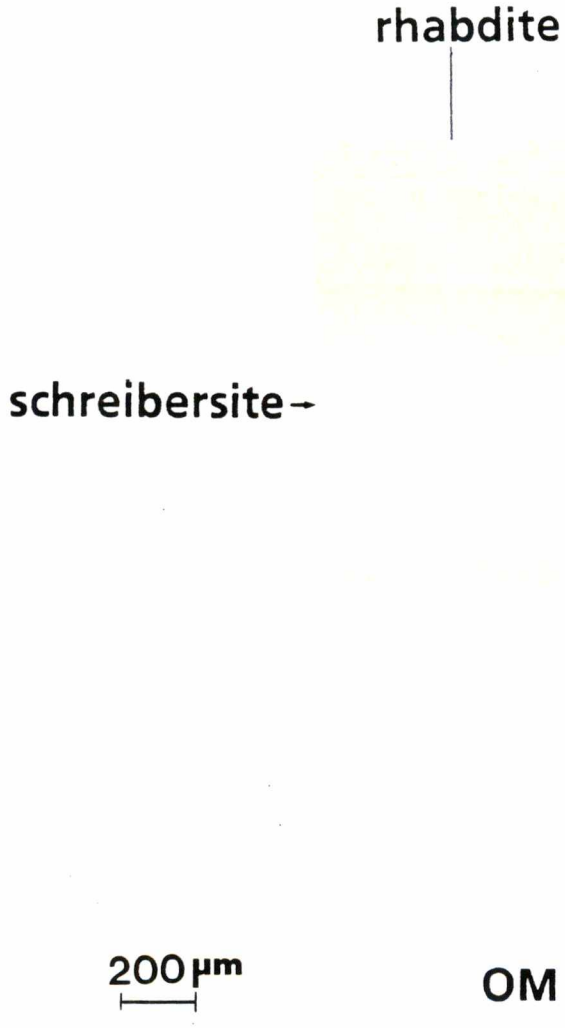

Figure 19. Micrograph of a very large schreibersite grain in sample C which has denuded the surrounding area of rhabdite.

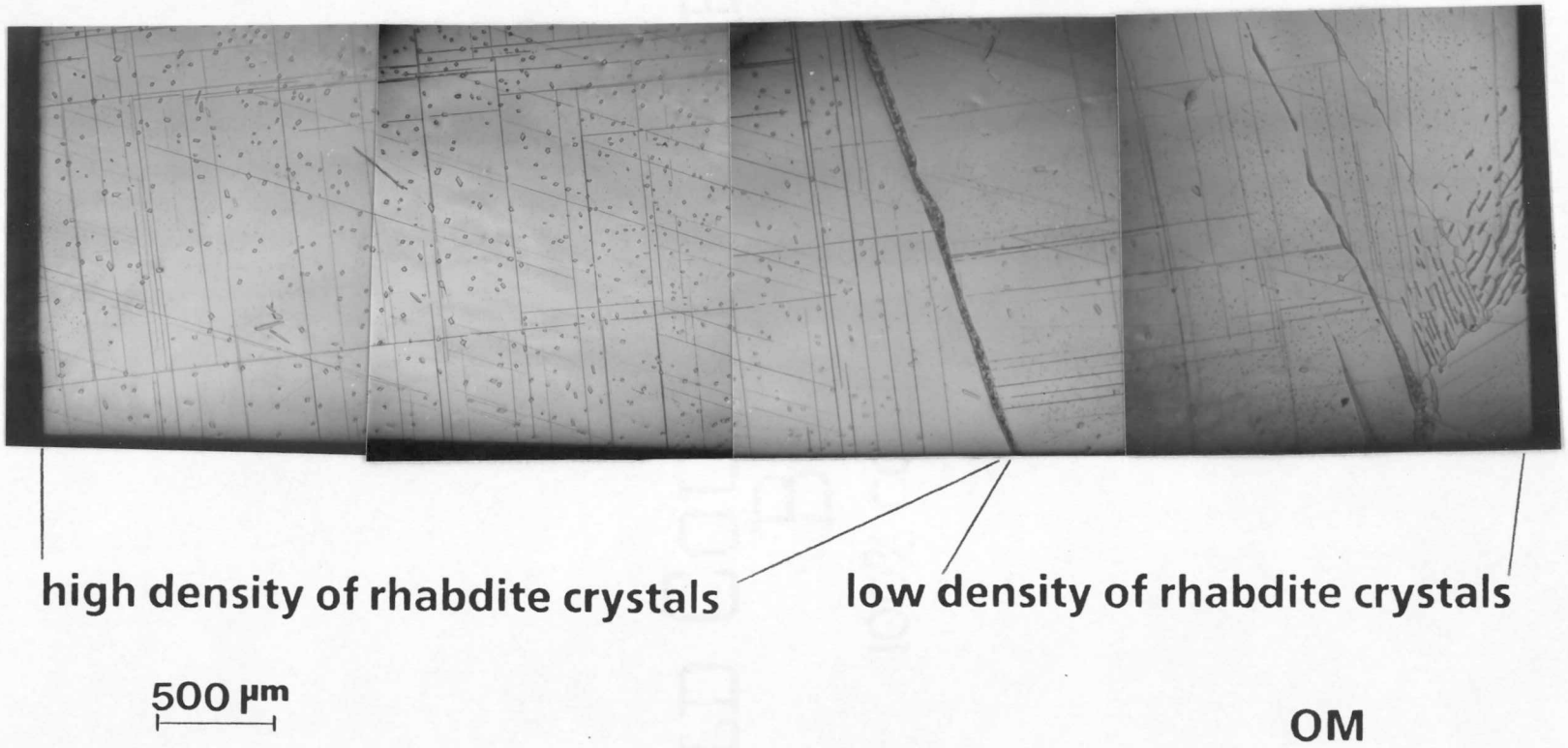

Figure 20. Edge of sample D' showing high density of rhabdite in one grain, low density in another.

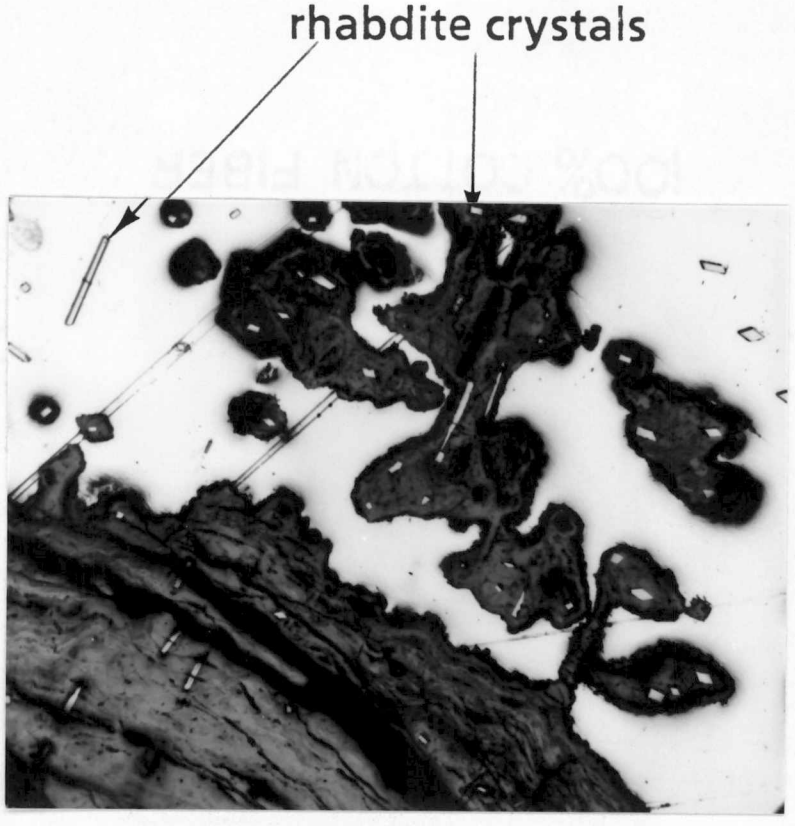

Figure 21. Grey oxide on outer crust of sample A.

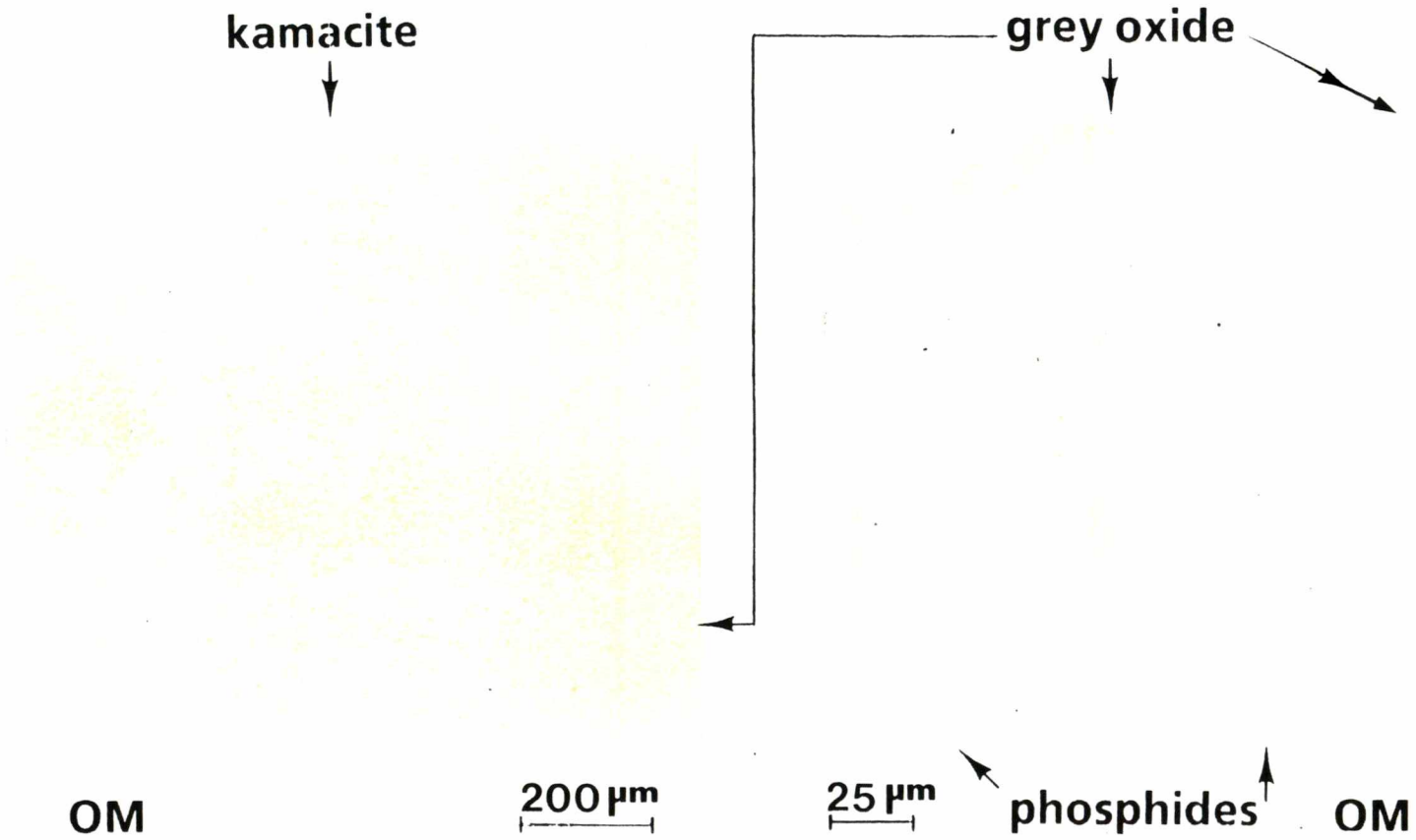

Figure 22. Grey oxide along cracks near meteorite's crust in sample A.

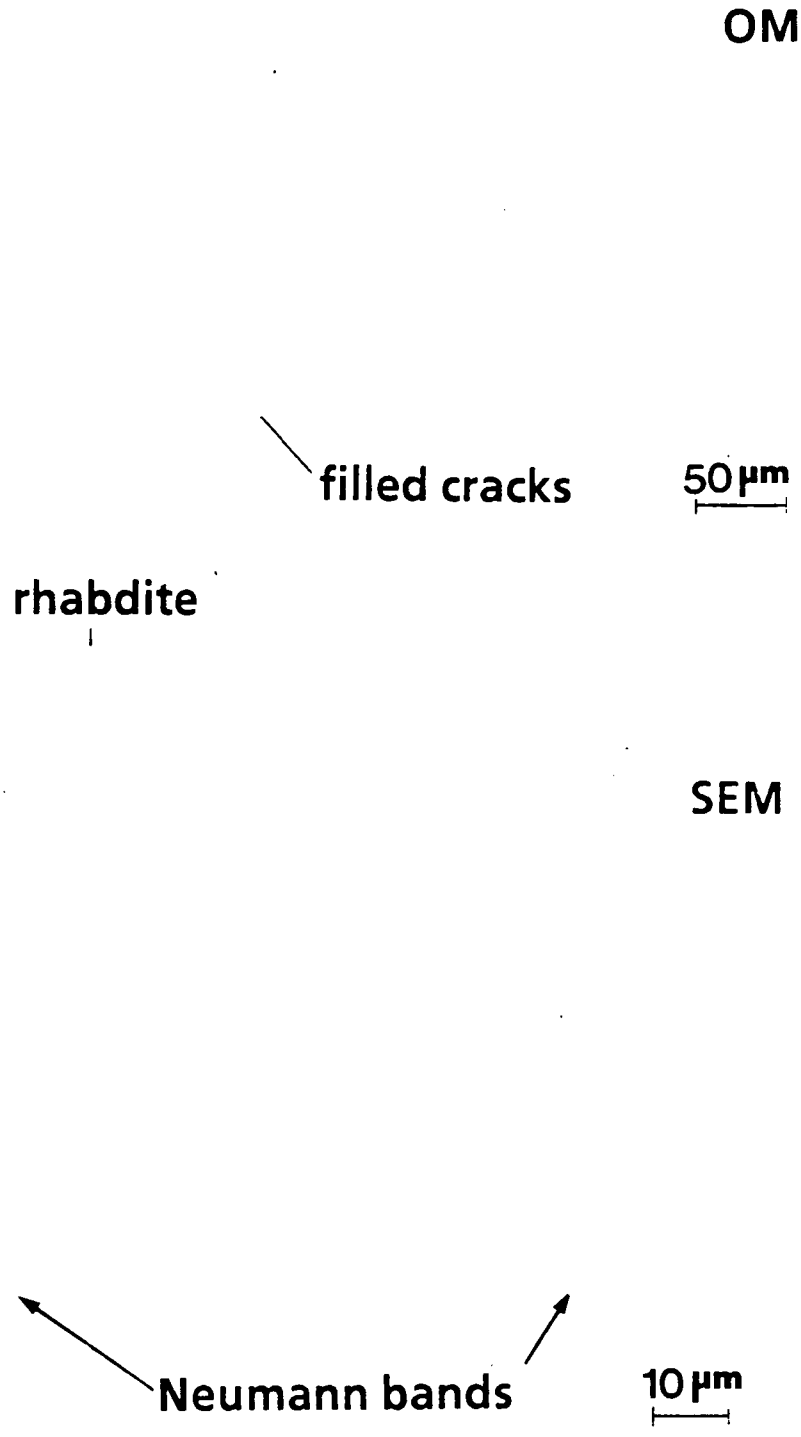

Figure 23. Grey phase filling cracks in sample C, from center of meteorite.

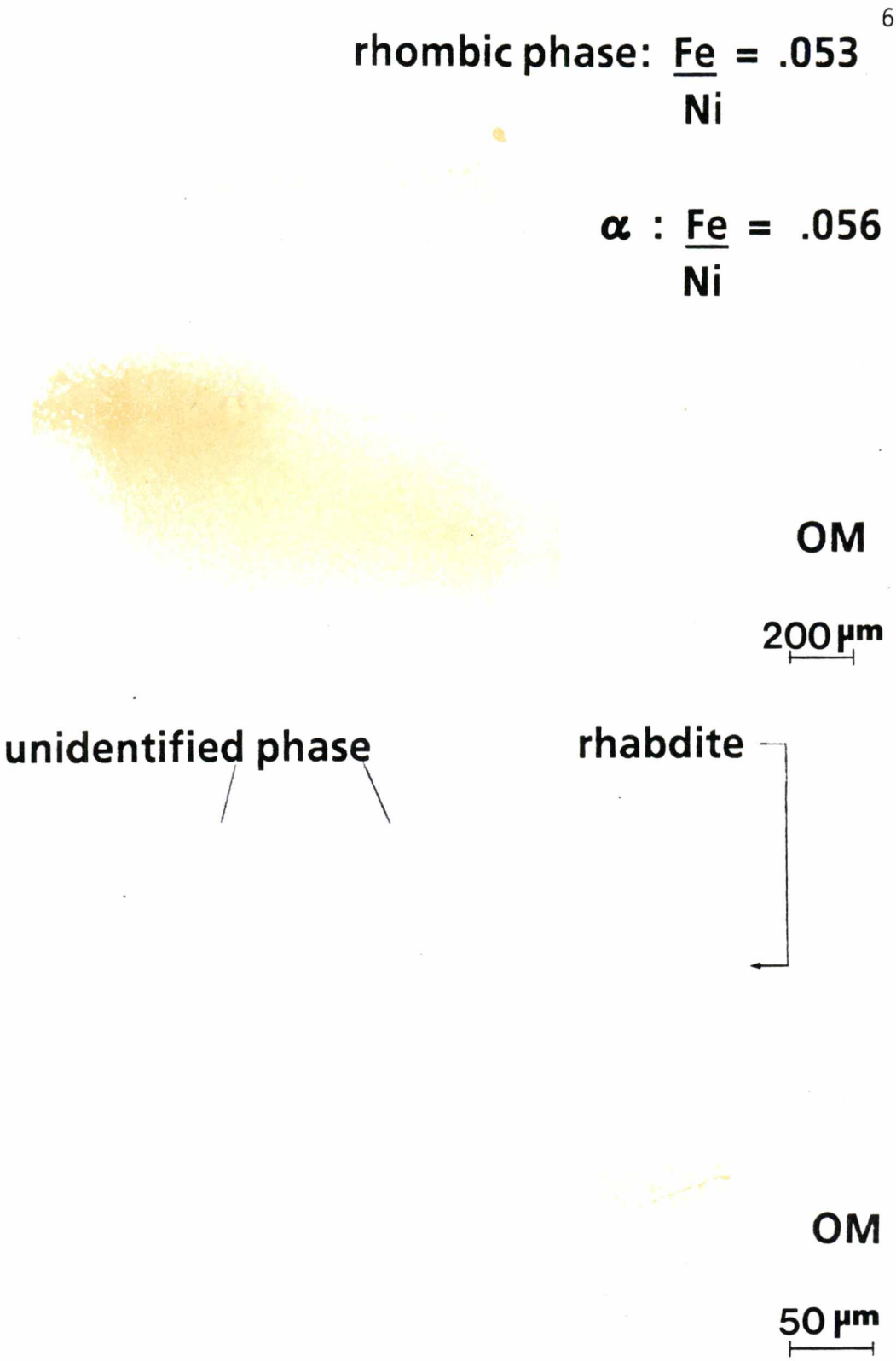

Figure 24. Unidentified rhombic phase.

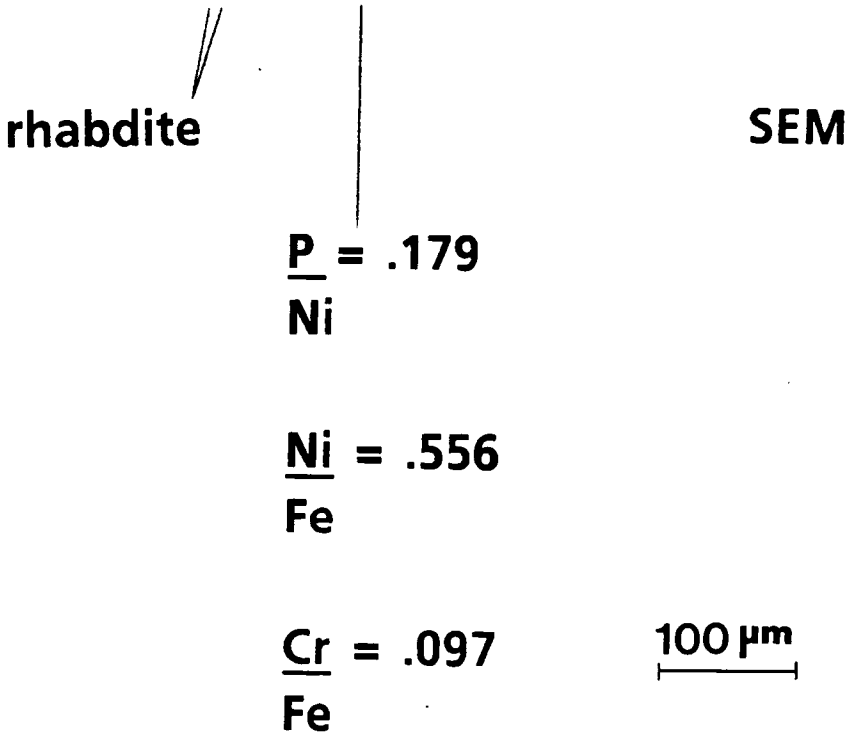

Figure 25. Micrographs showing Cr-bearing inclusions.

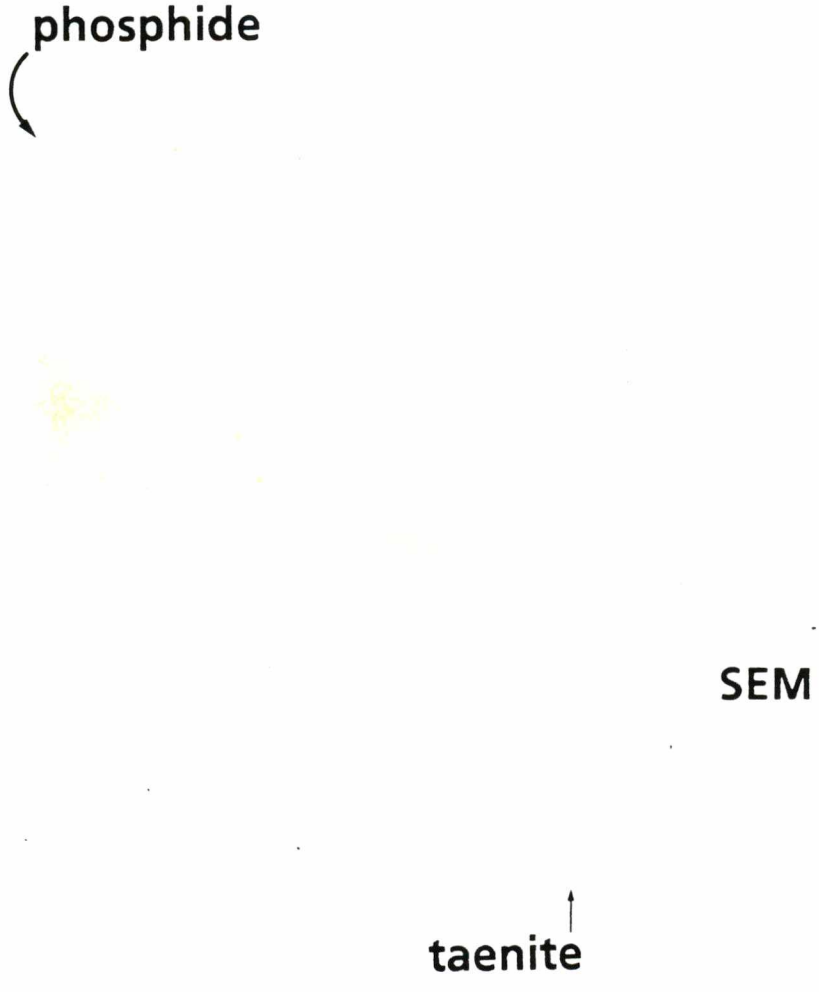

Figure 25 (continued)

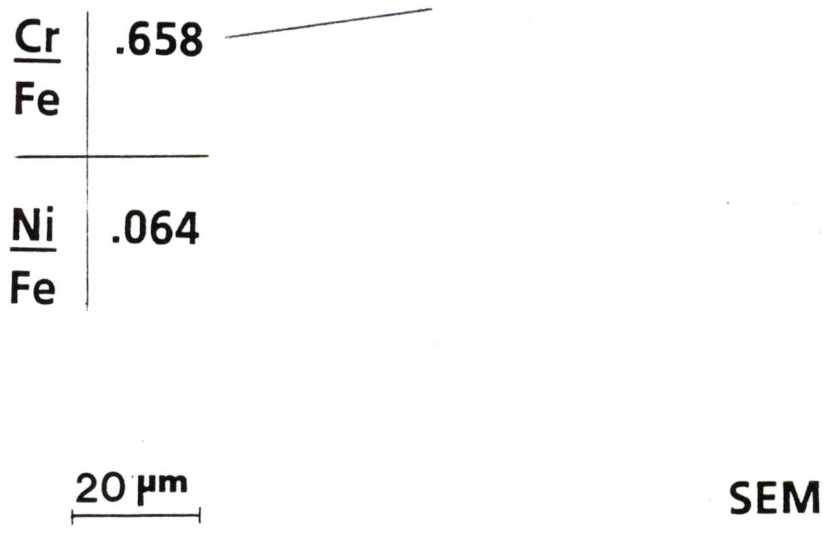

Figure 25 (continued)

impossible to tell whether these particles actually contain Fe and Ni or not. These inclusions are suspected to be either chromite ($FeCr_2O_4$) or carlsbergite (CrN), although most are much smaller than the 1 x 5 micrometer carlsbergite inclusions that Buchwald has reported seeing in the Arispe [52].

3. White Rims Around Schreibersite

In samples C and D' there were white rims around schreibersite that would sometimes tarnish streaky brown within a few days after etching (Figure 26). These inclusions showed only iron in the EDS, and we suspected they were carbides—either cohenite or haxonite. Viewing under polarized light showed that these inclusions were active, like cohenite nests. This indicated that these suspected carbides were not the cubic phase haxonite. From Buchwald's description of the Arispe [52], they are probably cohenite, but why these inclusions developed a brown tarnished layer after only a few days while the cohenite nests remained unchanged after a couple of months remains unexplained.

4. Zn- and S-Bearing Inclusion

One particle was found that appeared to contain Zn and S (Figure 27); this inclusion could be sphalerite.

D. Neumann Bands

Neumann bands are present throughout the meteorite. They can be seen in the Widmanstatten kamacite plates, but are not seen in

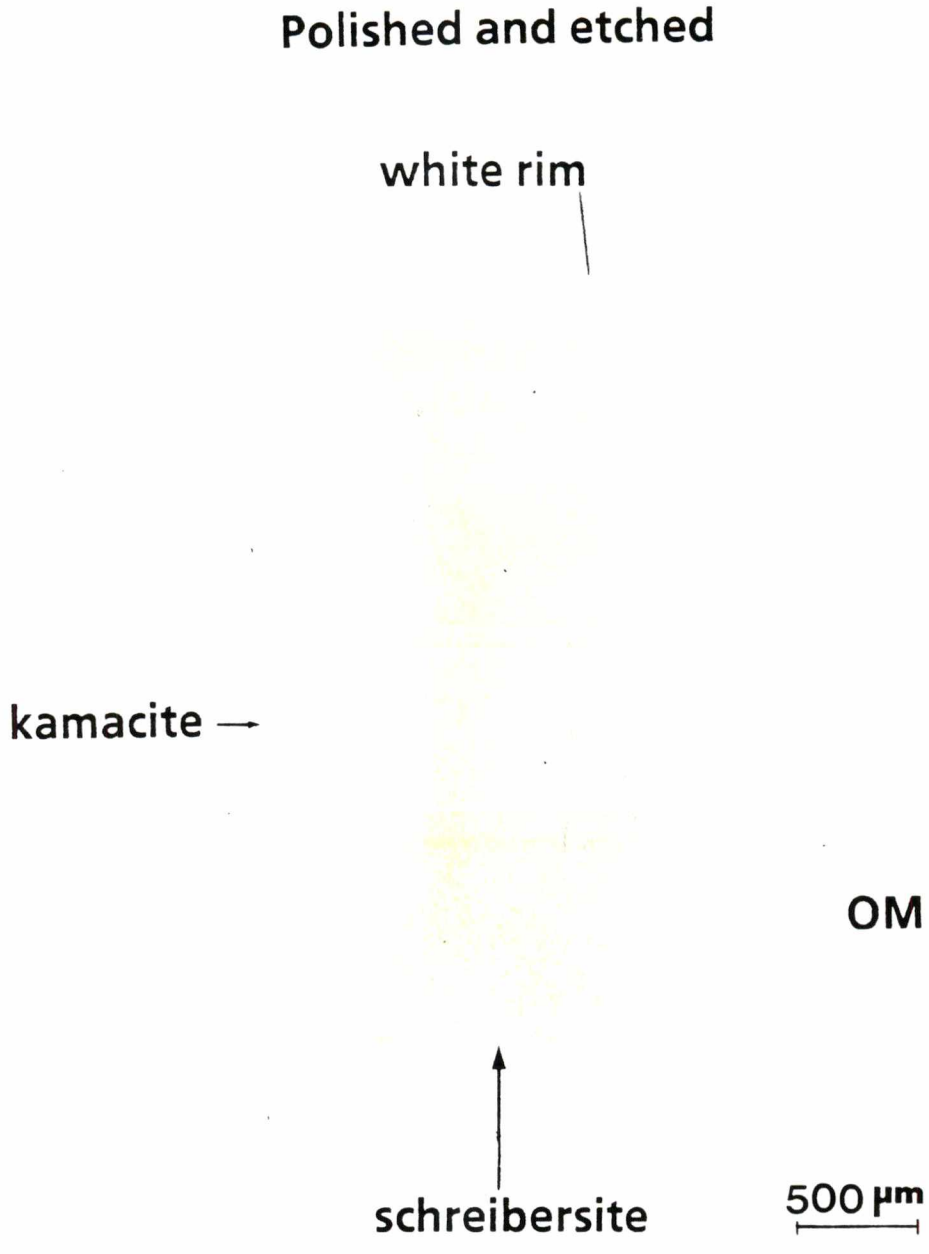

Figure 26. Streaky brown tarnishing inclusions on sample C. Notice the brilliant white color of this phase in the freshly polished condition.

Polished and etched several days earlier

OM

200 µm

schreibersite Brown-tarnishing inclusions

Freshly polished, unetched

OM

200 µm

Figure 26 (continued)

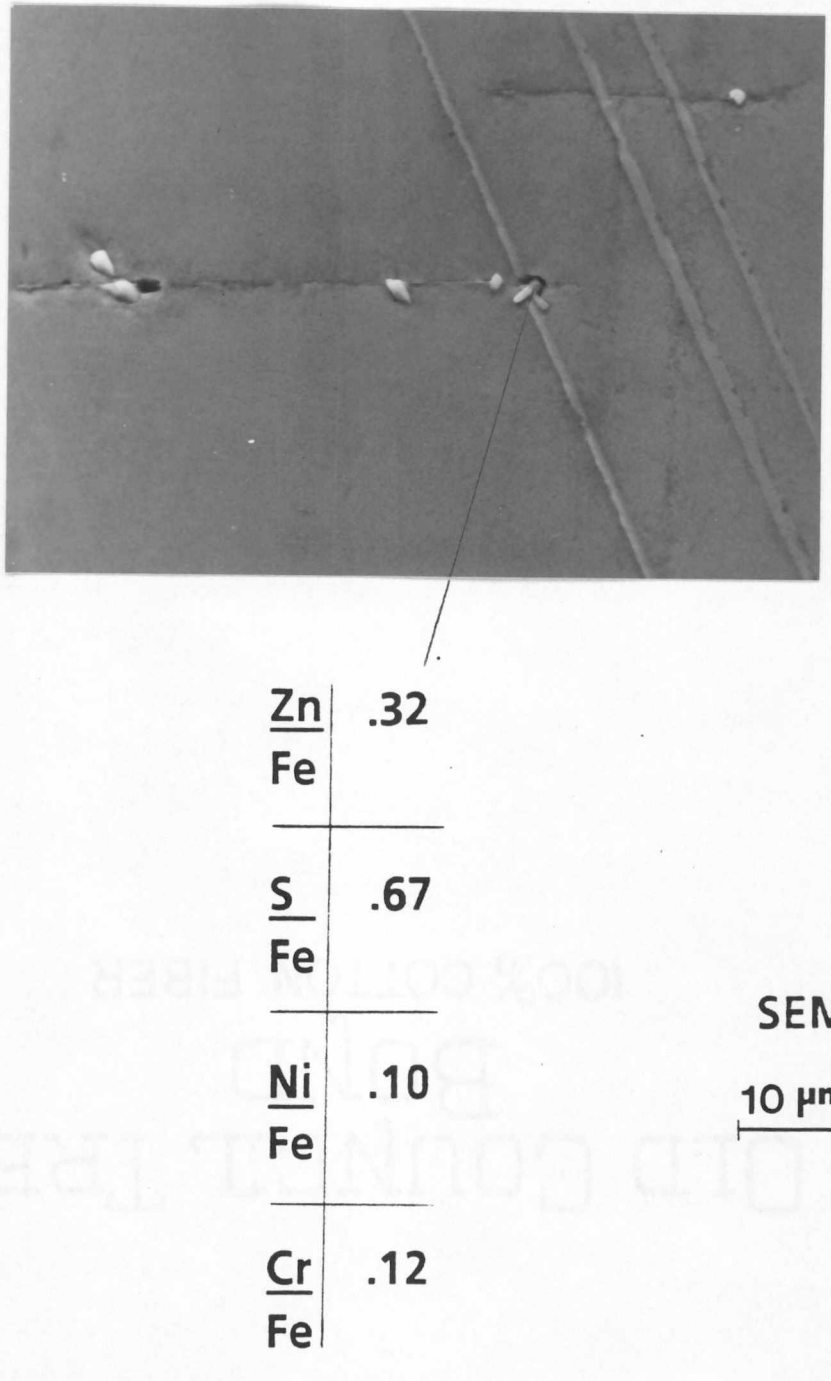

Figure 27. Particle containing Zn and S.

kamacite within plessite. They are highly orientation sensitive: Neumann bands are much denser on some grains in samples C (Figure 28), D', and B (Figure 29) than on other grains in these samples.

Sample A displayed considerably fewer Neumann bands than the other samples (Figure 30). Also on this sample, unlike the others, at low magnifications the Neumann bands frequently appeared to be decorated with fine precipitates (see Figure 30). Investigation under the SEM at higher magnifications, however, seldom revealed any particles along these bands.

In the scanning electron microscope, the Neumann bands sometimes appeared to have a finite width as if a track had been cut in the sample (Figure 31). These wide Neumann bands many times would appear pinched off in places (Figure 32).

E. Plessite

In the Arispe meteorite the retained taenite can break down into plessite with a wide variety of morphologies depending on whether the stringer is near a cohenite nest or not.

1. In Bulk of Meteorite

In the bulk of the meteorite (away from cohenite nests) the plessite is generally in a microwidmanstatten pattern with martensite, or is present as degenerated comb plessite.

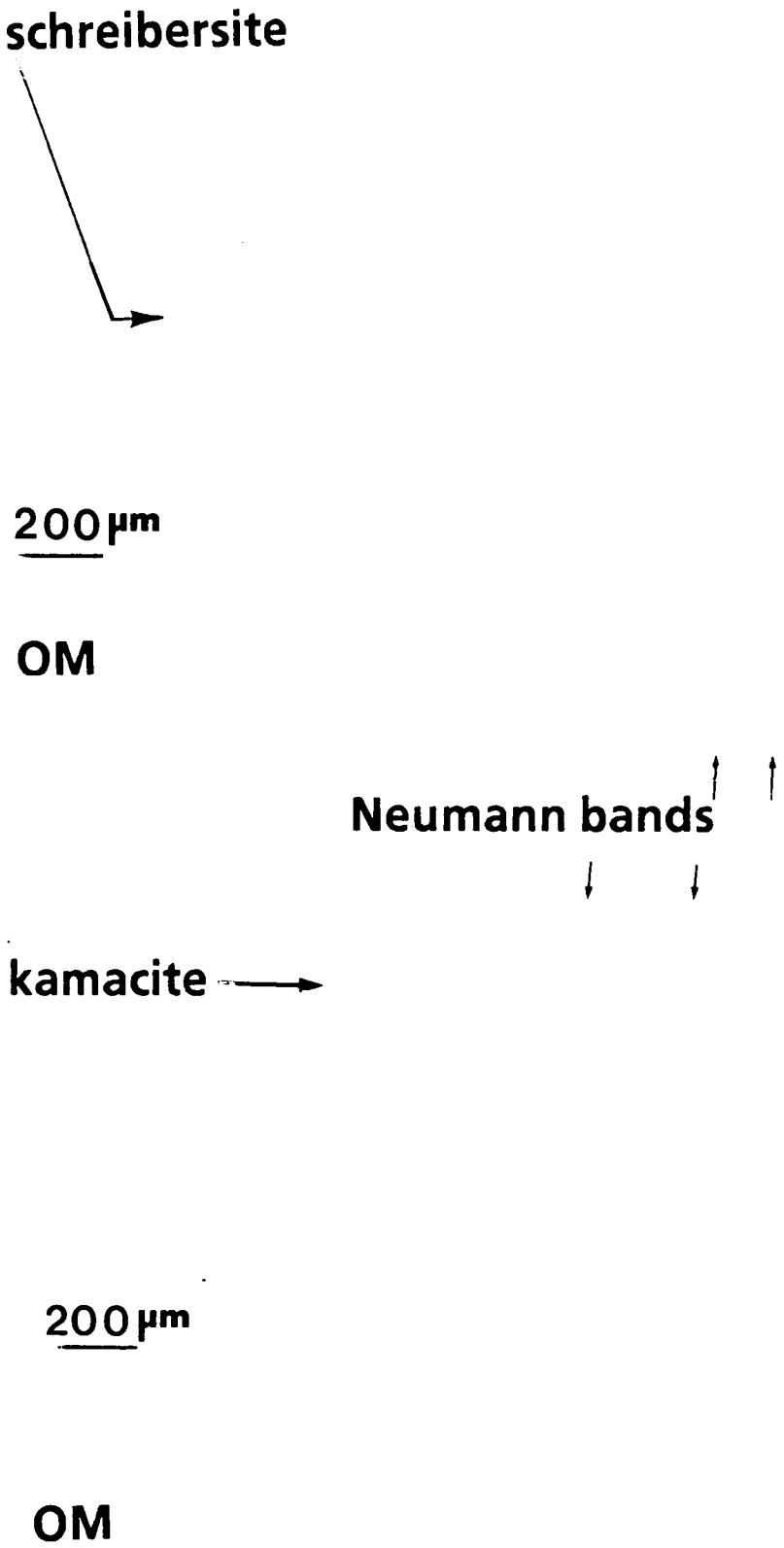

Figure 28. Dense Neumann bands in some grains in sample C.

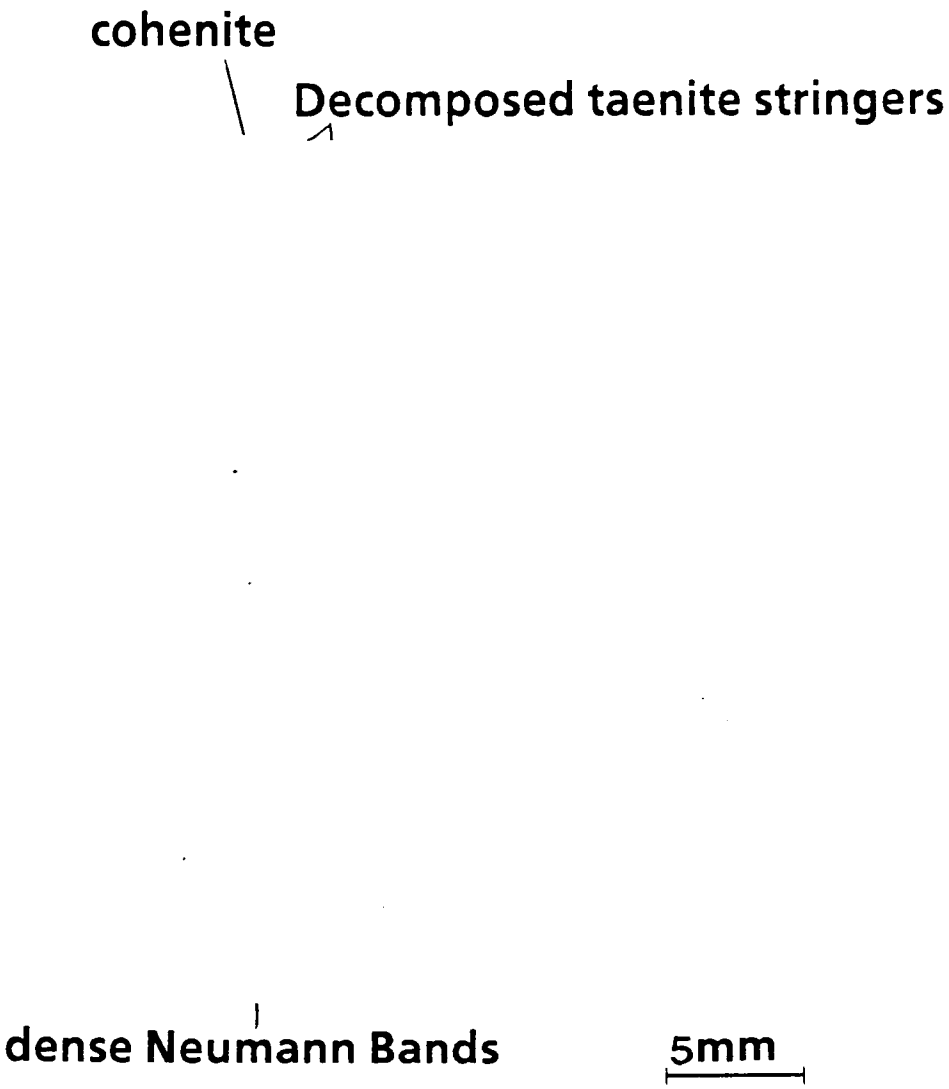

Figure 29. Neumann bands in sample B.

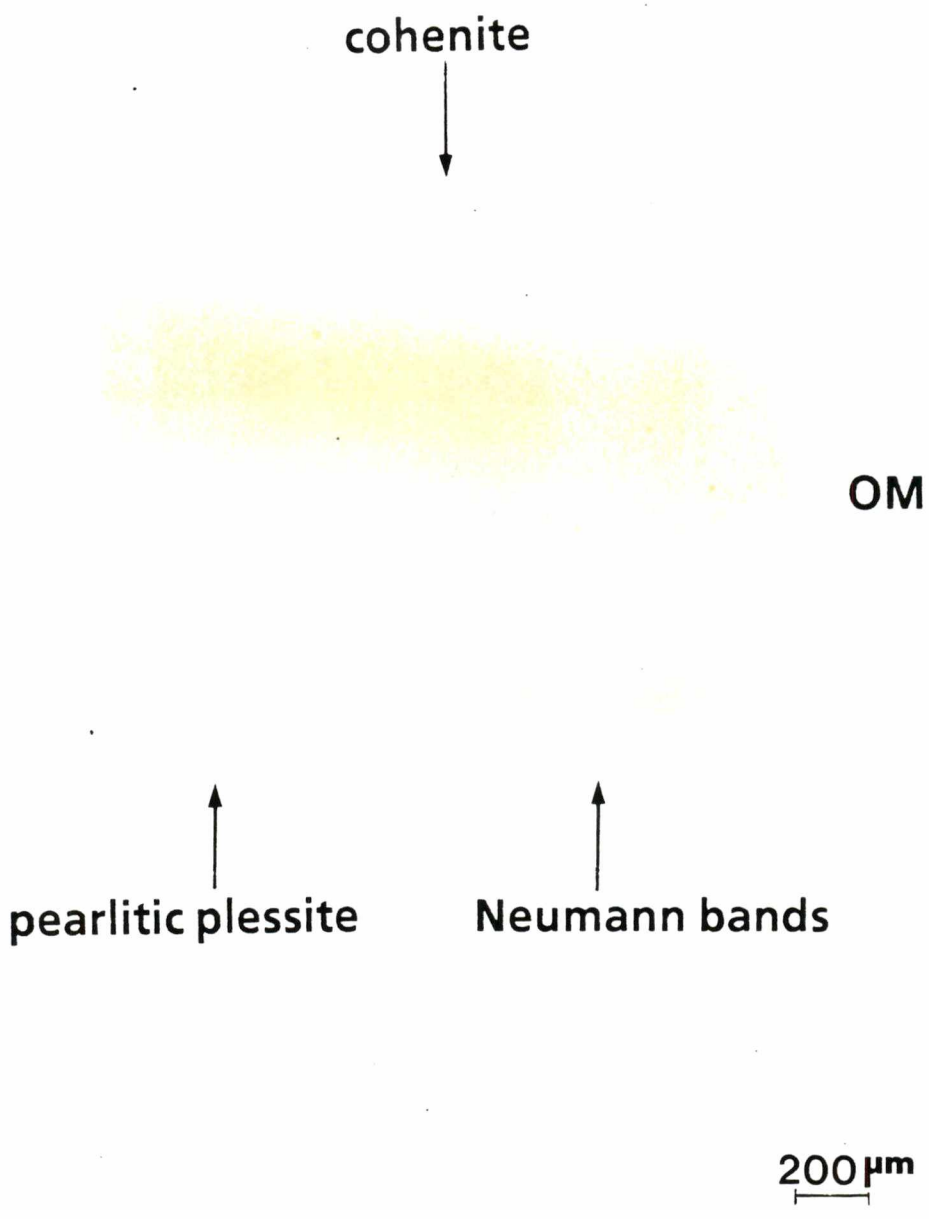

Figure 30. Neumann bands in sample A.

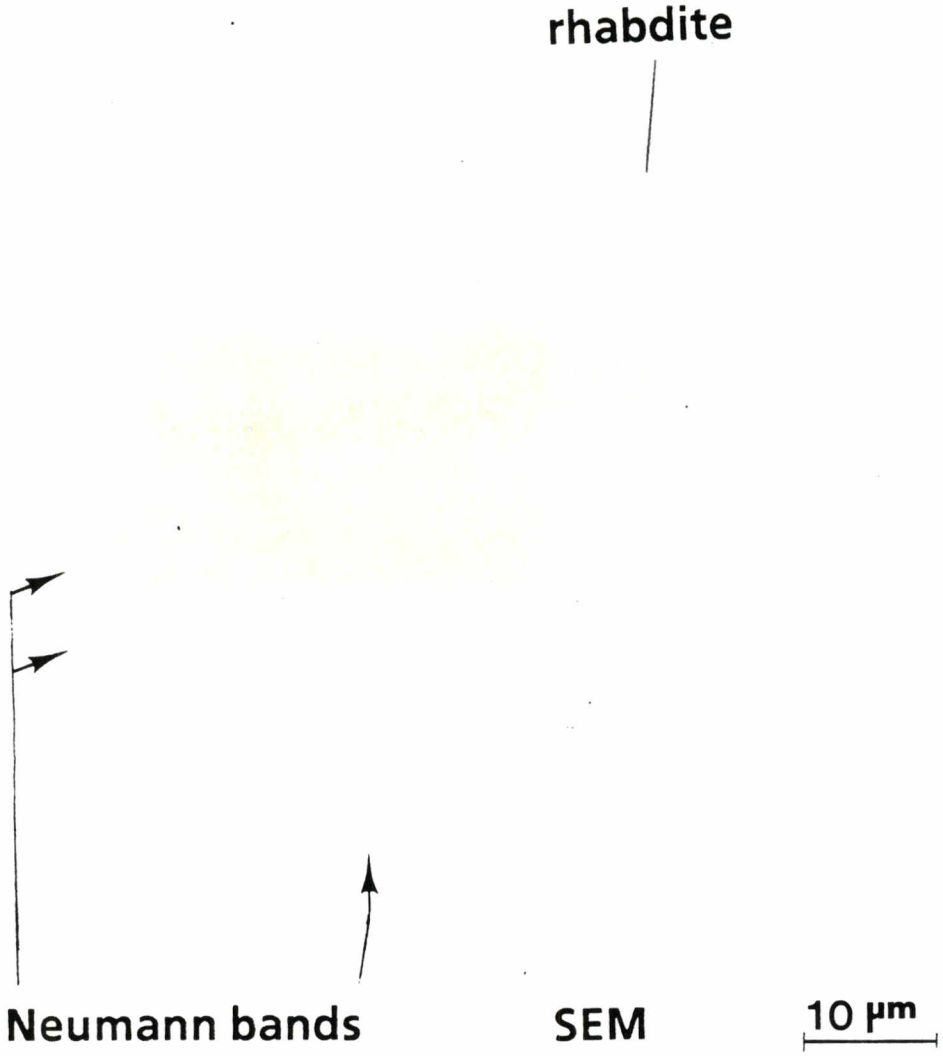

Figure 31. Neumann bands having finite widths. Notice the shattered rhabdite crystal.

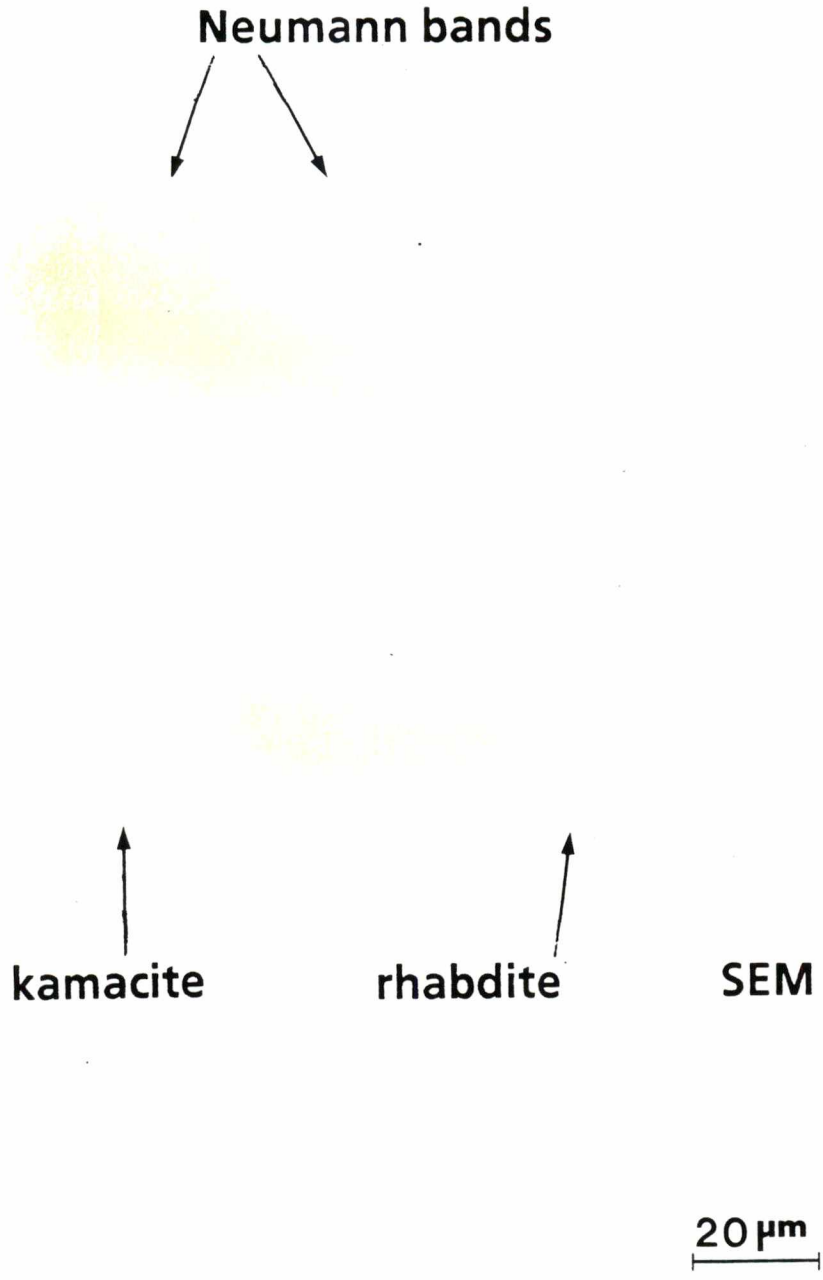

Figure 32. Scanning electron micrograph showing wide Neumann bands.

Microwidmanstatten pattern with martensite. Plessite is commonly found in a microwidmanstatten pattern. In this pattern, the kamacite has precipitated in the center of the stringers along the {111} planes of the retained taenite, just like the kamacite precipitated to produce the macroscopic Widmanstatten pattern. In this case though, the Ni content is higher, so the pattern will not be very coarse or complete (Figure 33). There will usually be a rim of retained taenite around the edge of the stringer, and also generous regions of retained taenite within the stringer. In Figure 34, some of these areas of retained taenite have even broken down into a smaller Widmanstatten pattern. In many cases, however, the thick taenite remaining after the microwidmanstatten pattern has formed breaks down into a fine martensite in the cores (Figure 35). Taenite strips which are thin appear to remain unchanged (Figure 36).

Comb plessite. Sometimes the plessite consists of only apparently undecomposed stringers (Figure 37). Other times, a taenite rim and some martensite along the edges are left (Figure 38). In Figures 37 and 38b, grain boundaries in the kamacite can also be clearly seen. The "cloudy zone" mentioned frequently in the literature is observable in these stringers at higher magnifications after heavy etching (Figure 39).

3D view of stringers—D-D'. In an attempt to more clearly visualize comb plessite, martensitic stringers, and stringers containing microwidmanstatten kamacite, piece D was cut and polished so

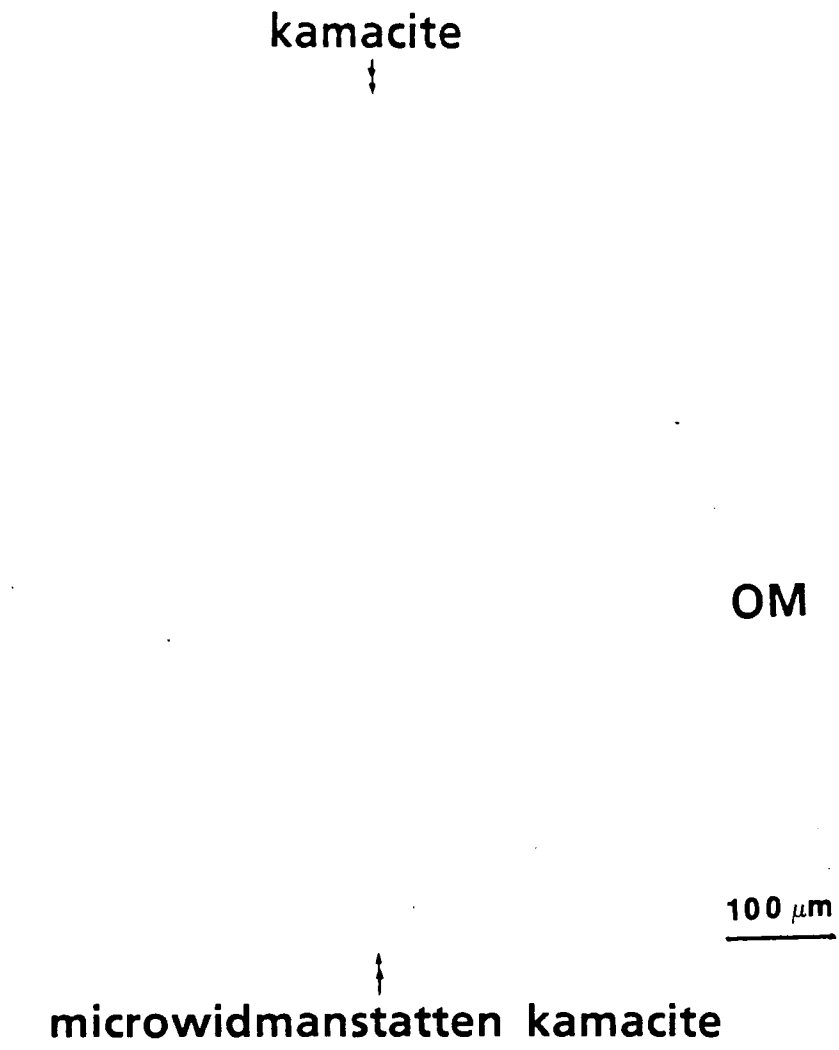

Figure 33. Taenite that has broken down into microwidmanstatten kamacite.

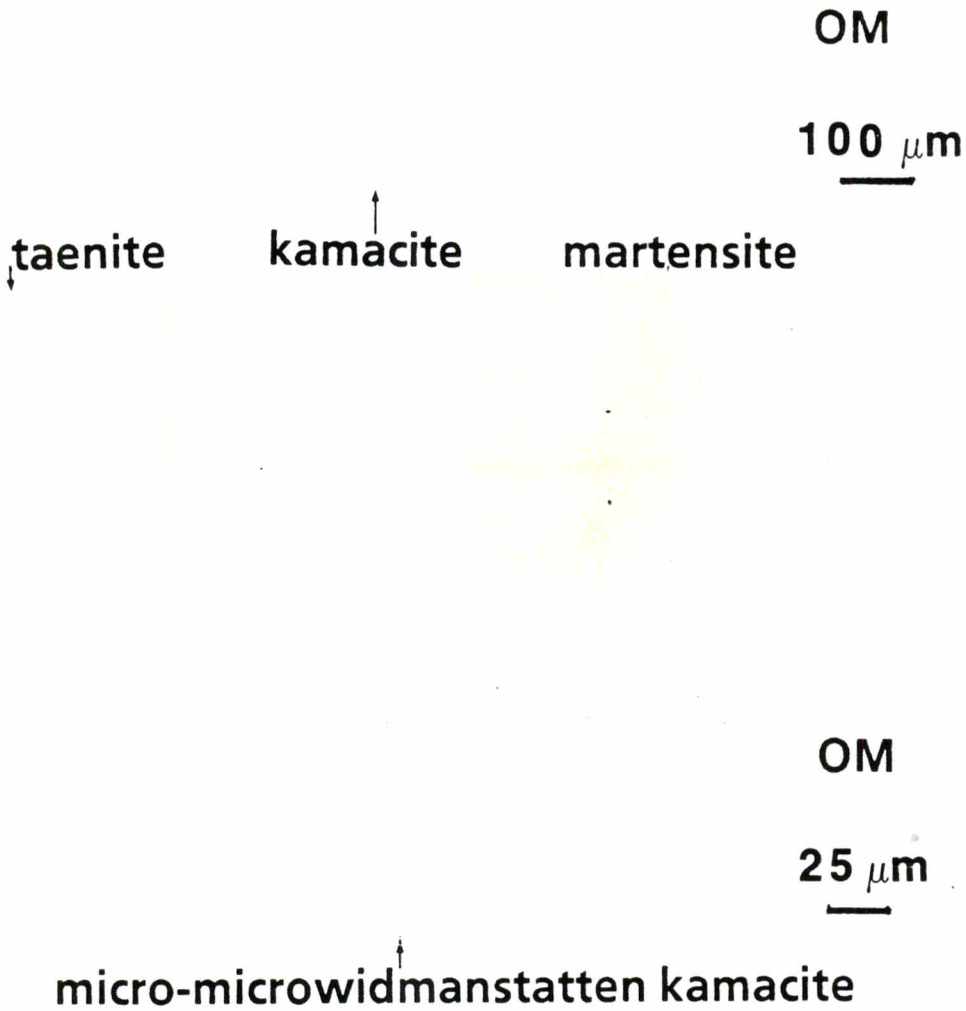

Figure 34. Microwidmanstatten kamacite. Here, the remaining taenite has decomposed to martensite in some areas, and to micro-microwidmanstatten kamacite in others.

Figure 35. Microwidmanstatten kamacite where the remaining taenite has decomposed into fine plate martensite.

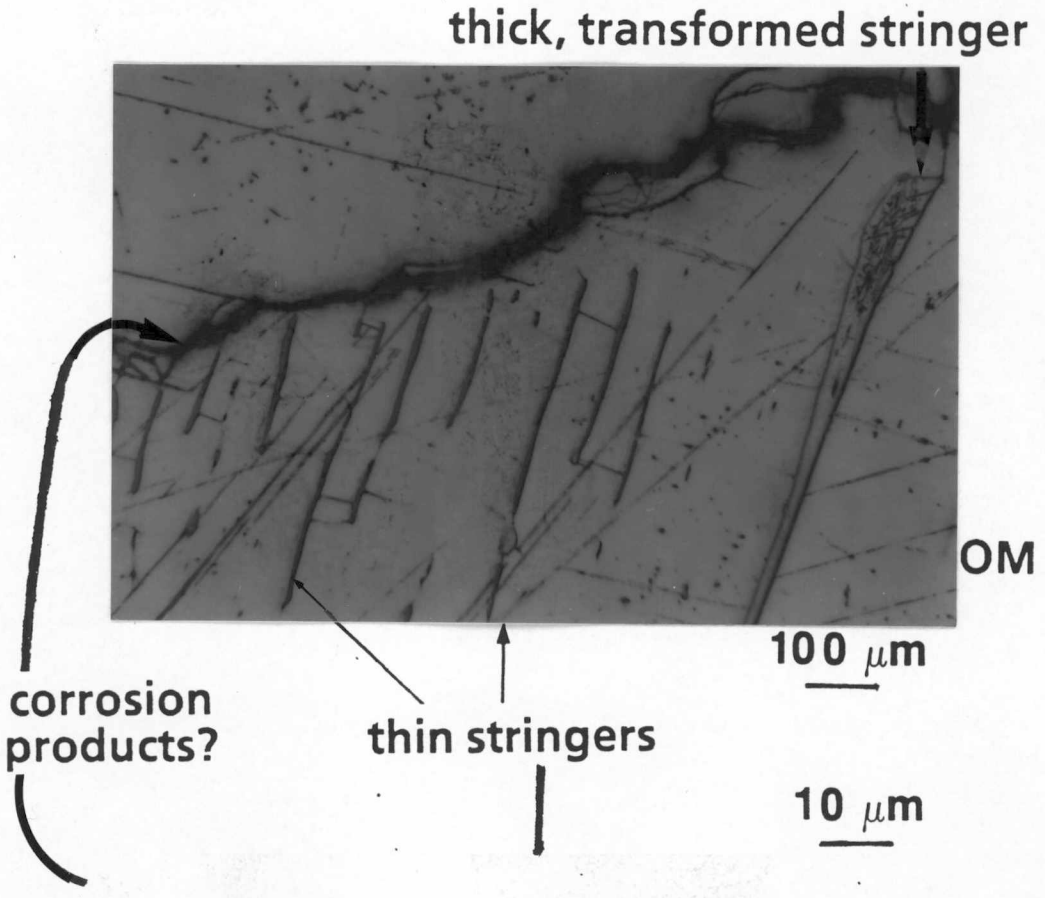

Figure 36. Thin stringers of taenite do not visibly transform.

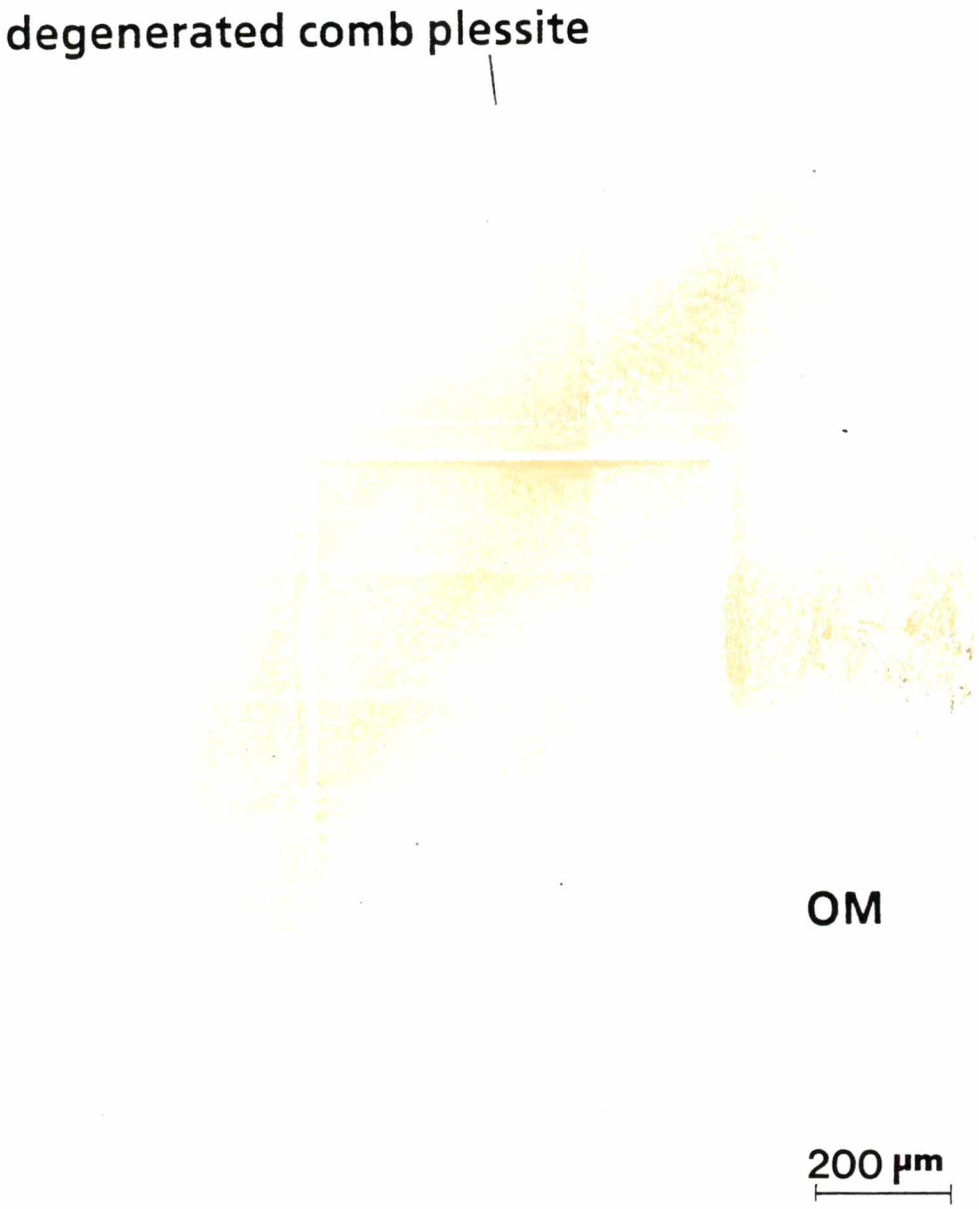

Figure 37. "Degenerated comb plessite": only unconnected taenite stringers remain here.

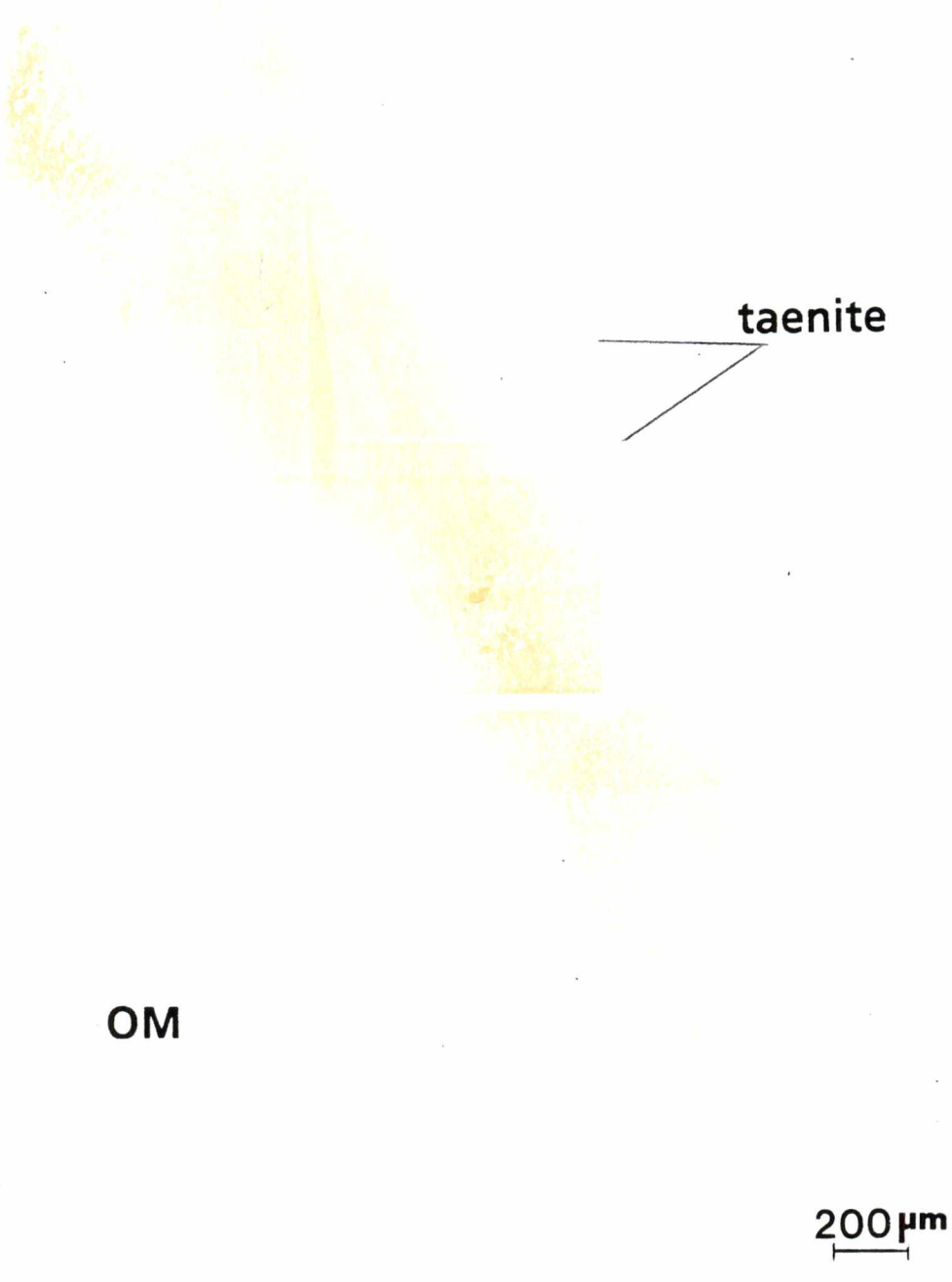

Figure 38. (a) Comb plessite in which a rim of taenite surrounds the plessite; (b) higher magnification view of this area. Notice the boundaries in the kamacite (arrows).

Figure 38 (continued)

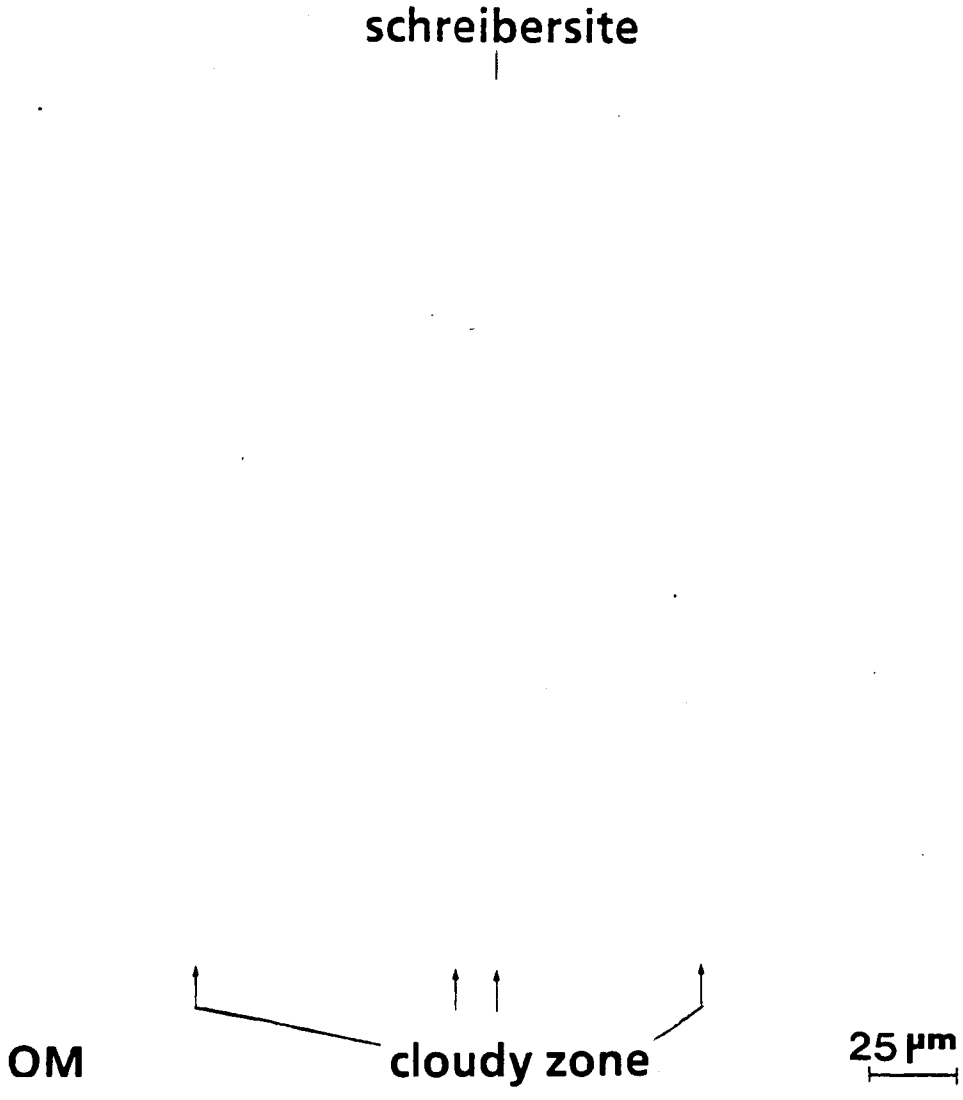

Figure 39. Thin taenite strips in comb plessite showing the "cloudy zone."

that the same plessite stringers could be viewed on two perpendicular faces.

From this sample, the plessite appears to be somewhat weblike (Figure 40), with stringers running through the sample as plates of varying thickness and interconnecting at various points on and below the surface.

Figure 41 shows a different stringer with a schreibersite inclusion on one face.

Neumann bands can also be seen (Figure 42) along the intersection of the two perpendicular faces; the Neumann bands are plate-like, cutting both faces of the sample. They are not parallel to the stringers.

2. Near Cohenite Nests

Near the cohenite nests the plessite is many times pearlitic, but can also be spheroidal or martensitic. These morphologies resemble the pearlite, spheroidite, plate martensite, and bainite seen in steels, so I will refer to them by these names.

Pearlite and spheroidite. Pearlite is found in over half the plessite stringers that run through the cohenite nests. The taenite pearlite lamellae are generally continuous, and there is usually a rim of taenite, continuous with the taenite lamellae, along the edges of the stringer (Figure 43).

The pearlite grows in well-defined colonies at times (Figures 44 and 45), although these colonies are generally connected

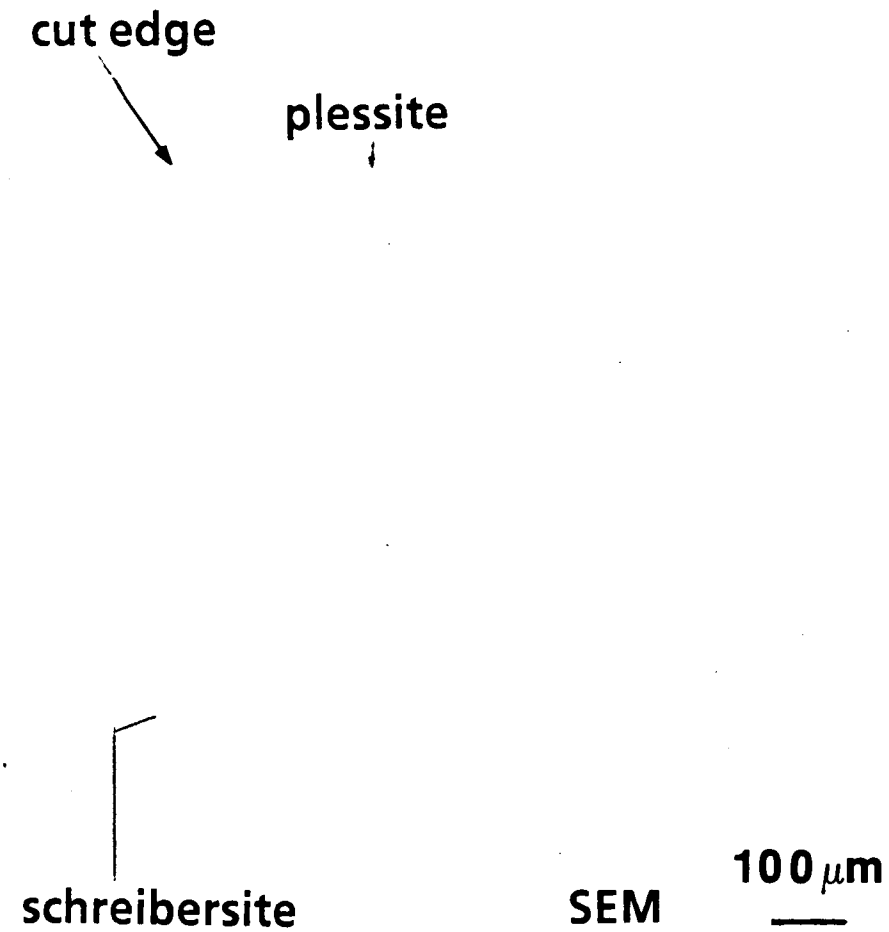

Figure 40. Scanning electron micrograph of plessite on two perpendicular faces.

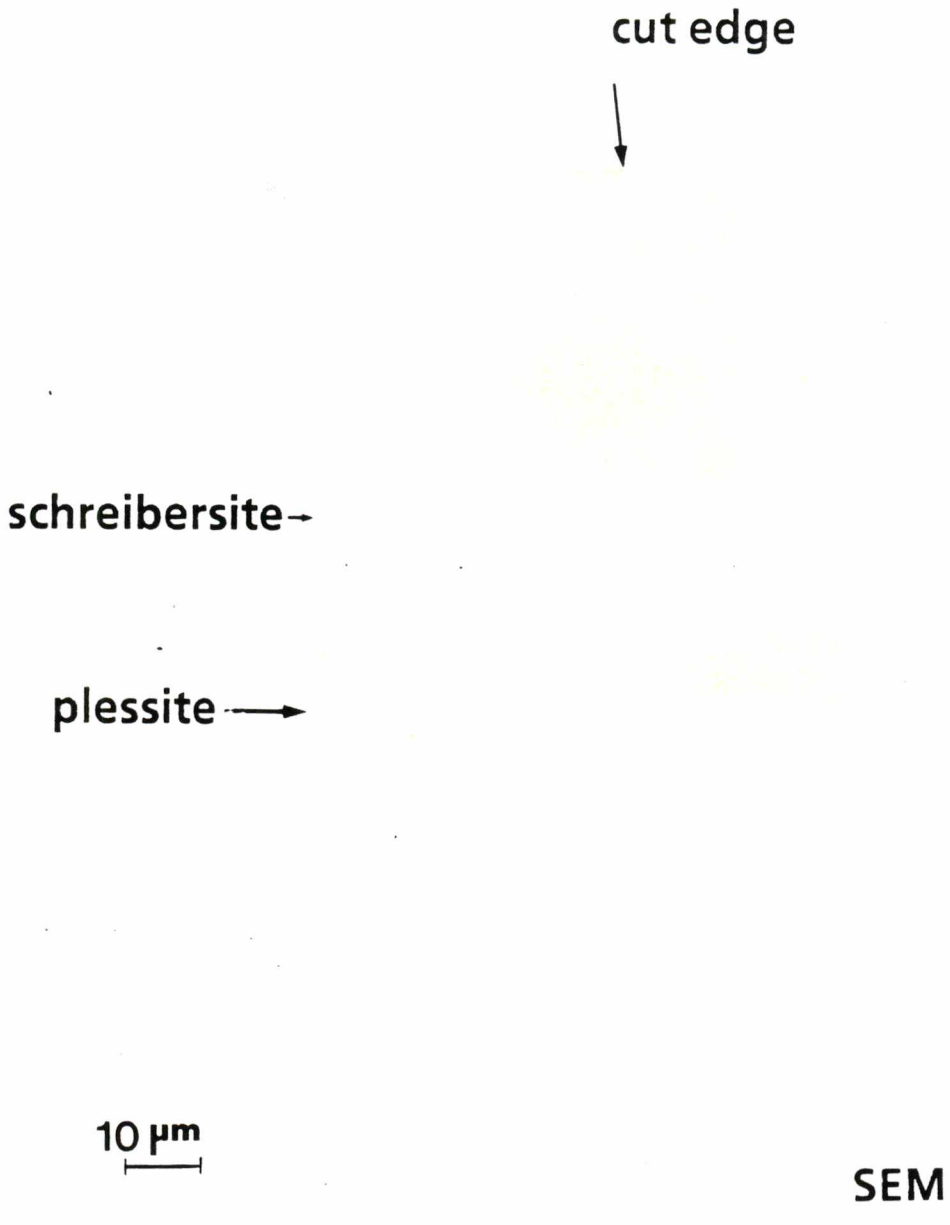

Figure 41. Schreibersite running alongside a plessite stringer. The schreibersite grain does not surface on the other face of the sample.

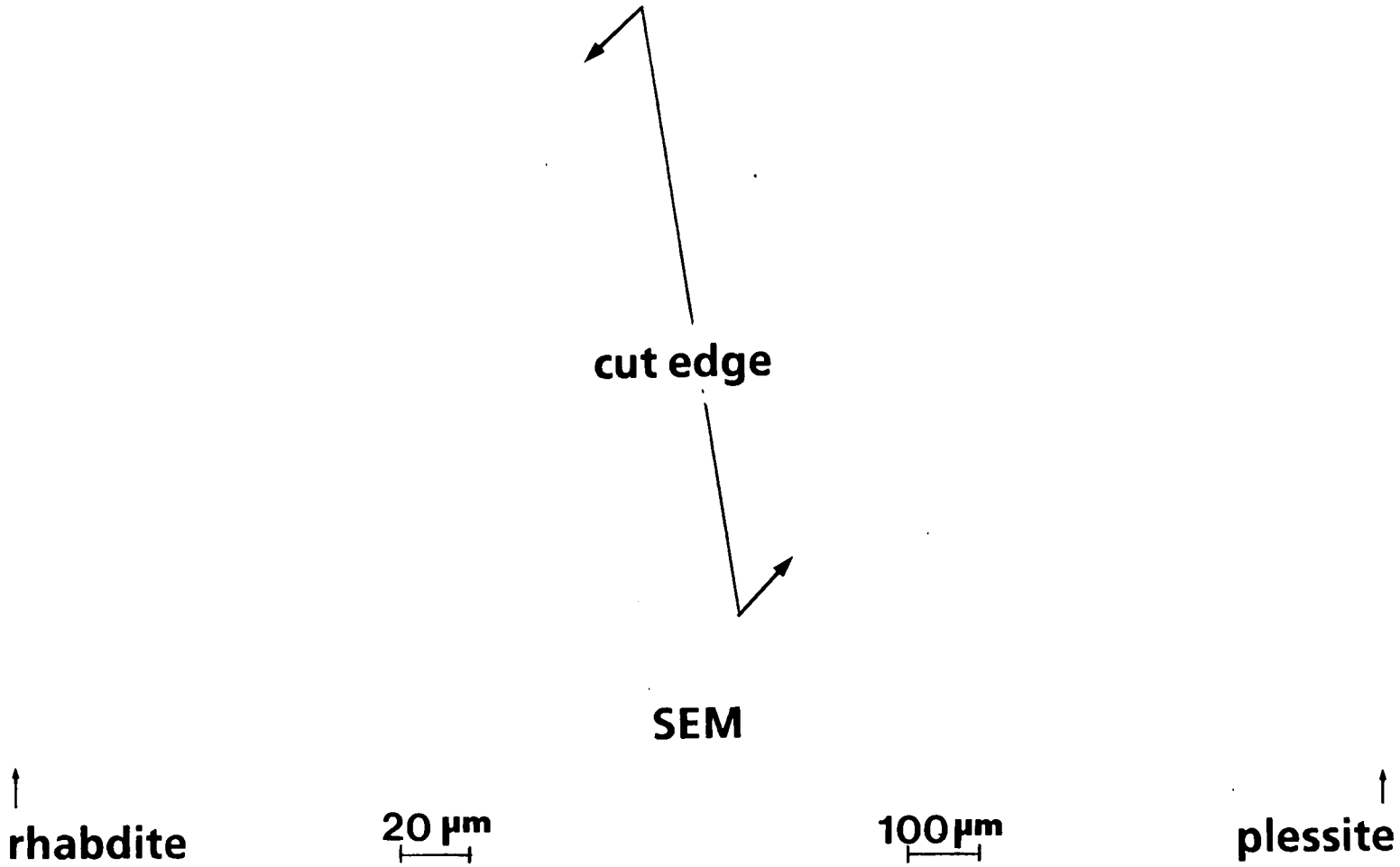

Figure 42. Neumann bands on two adjacent faces of sample D.

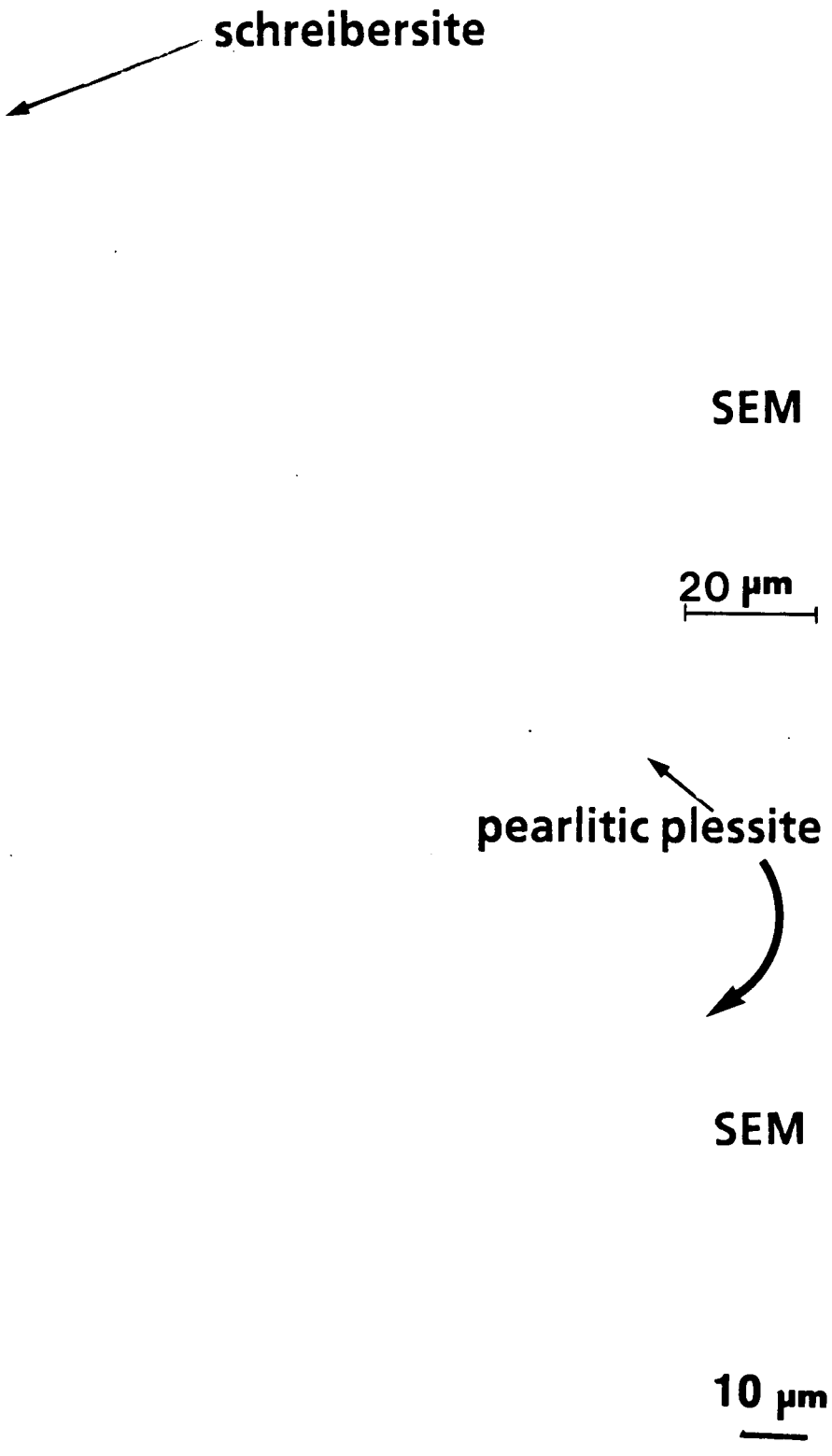

Figure 43. Scanning electron micrographs of pearlitic plessite.

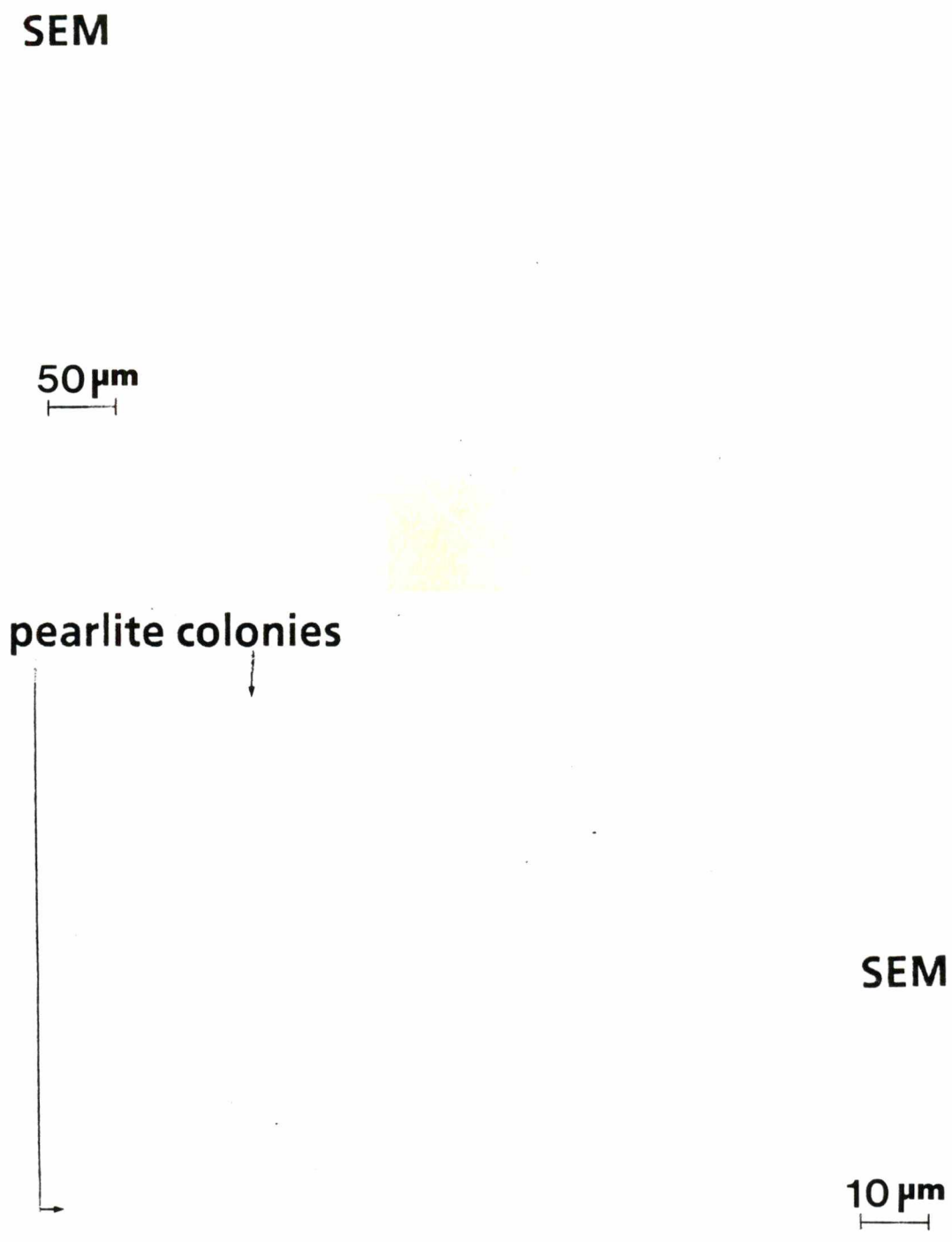

Figure 44. Pearlitic plessite growing in well-defined colonies on sample B. Apparently, some of the pearlite here has begun to spheroidize.

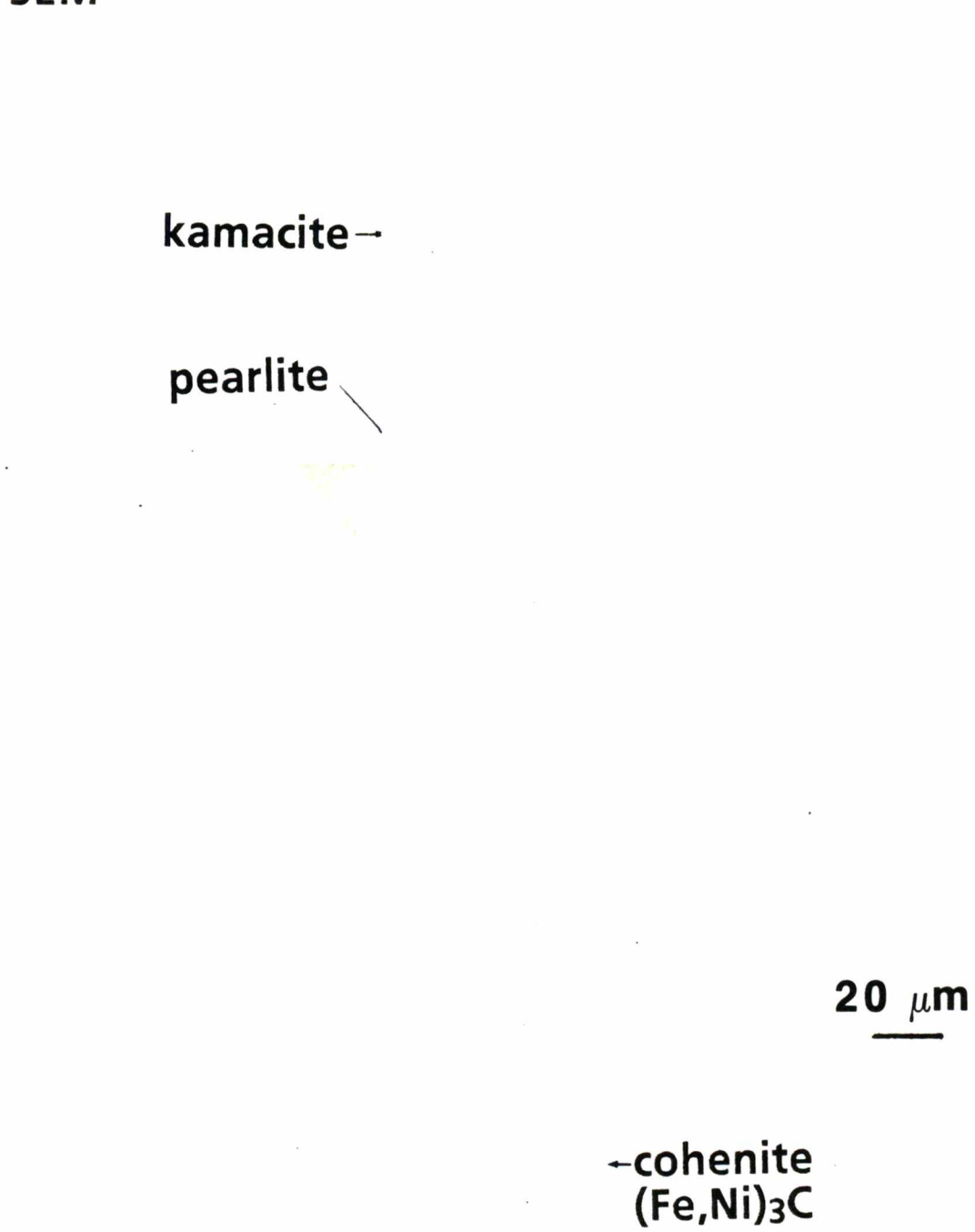

Figure 45. Pearlitic plessite displaying different orientations.

by a few taenite lamellae that loop from one colony to the next. From the varied orientations of these colonies, it appears that the pearlite nucleated in several locations simultaneously, but maintained identical crystallographic orientations (the crystallographic orientation must be very close to allow one taenite lamella to be part of two different colonies). There do not appear to be any boundaries etched out in the kamacite between these colonies.

Pearlite can make up the entire stringer (Figure 46), or can coexist with other morphologies, such as spheroidite (Figure 47).

Spheroidite is fairly common near the cohenite nests. It is obvious that the taenite in the spheroidite is spherical as opposed to rod-like for three reasons. First, cutting rods at oblique angles will produce ellipses of taenite, but we have only seen circles. Second, the circles are of various sizes, which is what would be obtained if randomly located spheres were cut. Third, the pearlite generally has very periodic, even spacing, so if these were rods and were cut to make circles, the circles would be evenly spaced and in straight rows, not randomly scattered as we see.

In the pieces observed in this study, the spheroidite always occurred with pearlite in the same stringer. It can occur as very large sized circles (Figures 48 and 49), or as relatively small circles of taenite that have diameters roughly the same as the thickness of nearby pearlite lamellae (Figures 50 and 51). When the taenite circles are extremely large, they may show cloudy zones after very heavy etching just as the taenite stringers do (Figure 52).

OM

200 µm

Neumann band

OM

25 µm

pearlitic plessite

Figure 46. A stringer on sample A composed entirely of pearlitic plessite. Notice the Neumann band displaced across the plessite.

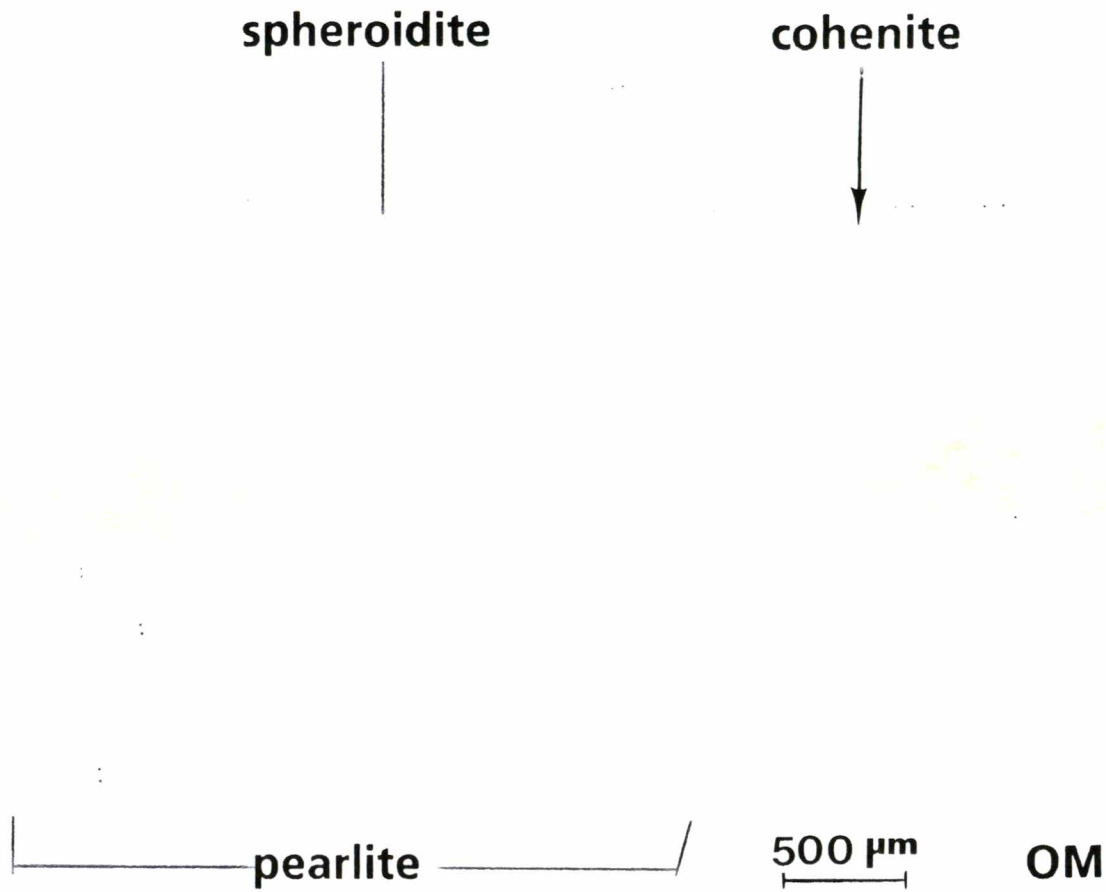

Figure 47. A stringer on sample A displaying coexisting pearlite and spheroidite.

Figure 47 (continued)

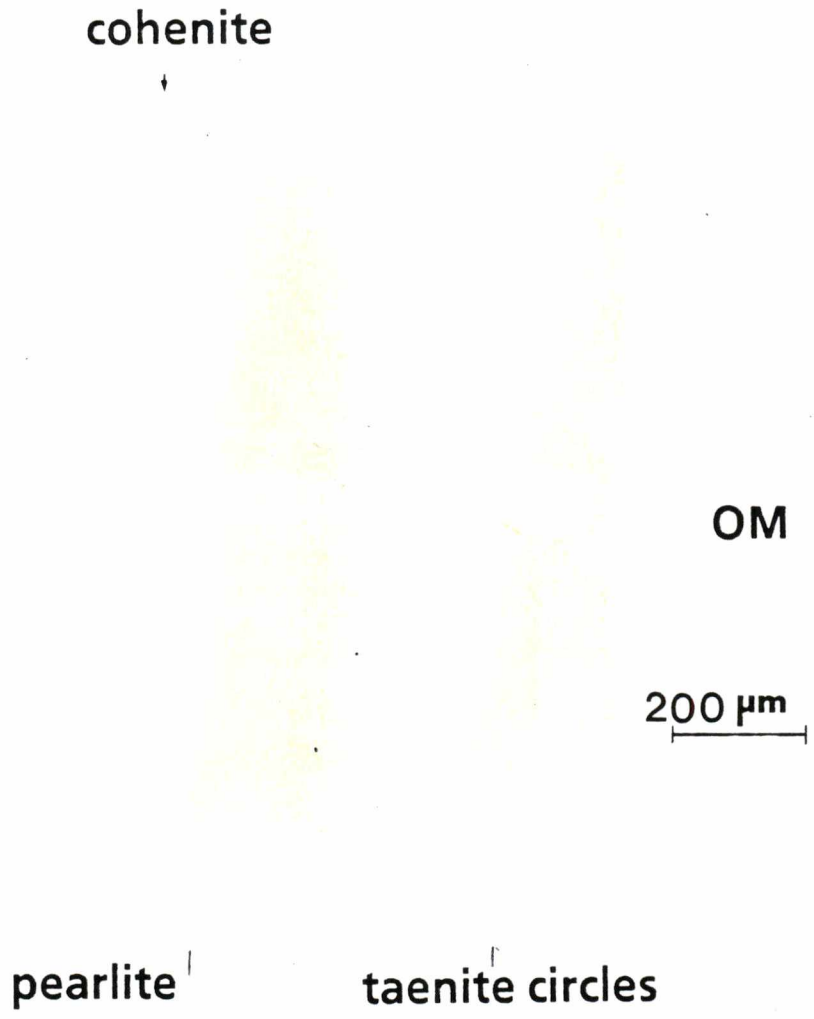

Figure 48. A stringer in sample A showing large circles of taenite.

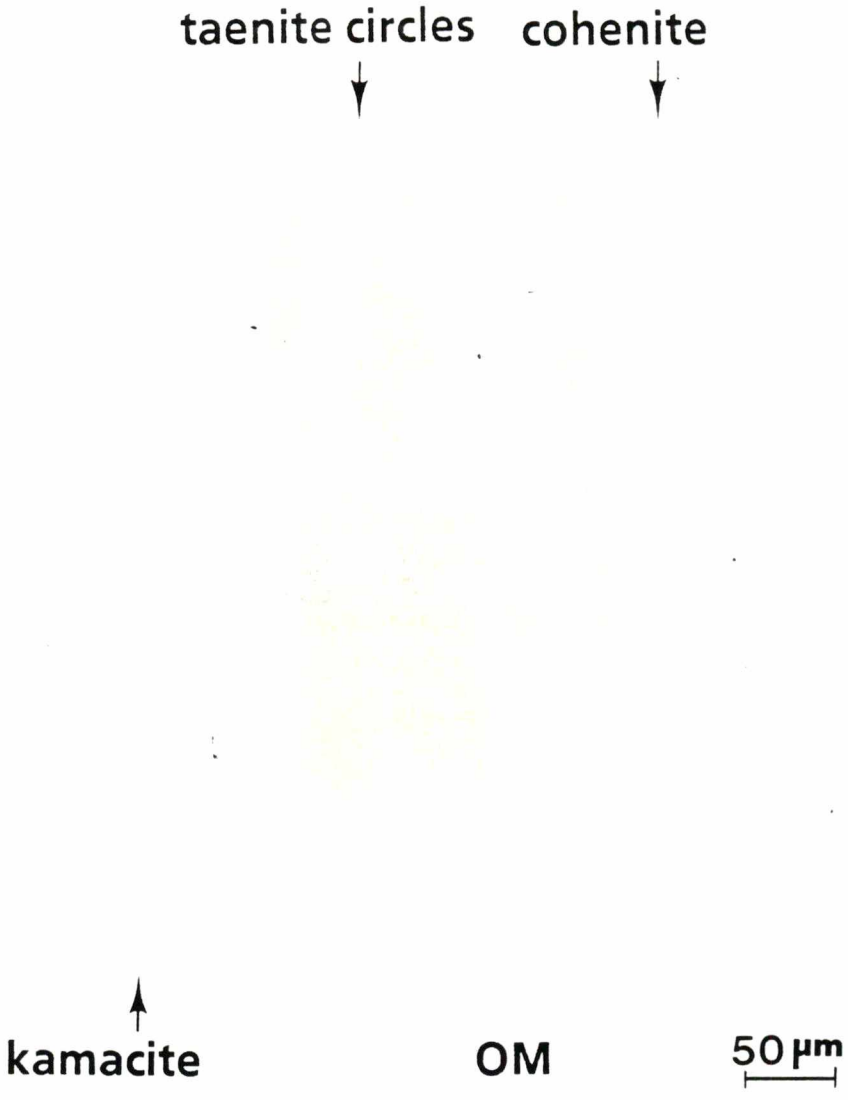

Figure 49. Part of a stringer in sample B showing large circles of taenite.

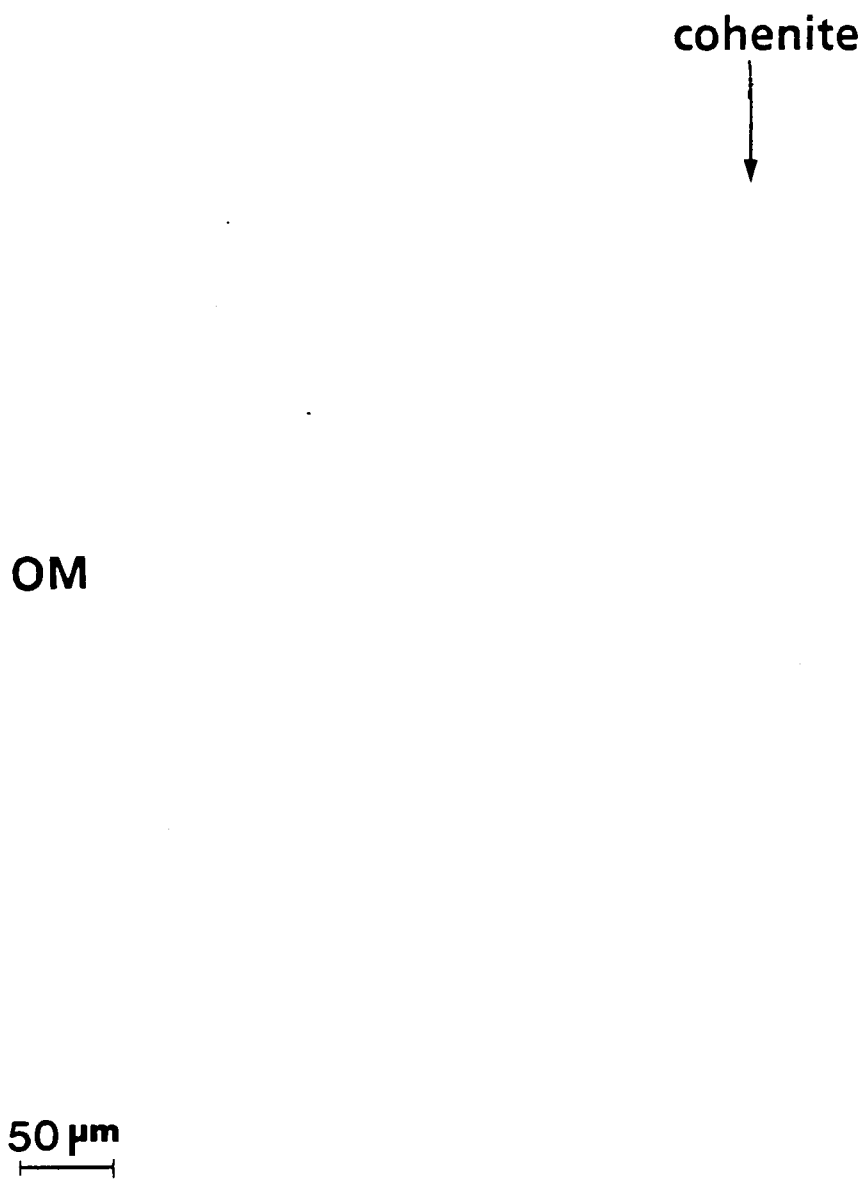

Figure 50. Circles and lamellae of taenite on sample B.

Figure 51. Very small taenite particles mixed with pearlite in sample B.

Figure 51 (continued)

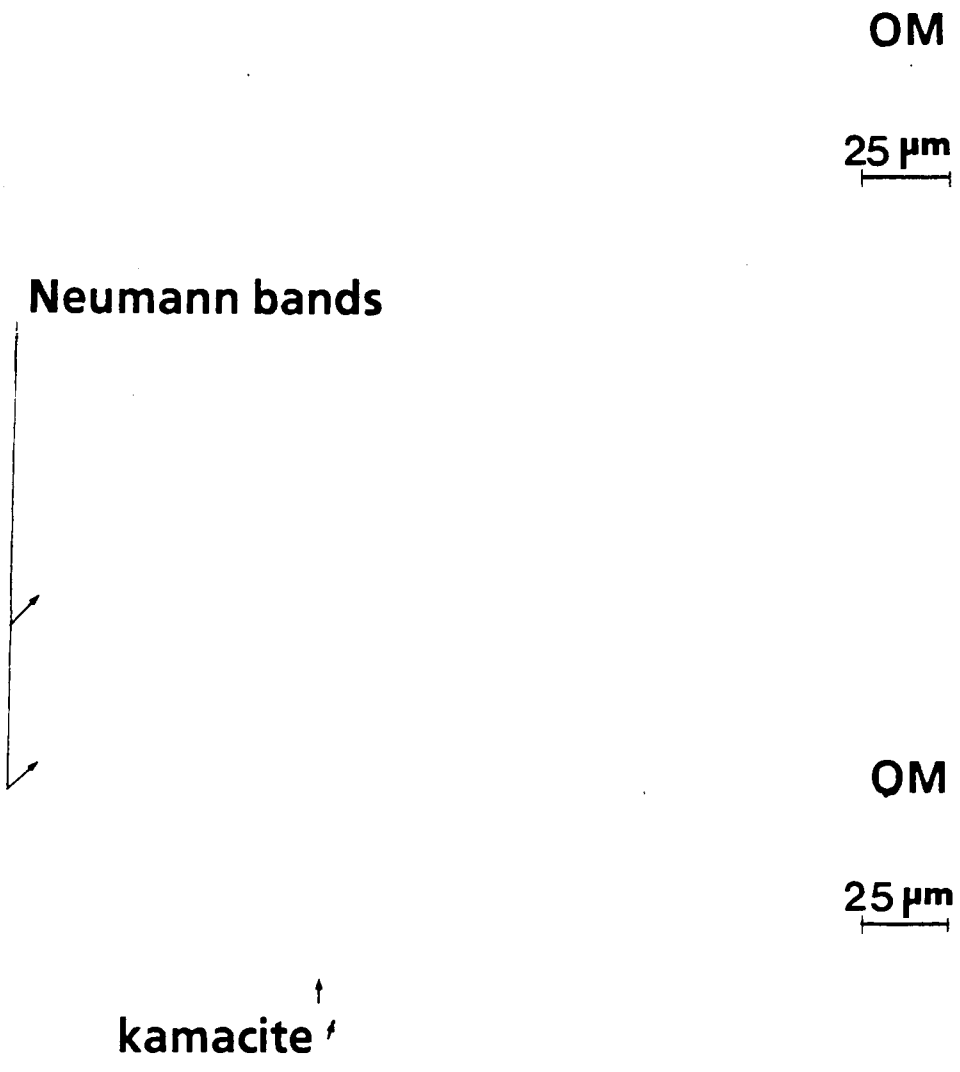

Figure 52. Taenite circles showing cloudy etching.

Martensite. Martensite is another common decomposition product. It occurs as either very coarse plates in the center of a stringer (Figure 53), or as very fine plates interspersed with kamacite (Figure 54). Where kamacite plates are mixed with martensite, it is obvious that the kamacite formed before the martensite, as the martensite has filled in the spaces between kamacite plates (Figure 55). The martensite plates never reach the edges of the stringers, but remain in the cores (Figure 56).

Many times there is a layer of coarse martensite surrounding fine martensite (Figure 57), or the fine martensite will give way to coarse martensite as the stringer becomes thin (see Figure 54).

Taenite inclusions are frequently seen in cohenite. Generally these inclusions are too small to decompose, but Figure 58 shows a taenite inclusion that formed a few needles of martensite. (Notice this inclusion has also been cracked, which is unusual to see in a ductile metallic phase.)

Combinations of martensite and pearlite. Martensite and pearlite can coexist in the same stringer. Pearlite will be in one end, generally the end toward the core of the cohenite nest, and will suddenly give way to martensite toward the middle of the stringer (Figures 59 and 60).

Martensite can also occur locally in stringers where the outer layer of taenite has remained unusually thick (Figure 61).

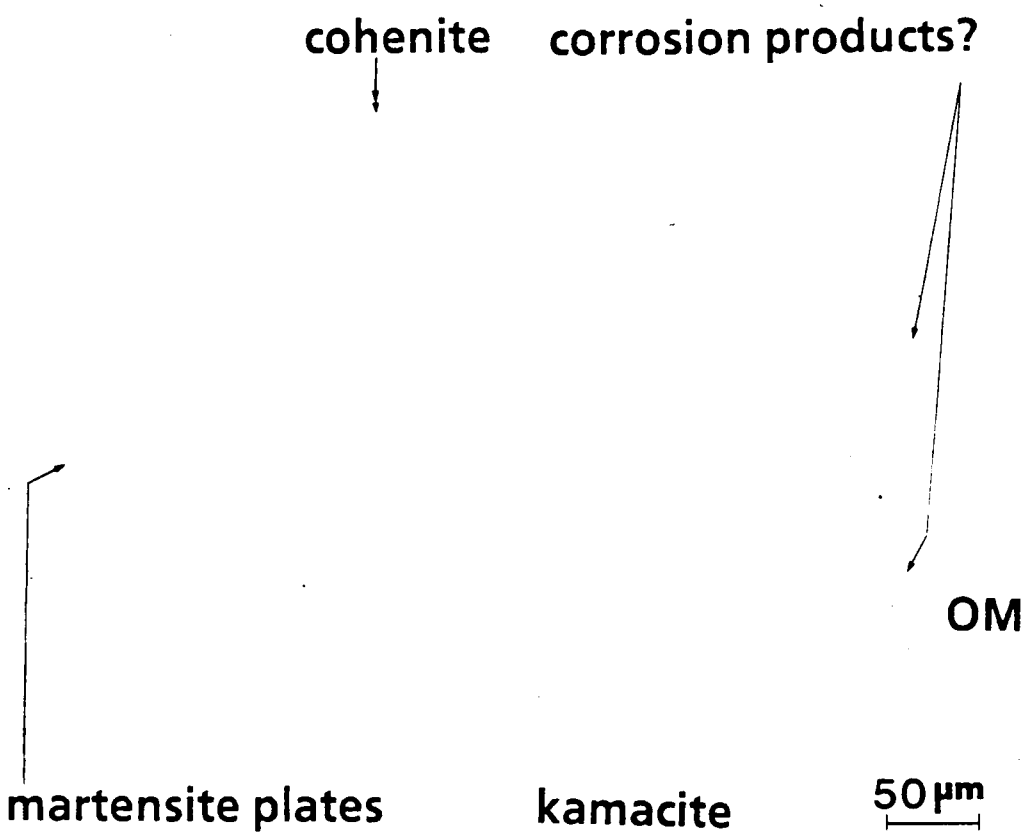

Figure 53. Coarse martensite plates in a stringer in sample A.

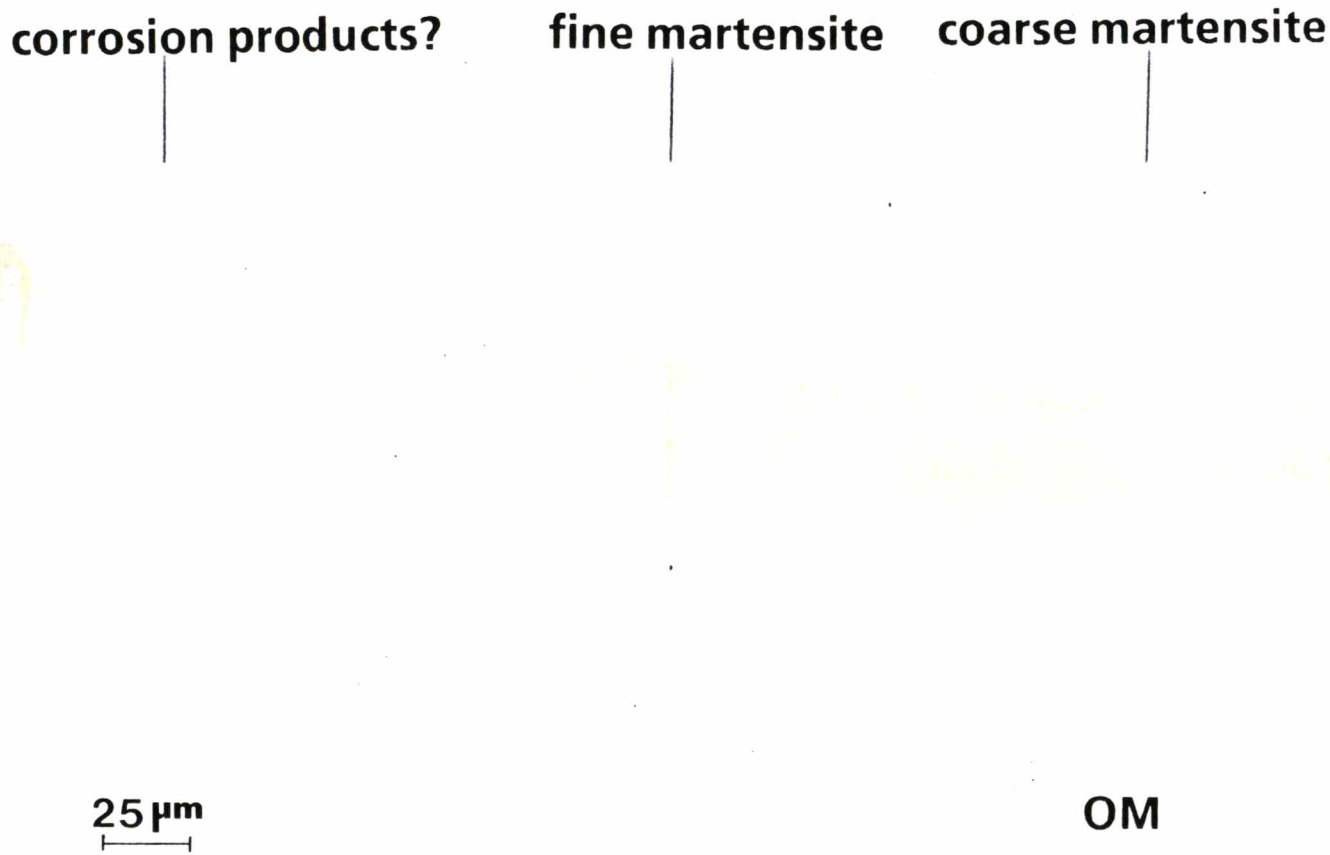

Figure 54. Fine martensite that has formed between platelets of kamacite in a stringer in sample A.

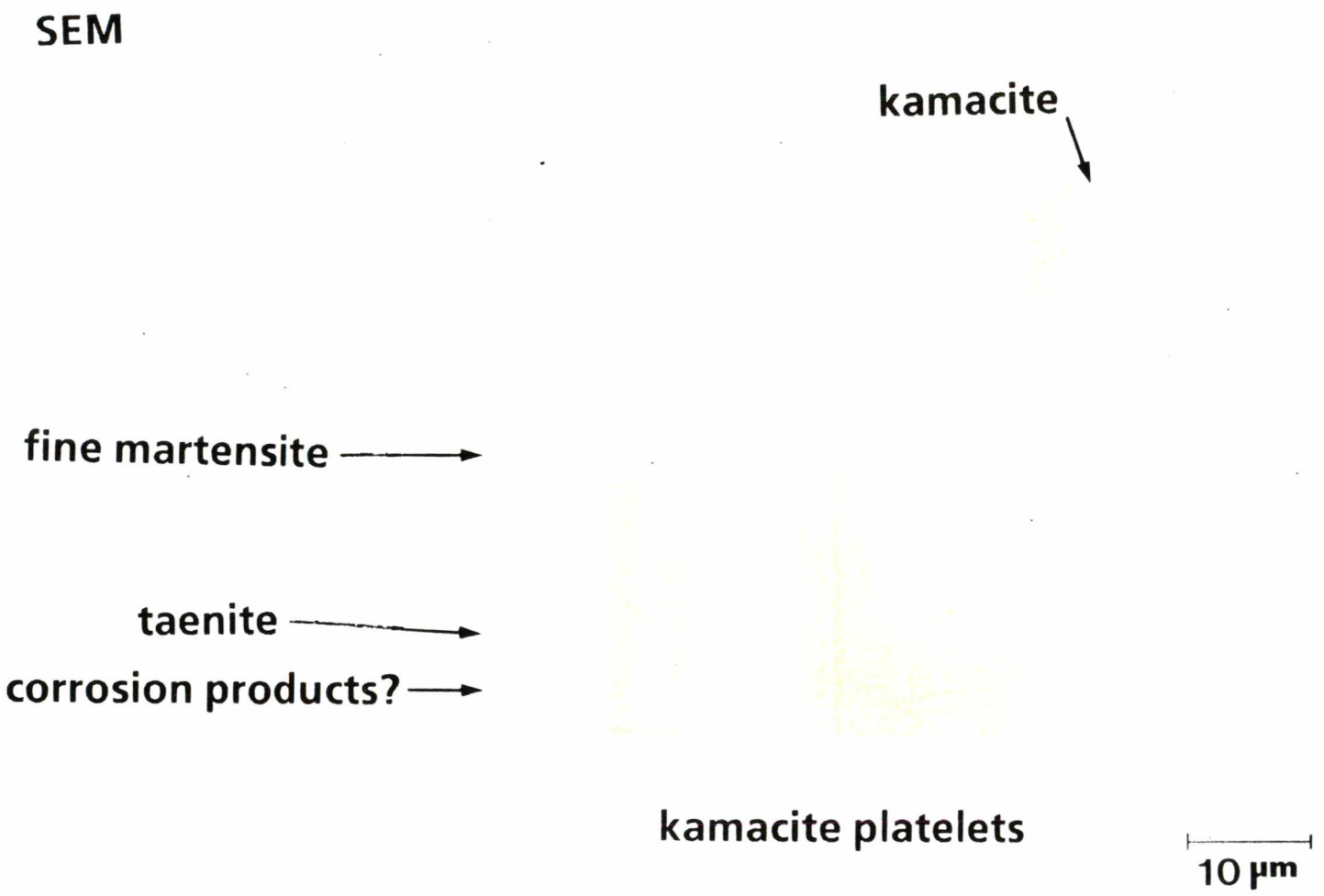

Figure 54 (continued)

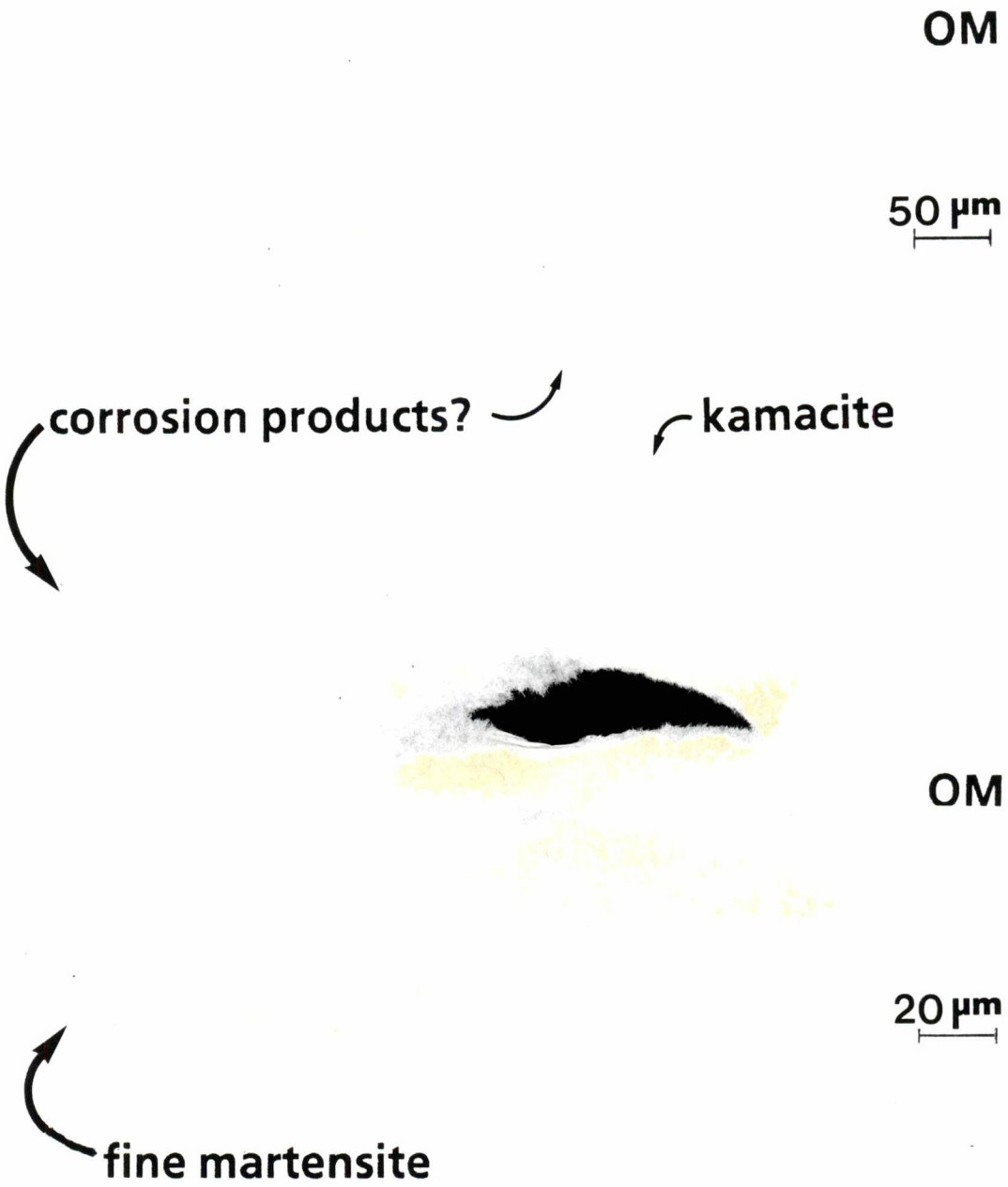

Figure 55. Fine martensite needles that have formed around kamacite grains. (This stringer is the same as the one shown in Figure 54, but the photographs in Figure 54 were taken after repolishing the sample several times and thus removing the surface layer of the metal.)

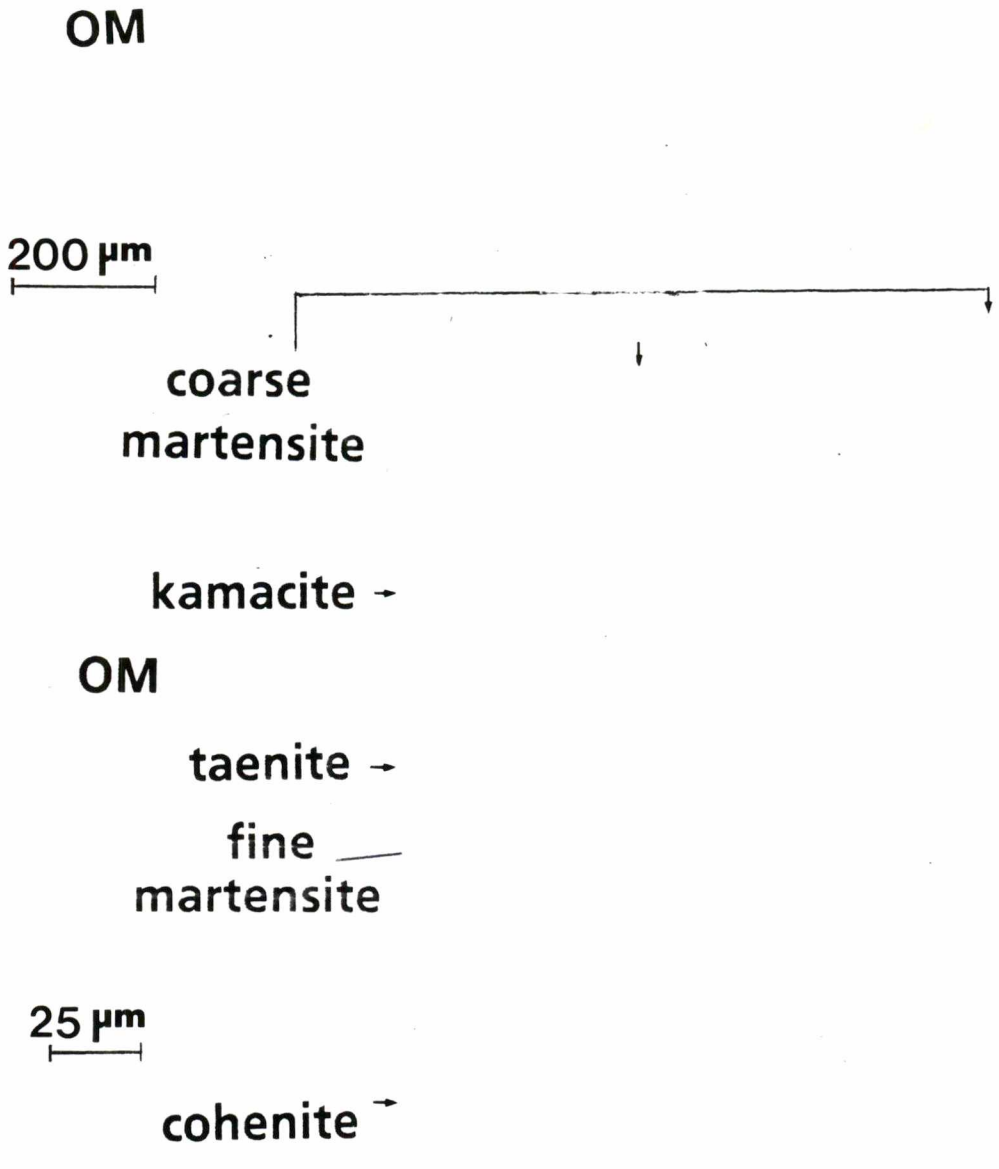

Figure 56. A martensitic region in sample B.

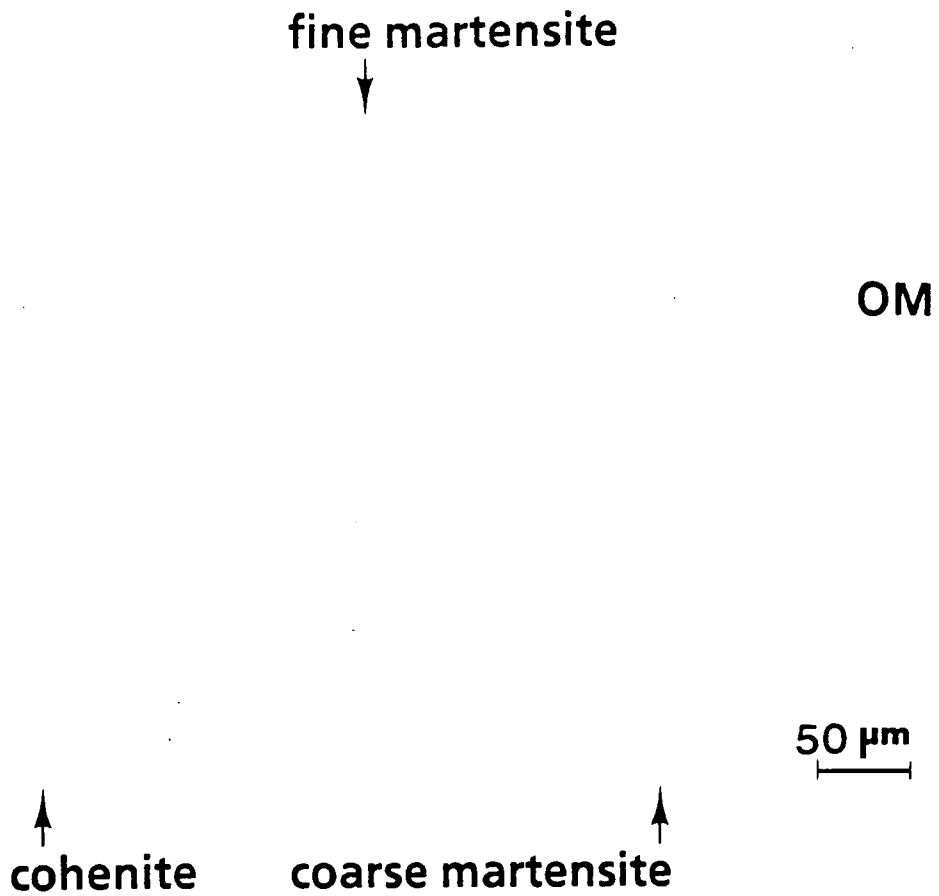

Figure 57. Coarse martensite surrounding fine martensite.

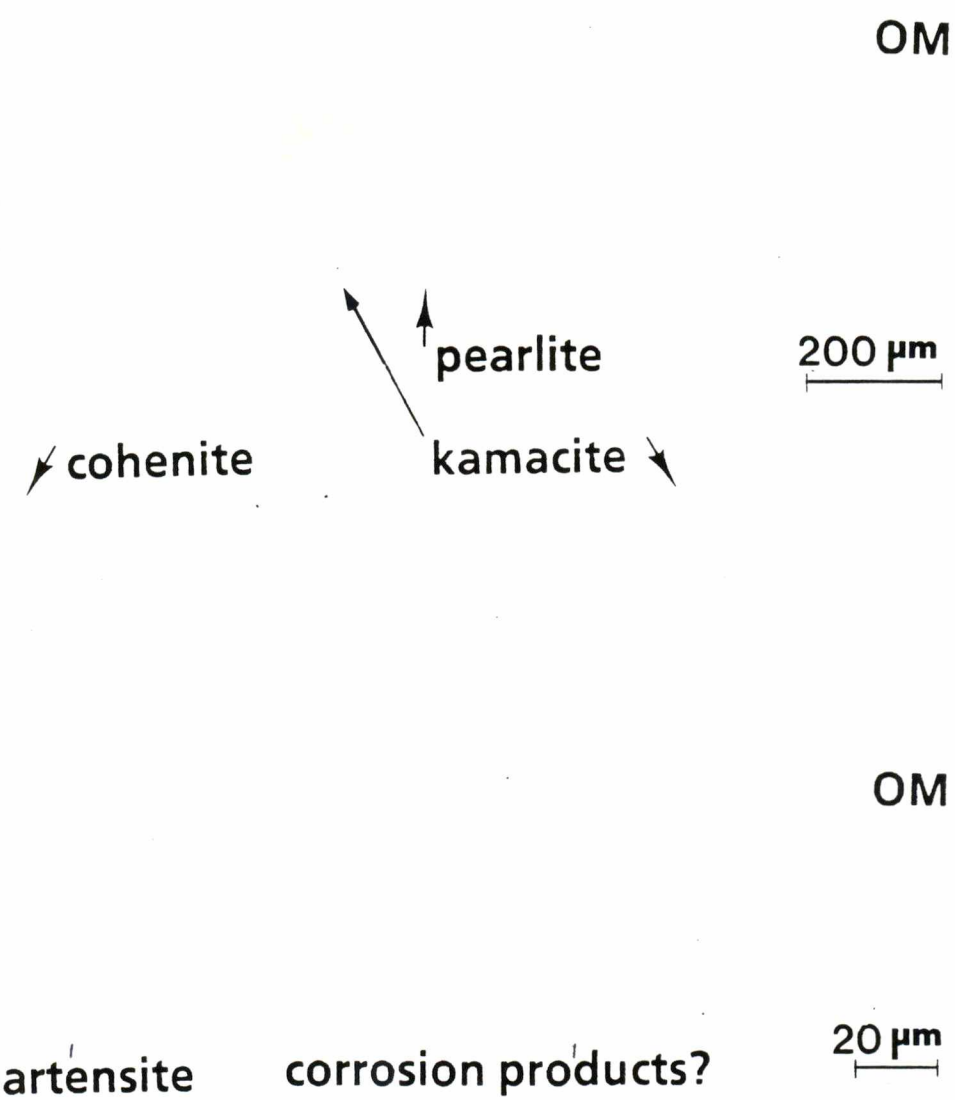

Figure 58. Cracked taenite inclusion in cohenite that has partially decomposed to martensite.

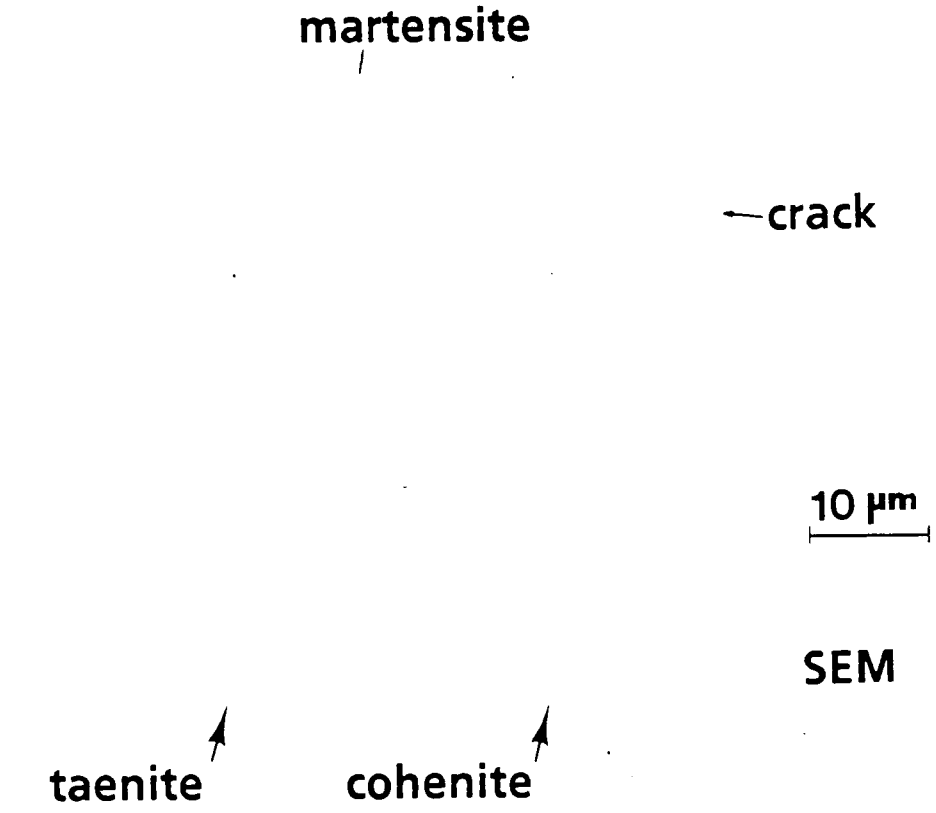

Figure 58 (continued)

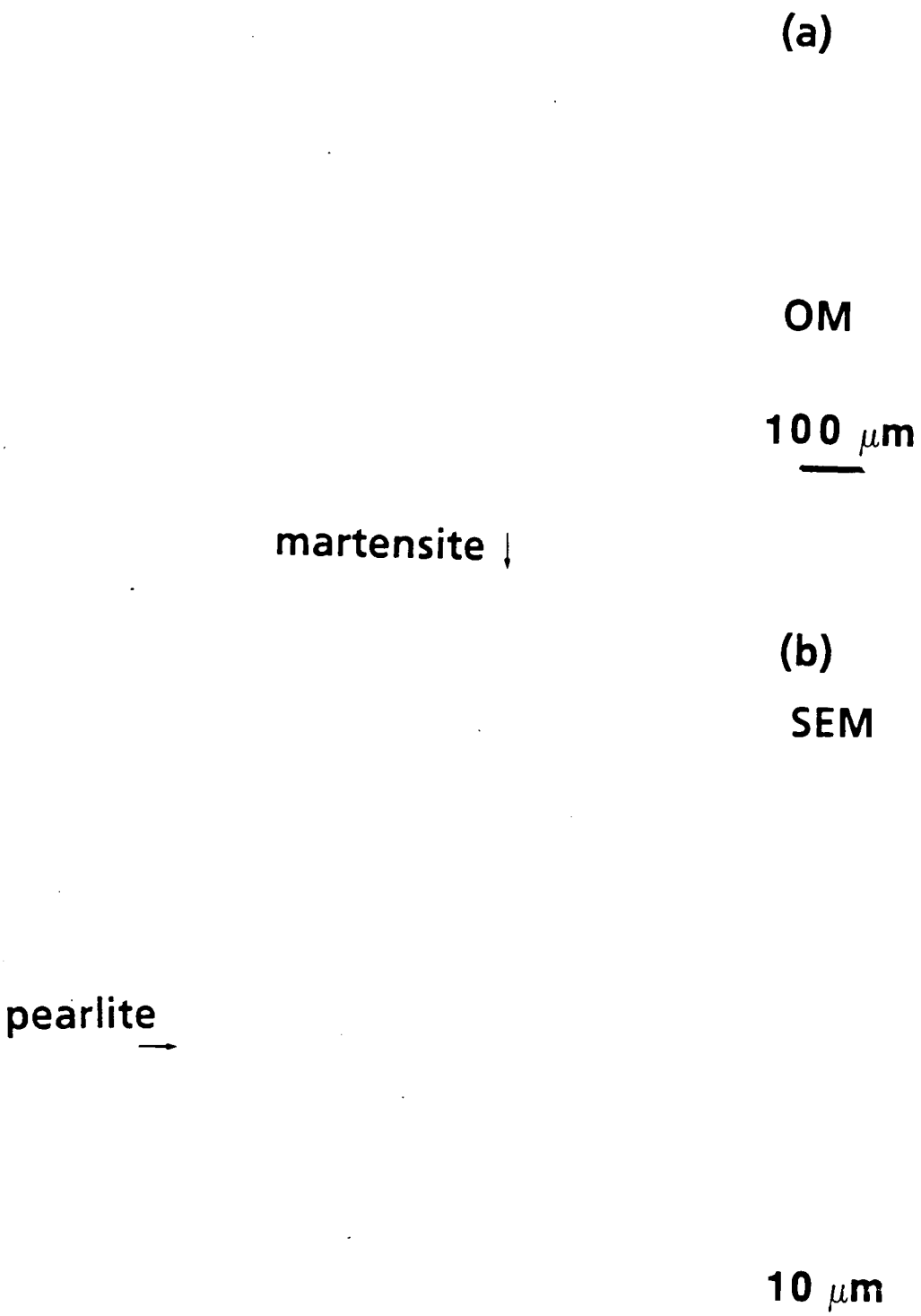

Figure 59. A stringer in which there is a martensite-pearlite interface (top, arrow). Below is a scanning electron micrograph of this interface.

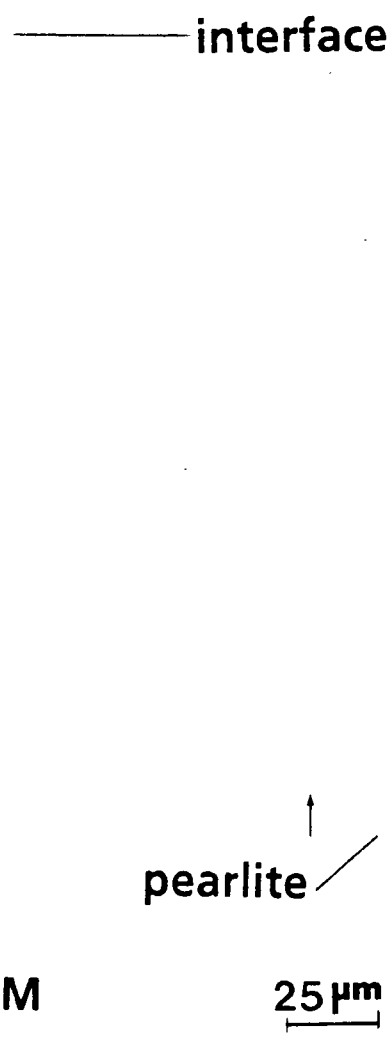

Figure 60. A stringer with an interface between pearlite and micro-widmanstatten kamacite with martensite.

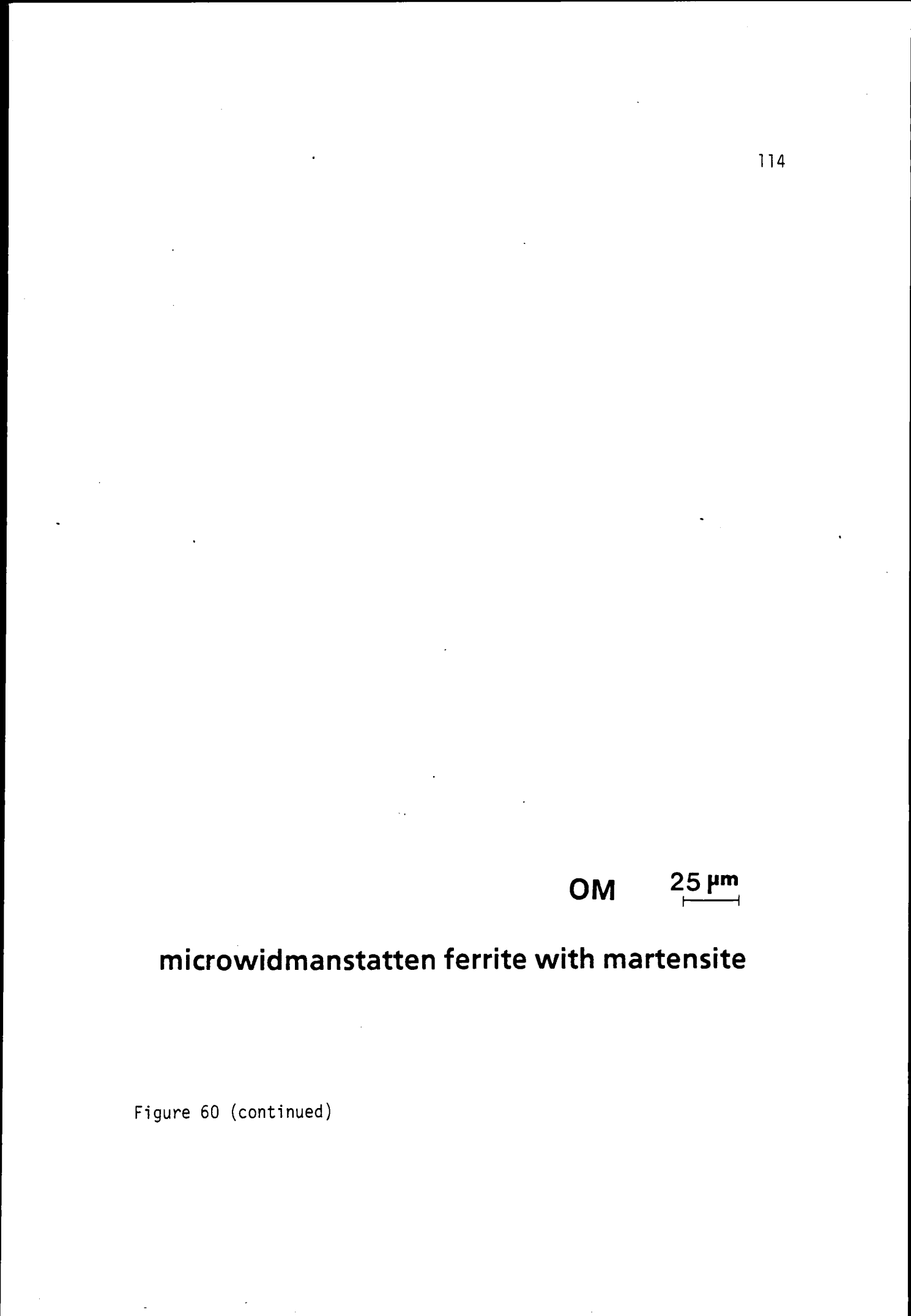

Figure 60 (continued)

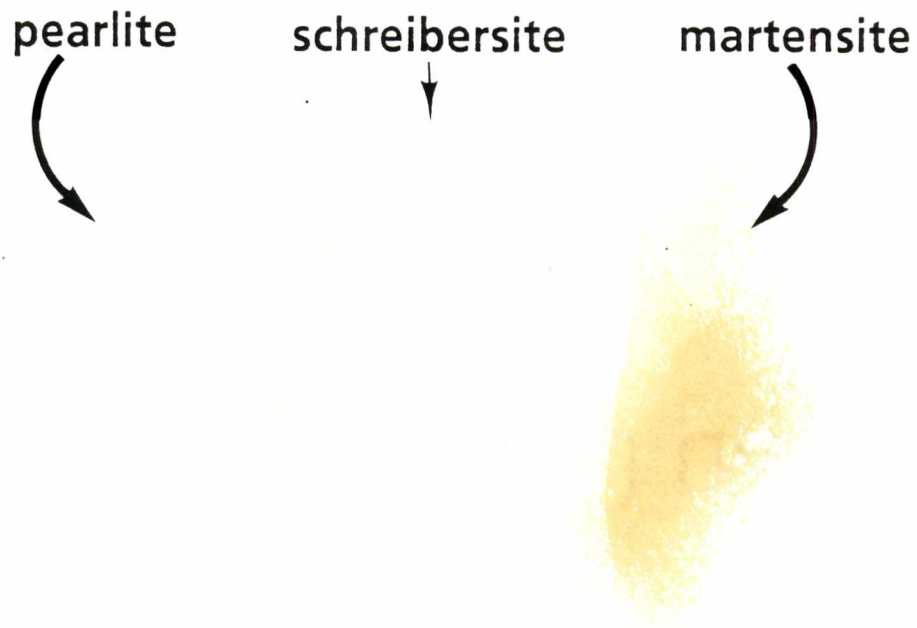

SEM

20 µm

Figure 60 (continued)

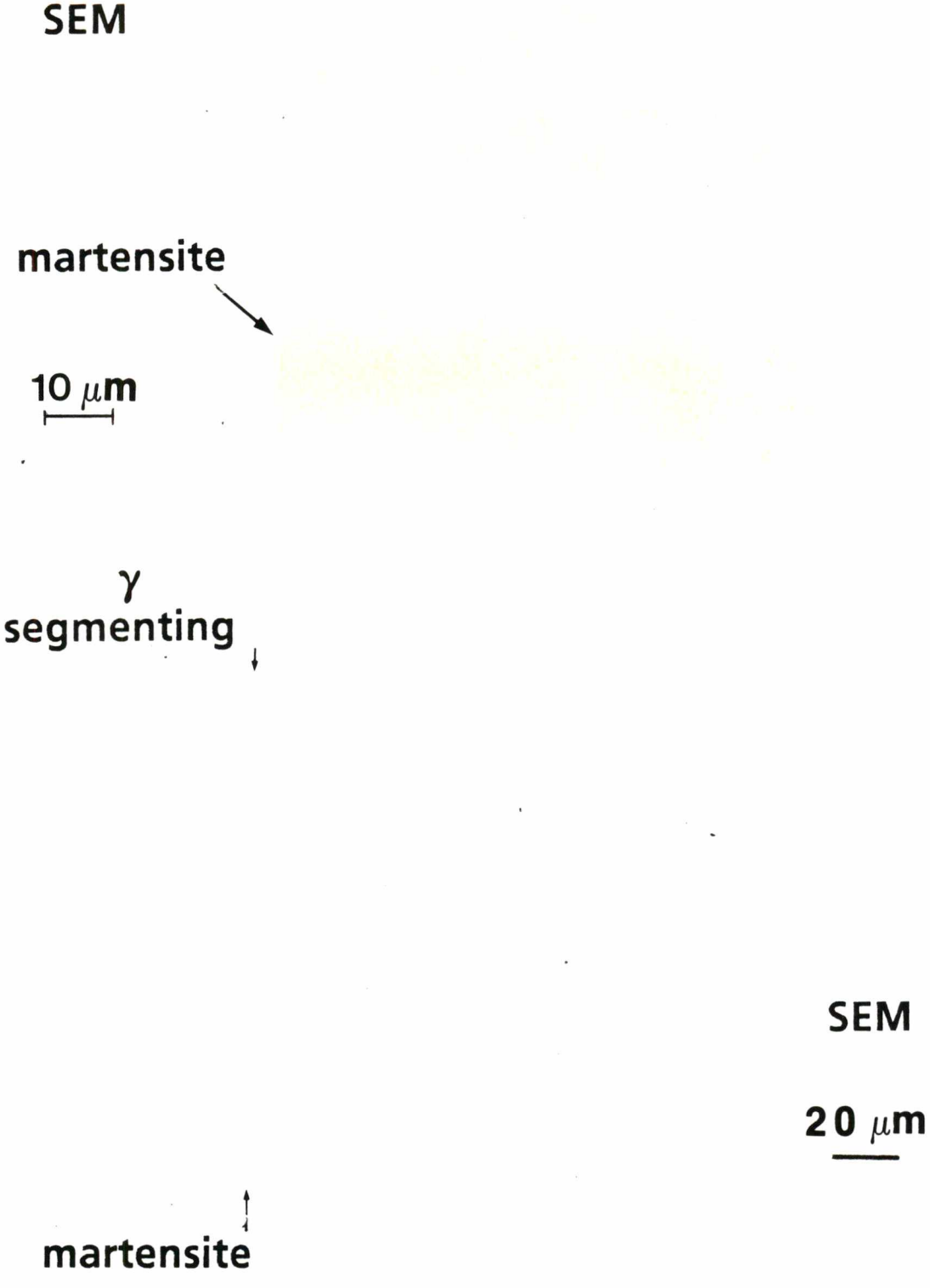

Figure 61. Martensite occurring locally in thick taenite along the edge of stringers.

Others. On one stringer, a bainitic appearing area was seen (Figure 62). Notice the structure in this case appears to grow from a boundary toward the stringer center, and not from the center out.

Pearlite occasionally occurs mixed with the microwidmanstatten kamacite. Figure 63 shows both coarse and fine pearlite in between microwidmanstatten kamacite plates.

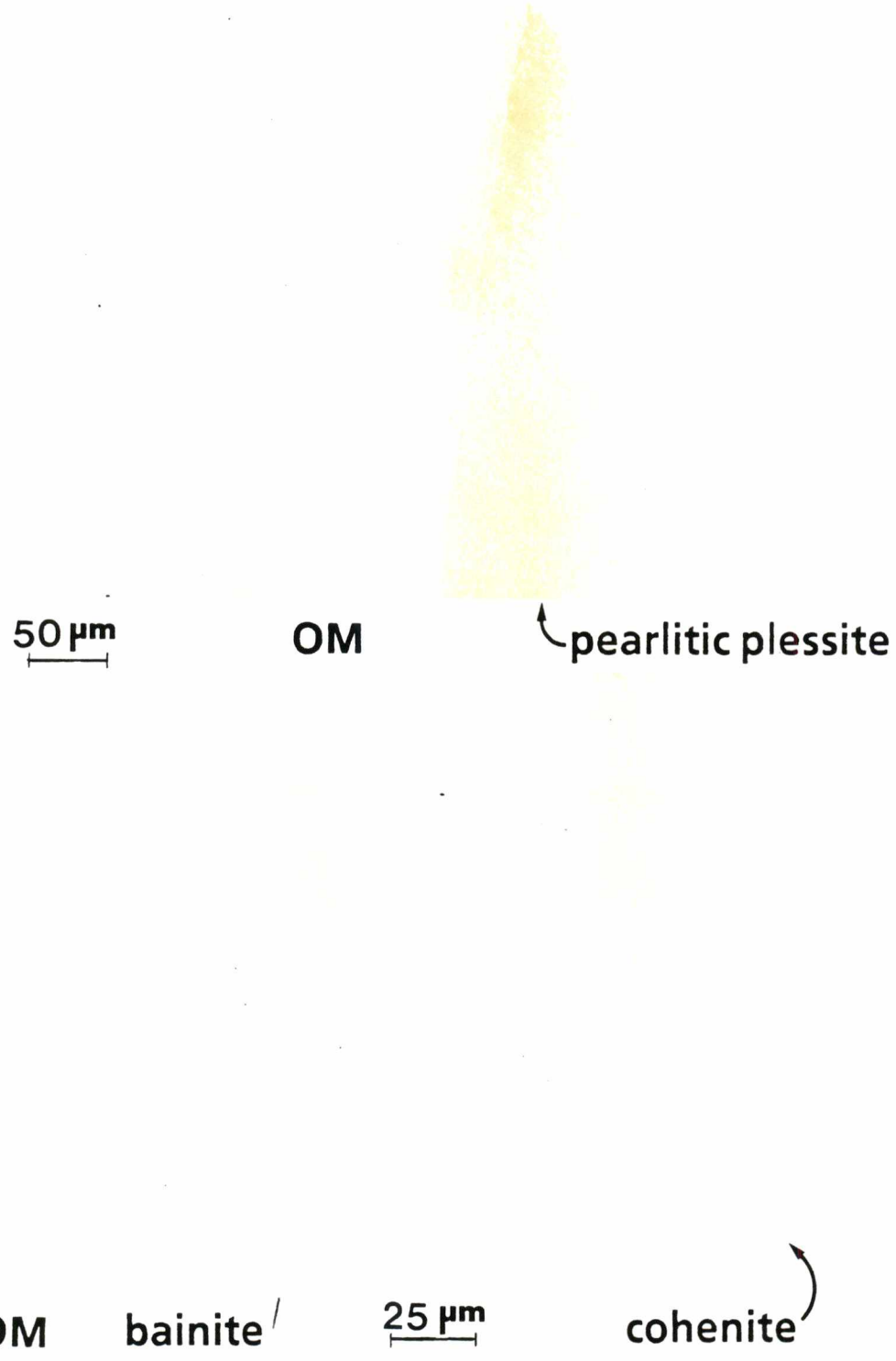

Figure 62. Bainitic region in sample B.

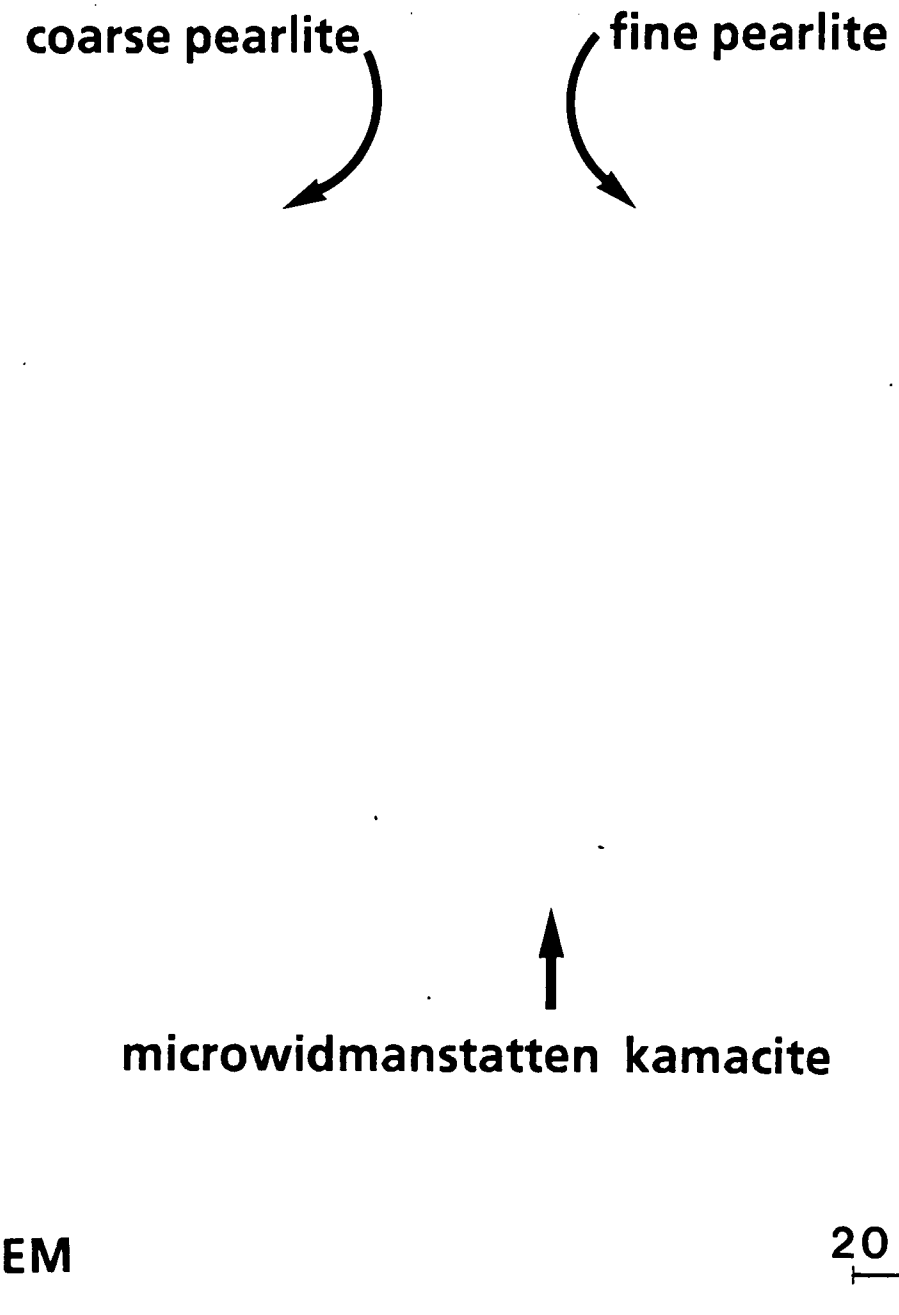

Figure 63. Coarse and fine pearlite mixed with microwidmanstatten kamacite.

CHAPTER VIII

DISCUSSION

> . . . it cannot be considered at complete structural equilibrium if the precipitate is dispersed as finely divided particles. Whether the precipitate is in the form of Widmanstatten particles, fine particles of irregular shape, or as lamellae in a cellular precipitate, coalescence and spheroidization will occur continuously by diffusion until, at last, the system consists of one lump of precipitate, whose shape is consistent with minimum surface energy, in a mass of depleted matrix ([55], p. 85).

This quote sums up the current belief on the subject of equilibrium microstructures. Why, then, is this not the case throughout the Arispe? Either the meteorite is not in equilibrium, after millions of years in space and an extremely slow cooling rate, or we must redefine equilibrium.

In this discussion, several aspects of the structures we see (Neumann bands, pearlite, martensite, spheroidite, and phosphides) and the sequences of their formation are discussed in an attempt to establish how these structures formed. However, due to time constraints in this experimental work, a detailed examination of possible mechanisms and theories of the formation of the structural features is not presented here.

I. THE FORMATION OF THE STRUCTURES IN THE ARISPE

The mechanism of formation of the Widmanstatten kamacite is undisputed and straightforward: it formed by general precipitation from supersaturated taenite as it cooled below about 800 °C. The

origins of many of the other structures in the Arispe, such as Neumann bands, pearlite, martensite, and spheroidite remain open to speculation.

A. Neumann Bands

Neumann bands are the result of a preterrestrial shock (impact). Their formation is highly orientation sensitive; they propagate in homogeneous BCC phases only along {112} planes that are oriented in a certain way with respect to the impact direction.

Most of the Neumann bands in this slice of the Arispe are thin and straight and of a constant width (Figure 31, p. 75), but some appear to be pinched off and segmented (Figure 32, p. 76), which may be due to reheating. If this is the case, then the Neumann bands probably formed at two different times: the meteorite was impacted, slightly annealed, then impacted again to produce new, sharp Neumann bands.

Neumann bands are seen in comb plessite (Figures 37 and 39, pp. 82 and 85), but not in pearlitic plessite or spheroidite. This indicates that the meteorite was probably impacted after the formation of the comb plessite, but before the pearlite and spheroidite formed; although as Neumann bands are orientation sensitive, it could be that the kamacite in the pearlitic plessite and spheroidite was not oriented properly with respect to the impact direction to form twins.

B. Pearlite

Pearlite cannot be rationalized by the accepted (as of 1980) Fe-Ni phase diagram (Figure 4, p. 32). Taenite (with less than 25% Ni) coupled with FeNi exists in meteorites [44], but the phase diagram predicts kamacite and ordered phases as the only structures that exist below 350 °C and 50% Ni. (No phase with more than 50% Ni has been reported in meteorites.)

The phase diagram predicts that the taenite stringers will decompose to kamacite and $FeNi_3$ by a eutectoid reaction. This may well produce a lamellar structure, but the higher Ni phase in the pearlite is definitely below 50% Ni (as evidenced by comparing K_α peak heights on the EDS; the Ni peak is seldom more than even half as high as the Fe peak).

Albertsen, Nielsen, and Buchwald [44] and Goldstein and Williams [49] have proposed revised Fe-Ni phase diagrams (Figure 64); however, the only low temperature phases shown on these diagrams are α and FeNi. Chamberod (Ref. 7 from Albertsen et al. [44]) reported finding Fe_3Ni in Fe-Ni alloys, which was the basis for showing this phase in Figure 4, but Albertsen, Nielsen, and Buchwald [44] suggest that this reported Fe_3Ni phase was actually disordered γ, and that superlattice reflection spots reported were due to ordered FeNi; thus Fe_3Ni should not be present in the phase diagram at all.

None of these diagrams, however, explains the existence of disordered γ (less than 25% Ni) at low temperatures (although Goldstein states that he expects that the cloudy zone is comprised of FeNi and

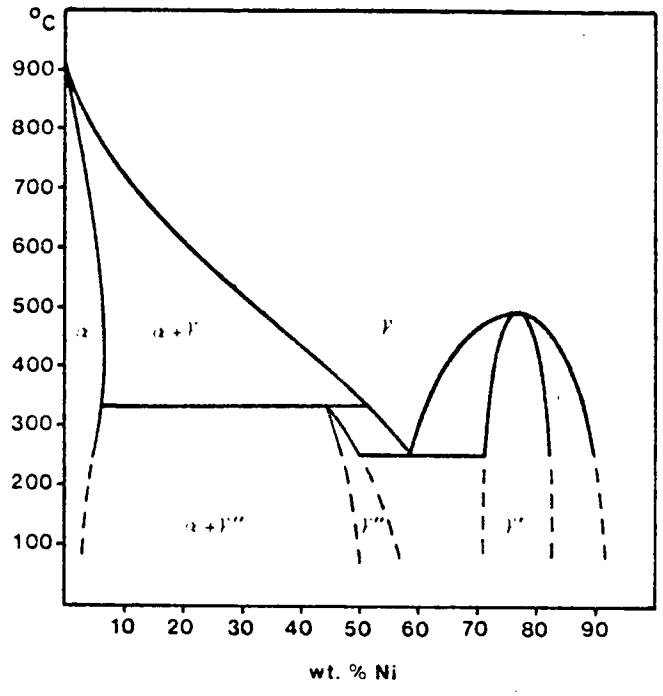

(a)

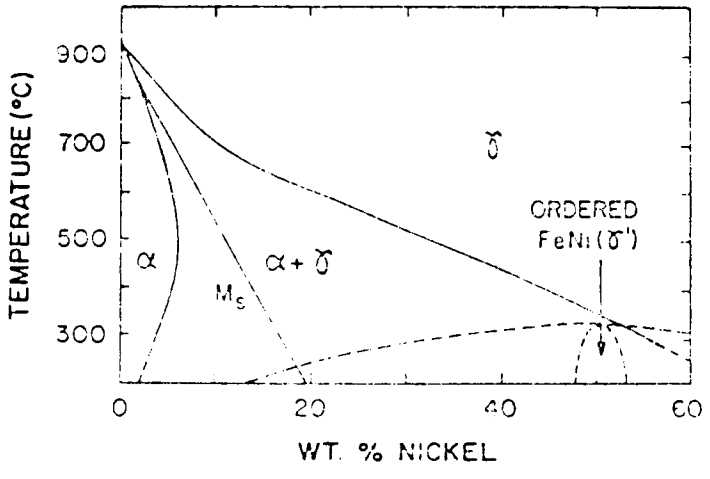

(b)

Figure 64. Fe-Ni phase diagrams proposed by (a) Albertsen, Nielsen, and Buchwald [44], and (b) by Goldstein and Williams [49].

α_2 [49], not FeNi and γ, on the basis of composition). Any phase diagram would almost have to have a γ (disordered) phase field around 25% Ni to accommodate Albertsen et al.'s reported γ phase. If there is a low temperature γ phase field present, then as the M-profile formed, the structure of the rim of the taenite would be governed by the 30-50% Ni region of the phase diagram and decompose to γ + FeNi, while the taenite cores would contain 0-20% Ni and would decompose to $\gamma + \alpha$.

One way pearlite could form is by precipitation of kamacite in the low Ni taenite. As the stringer's core cooled, the taenite would become increasingly unstable, until kamacite began to precipitate at various points in the stringer. As the kamacite lamellae grew, they would enrich the surrounding taenite in Ni, thus making these taenite lamellae more stable. It is not apparent to us though, why the kamacite would precipitate as lamellae; lamellae are generally thought of as a result of coupled growth.

Discontinuous precipitation is one such coupled process where lamellae can be produced. In discontinuous precipitation, one structure transforms completely into another. The transformation takes place by movement of a boundary, ahead of which the structure is unaffected, and behind which much coarser morphologies are present. It generally occurs at low temperatures where diffusion is extremely slow, too slow for general precipitation to take place. Discontinuous precipitation is favored by nuclei that form near grain boundaries, as solute atoms can diffuse more quickly along grain boundaries than

through the bulk of the grain. It produces lamellar structures with alternating solute-rich and solute-depleted plates. In the Arispe's pearlitic areas, however, no boundaries are seen (except between pearlite and spheroidite; these boundaries most likely formed much later than the pearlite).

C. Martensite

Martensite formation in Fe-Ni alloys depends strictly on temperature and chemical composition. Martensite will begin to form when the temperature drops below "M_s," the martensite start temperature. Transformation will continue until the temperature drops below "M_f" (martensite finish), at which time the structure will consist of 100% martensite with no retained taenite. (If the alloy never reaches M_f, there will be retained taenite present.) M_s and M_f can be drastically affected by alloying elements: increasing %Ni in Fe decreases the M_s and M_f temperatures, as does the addition of C.

Plate martensite occurs in Fe-Ni alloys above about 25% Ni [56], so evidently the regions that martensite needles formed in must be reasonably rich in Ni. Carbon content may also affect martensite morphology.

Sometimes there will be an abrupt change from, for example, martensite to pearlite (Figure 59, p. 112). It is puzzling why pearlite would cease growing in this instance and allow such a large area of taenite to remain available to form martensite. If temperature were a factor controlling the amount of pearlite (or in Figure 60

(p. 113), microwidmanstatten kamacite) formed, then one would expect to see the pearlite lamellae or microwidmanstatten plates become finer and finer as they continued to grow at increasingly lower temperatures; but instead, these structures are a constant size. Here, the implication is that pearlite had only nucleated on one end. In this instance, apparently the pearlite reaction ceased for some reason, leaving pearlite in one half of the stringer, and taenite in the other. As the temperature dropped then this taenite transformed to martensite.

What dictates the relative amounts of martensite and microwidmanstatten kamacite in stringers? Martensite and microwidmanstatten kamacite will both form in structures of the same size, and as far as we can tell, of the same composition. Some stringers are exclusively martensite with no microwidmanstatten kamacite, other stringers have well developed microwidmanstatten kamacite patterns with only small amounts of martensite in the edges. Carbon may play an important role in dictating the morphology of these areas, as martensite is seen more often in areas near cohenite nests than away from them; however, more work needs to be done to determine if any carbon (or other) gradients exist in these structures.

Figure 34 (p. 79) shows a stringer with a well-developed microwidmanstatten pattern that has a few regions of martensite near the edge. Perhaps the low Ni in the center decreased the stability of the γ and thus helped the microwidmanstatten kamacite process run more to completion, while the high Ni areas near the edge, being

comparatively stable, did not readily transform to microwidmanstatten kamacite, and thus eventually formed martensite as the temperature dropped. This theory falls short in explaining Figure 35 (p. 80) or Figure 56 (p. 108) (top photo), where martensite is present not only in the high Ni areas near the stringer edges, but also in the lower Ni cores, or Figure 51 (p. 100) which shows a martensitic area toward the center of a stringer only.

The significance of coarse martensite plates as opposed to fine ones is not understood. It is well established that in steels, the maximum size martensite plates can attain is directly related to the size of the austenite (γ) grains. In steels, the first plates will run from grain boundary to grain boundary, then subsequent plates will fill the remaining spaces, impinging on one another until there is little room left (see Figure 65). In the Arispe, however, the martensite plates do not run all the way across the grain. In Figure 57 (p. 109), for instance, the largest plates are found around the edges of the region, while the smallest plates are found packed into the center.

Also in the Arispe, the martensite plates appear to almost pass through one another, as opposed to merely impinging upon one another (Figure 66); and they lack the prominent midrib and internal striations seen in artificial Fe-Ni alloys.

In cases where pearlite is in contact with fine martensite and microwidmanstatten ferrite [Figures 67 and 60 (p. 113)], perhaps pearlite nucleated in the end towards the cohenite nest core, while

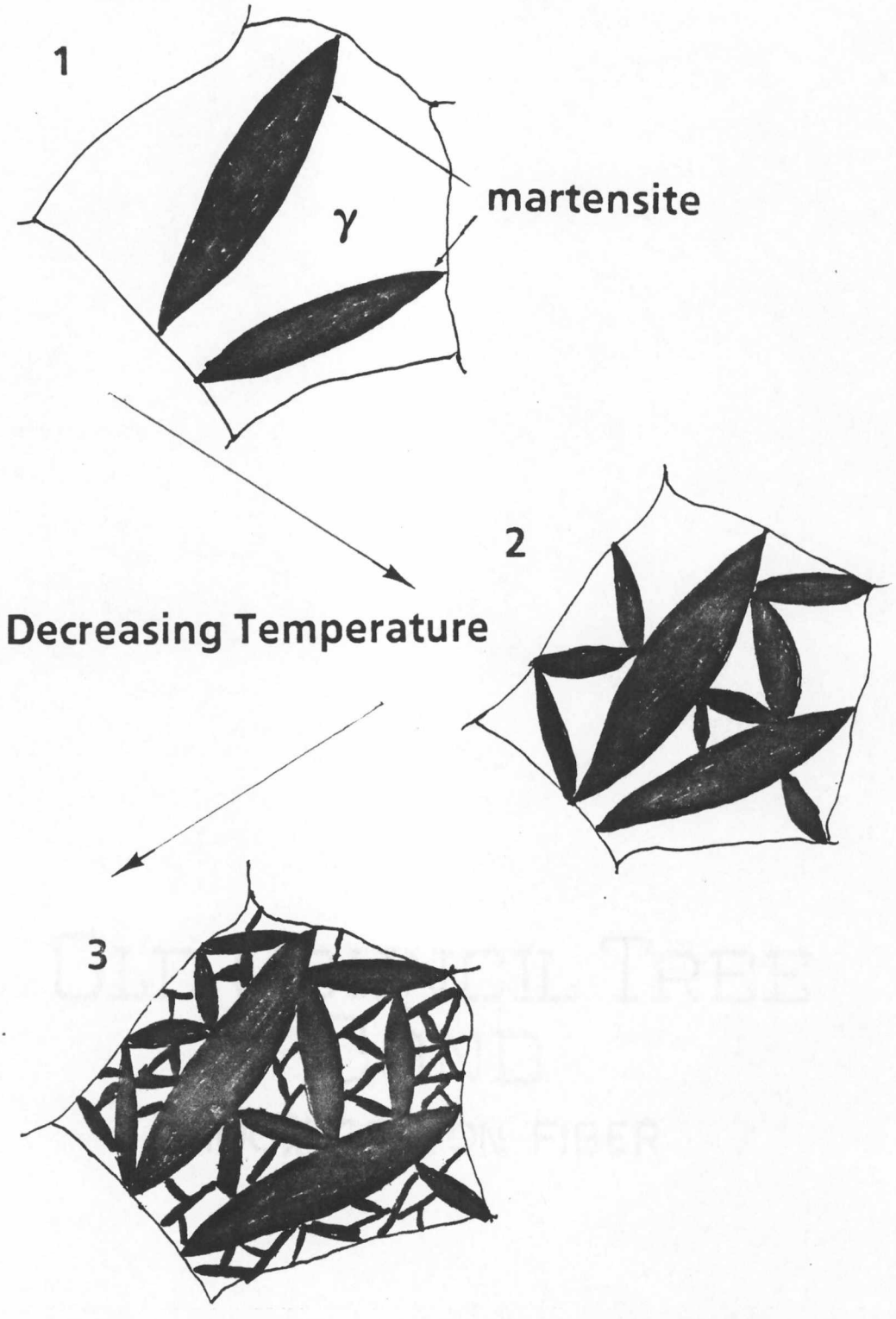

Figure 65. Drawing showing plate martensite formation in steels.

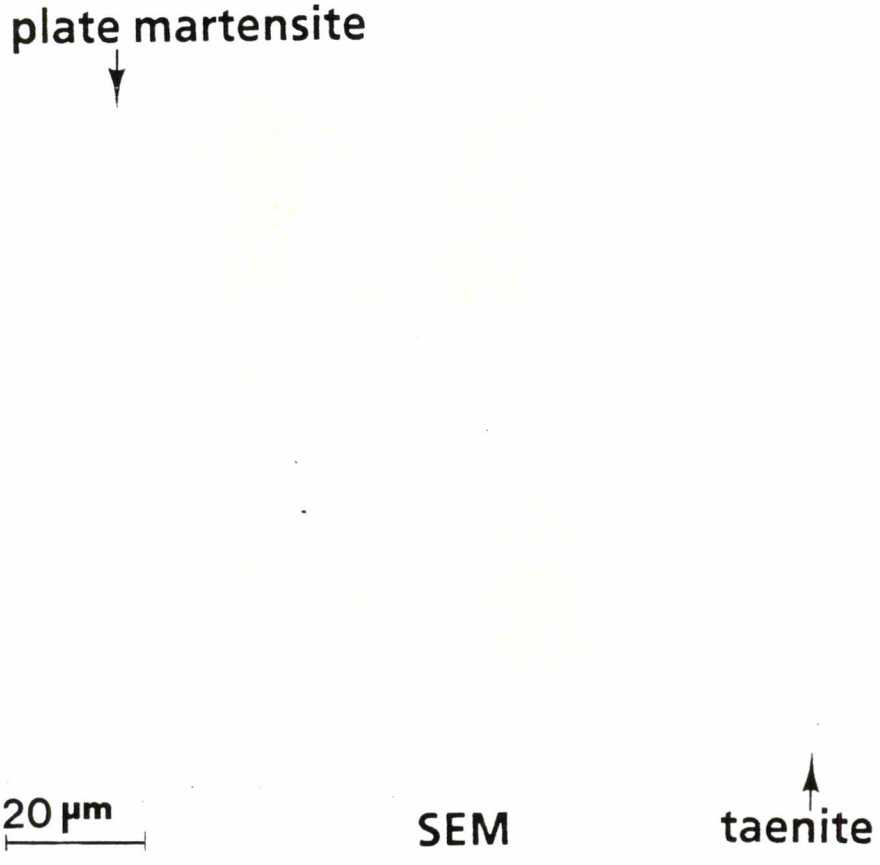

Figure 66. Typical plate martensite in the Arispe meteorite.

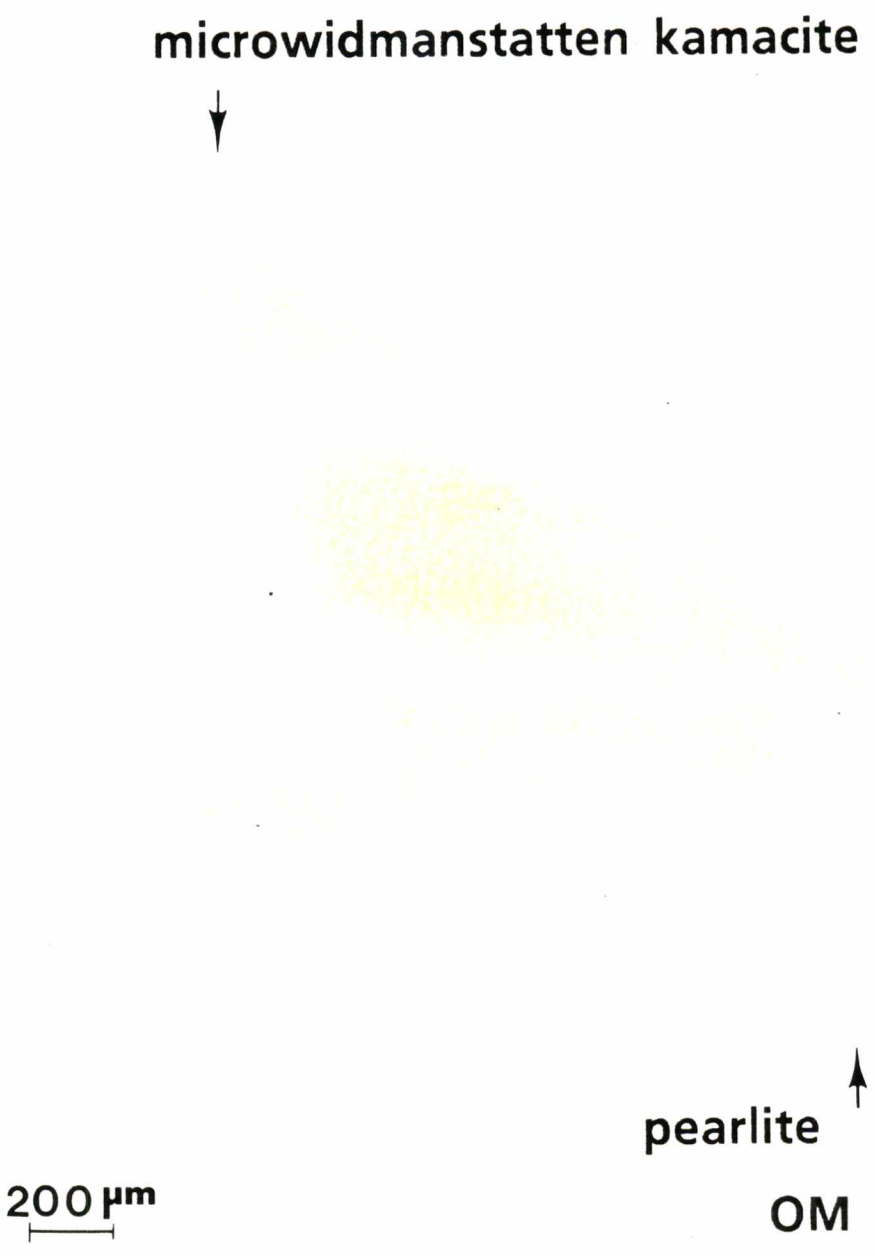

Figure 67. A stringer in sample B that goes from pearlite, to microwidmanstatten kamacite with varying amounts of martensite.

the microwidmanstatten kamacite nucleated in the other end of the stringer, farthest from the cohenite nest. When these two structures met each other, they ceased to grow. The earliest forming microwidmanstatten kamacite, that formed farthest from the cohenite nest, had a chance to form a very well-developed pattern, leaving only very thin strips of retained taenite. On the other hand, the latest forming microwidmanstatten kamacite plates had little opportunity to grow and coarsen, and therefore left large areas of retained taenite. When the temperature dropped below M_s and transformed the remaining taenite to martensite, more martensite formed near the pearlite interface in this stringer than in the end farthest from the cohenite nest.

D. Spheroidite

There is no evidence that spheroidite is a product of over-aged martensite, as spheroidite is always associated with pearlite, and also as there is so much sharp, clean, untempered plate martensite in the sample. All the spheroidite examined appears to have formed from pearlite.

Transformation from pearlite to spheroidite could occur by either segmentation of lamellae and subsequent coalescence of the particles, or by a boundary mechanism such as discontinuous precipitation, given the microstructures that we have seen.

In some areas (Figure 61, p. 116), pearlite and spheroidite are mixed, and the pearlite appears to be segmenting to form spheres (Figure 68). Figure 69 shows a spheroidite stringer that probably

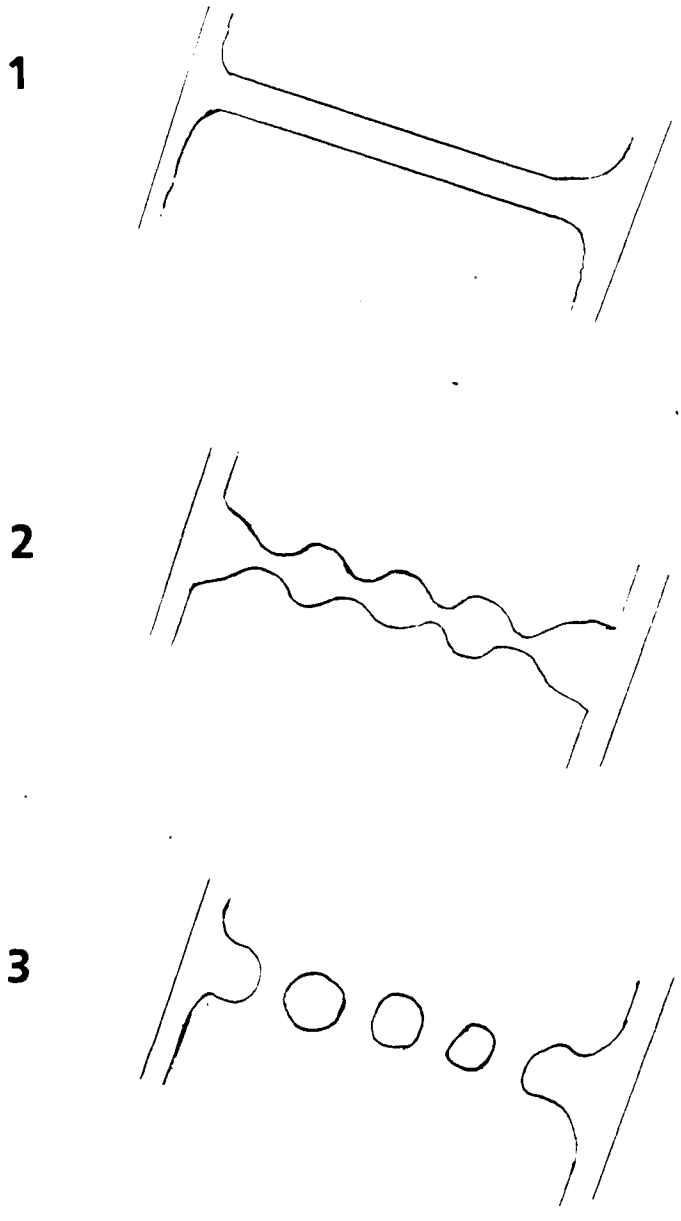

Figure 68. Schematic drawing of pearlite lamella segmenting to form spheroidite.

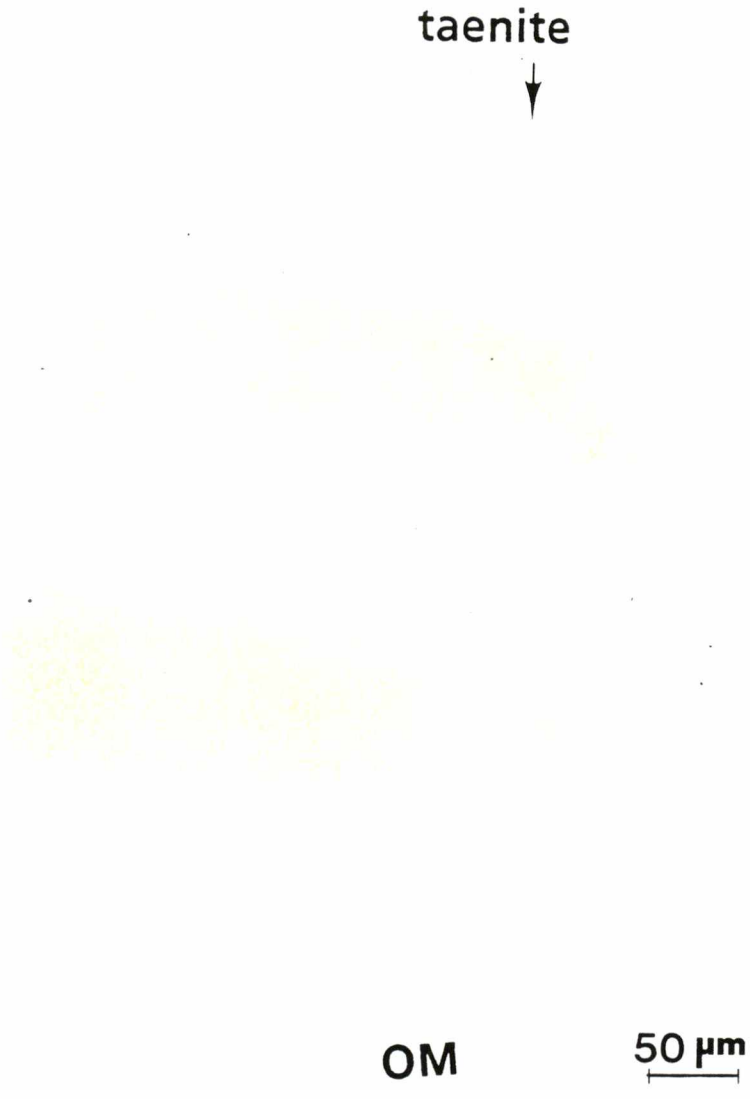

Figure 69. Part of the stringer of Figure 48 (p. 97) showing taenite pinching off to form spheroidite.

used to be pearlite. Small circles of taenite can be seen in various stages of breaking free from the thick taenite rim around the edge of the stringer.

Other places, the transformation appears to occur by a boundary mechanism. Boundaries may be seen between pearlite and spheroidite in Figure 70, and between spheroidite and microwidmanstatten kamacite in Figure 71. At some other interfaces between two morphologies, a boundary is not apparent, but still may be present (Figure 43, p. 90, bottom photo, from stringer shown in Figure 48, p. 97).

The stringer in Figure 72 features not only a boundary between spheroidite and pearlite, but also two regions of coarse pearlite that could be coarsening by discontinuous precipitation (Figures 73 and 74). (Upon repolishing and etching, the region in Figure 74 disappeared, indicating that this was a very shallow feature.)

Boundaries are not obvious, however, between the coarse and fine spheroidite on Figure 75, or between the fine spheroidite and pearlite in the same figure.

The structure of one stringer in sample B (Figure 76) also appears to be transforming by a boundary mechanism, but here, very fine pearlite appears to have nucleated from the sides of the stringer (Figure 77), making it doubtful that this area was once composed of coarse pearlite, unless this fine pearlite nucleated after the breakdown to spheroidite had begun (otherwise, this stringer would be composed of coarse pearlite surrounded by isolated colonies of fine pearlite, a situation that we have never seen). Actually, it is not

Figure 70. Part of the stringer of Figure 47 (p. 95) showing a boundary between pearlite and spheroidite.

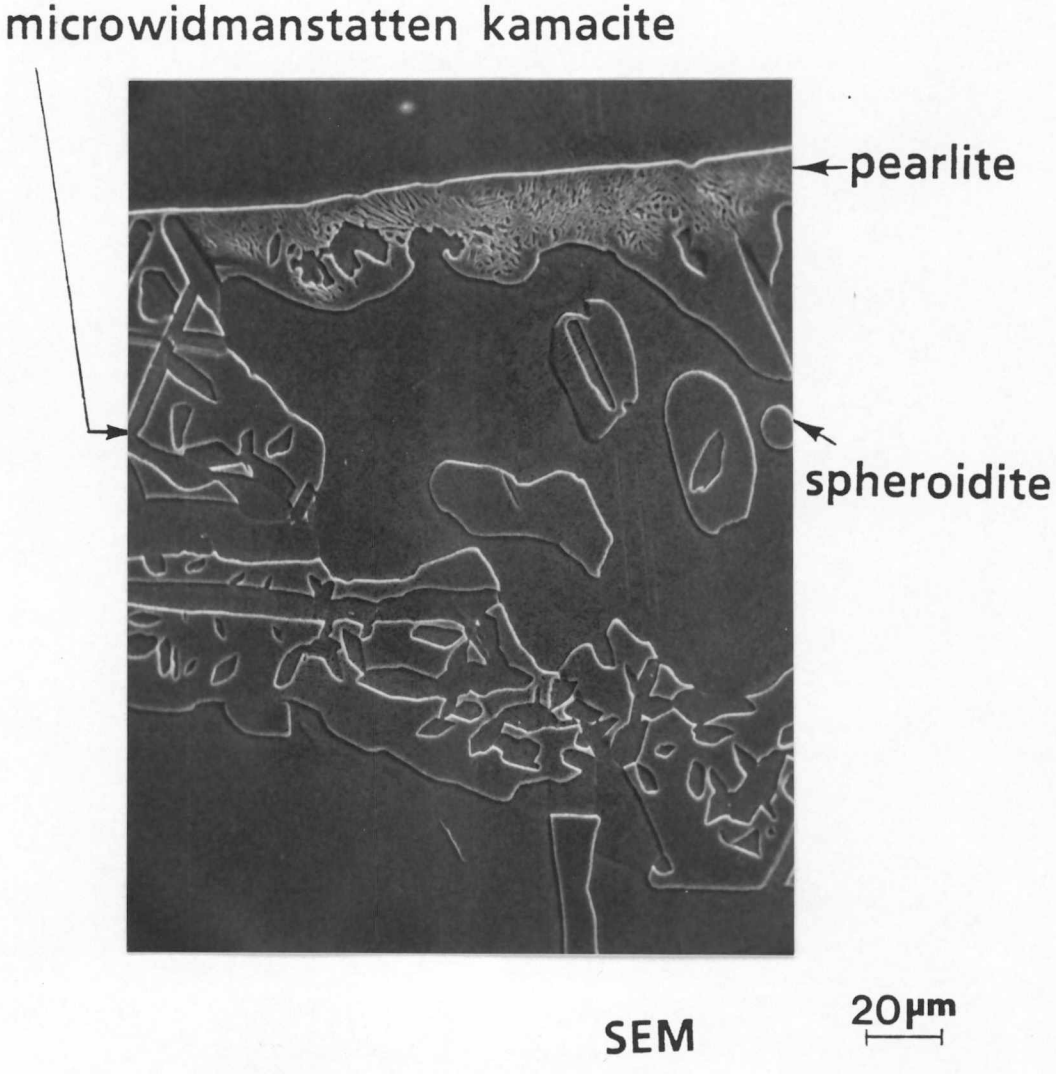

Figure 71. A stringer in sample B showing spheroidite and microwidmanstatten kamacite.

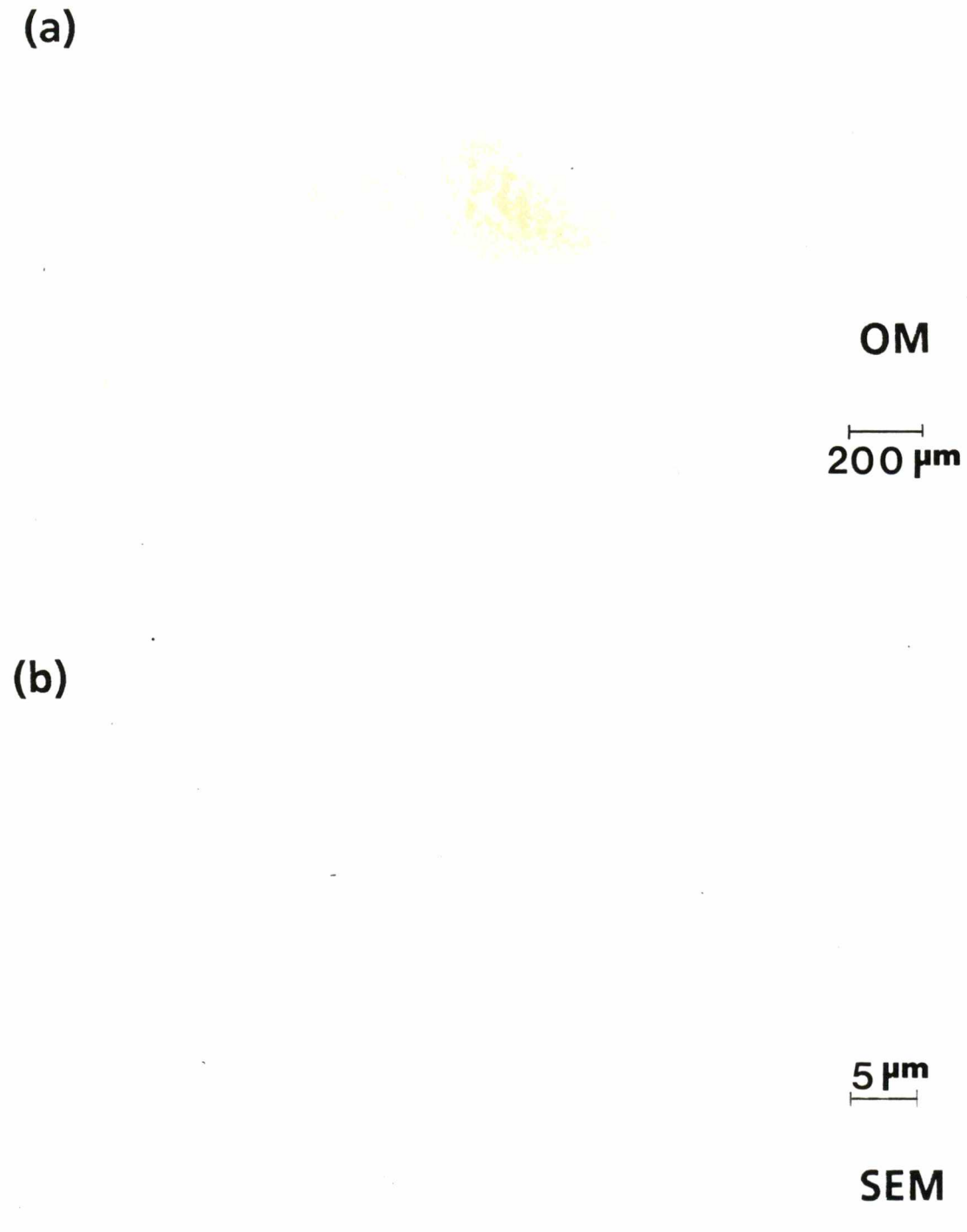

Figure 72. (a) A stringer in sample B with both pearlite and spheroidite. (b) Shows a higher magnification view of this interface.

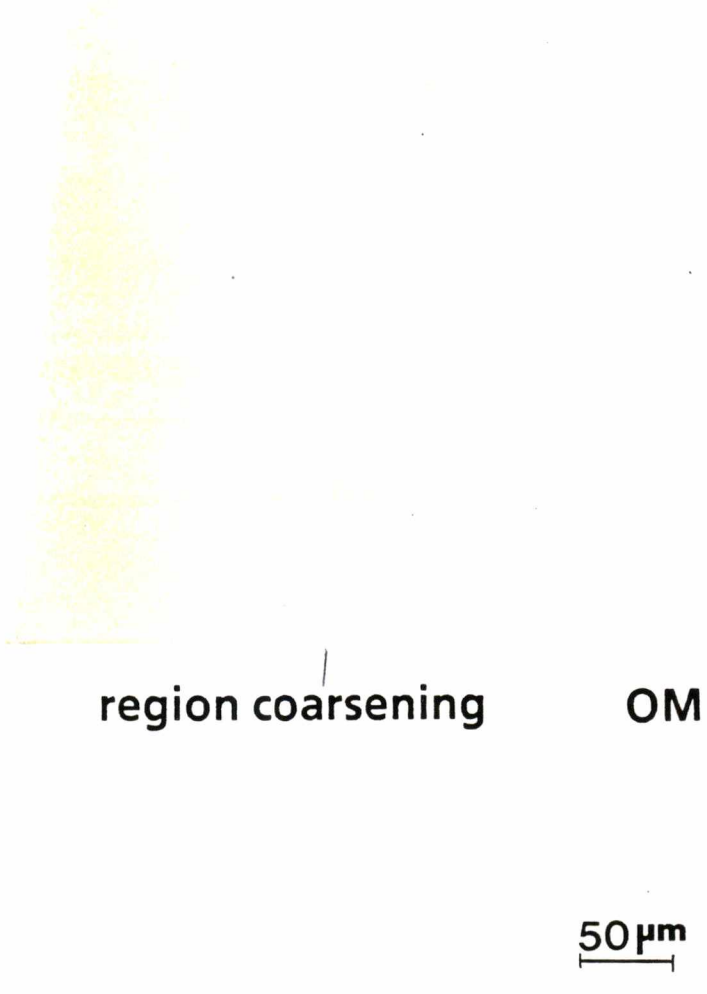

Figure 73. Region of pearlite from the stringer of Figure 72 coarsening by discontinuous precipitation.

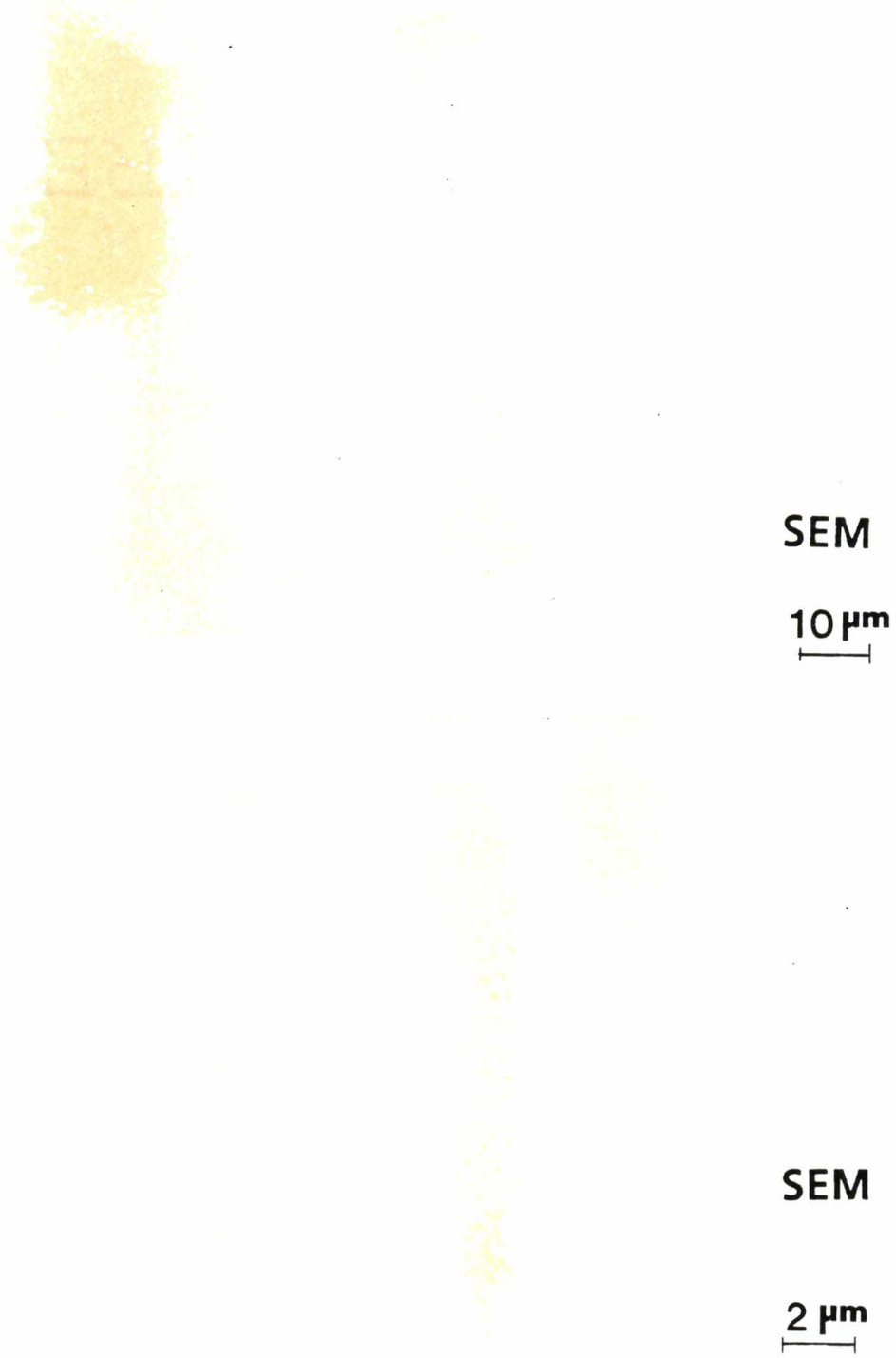

Figure 73 (continued)

Figure 74. A region from Figure 72 coarsening by discontinuous precipitation.

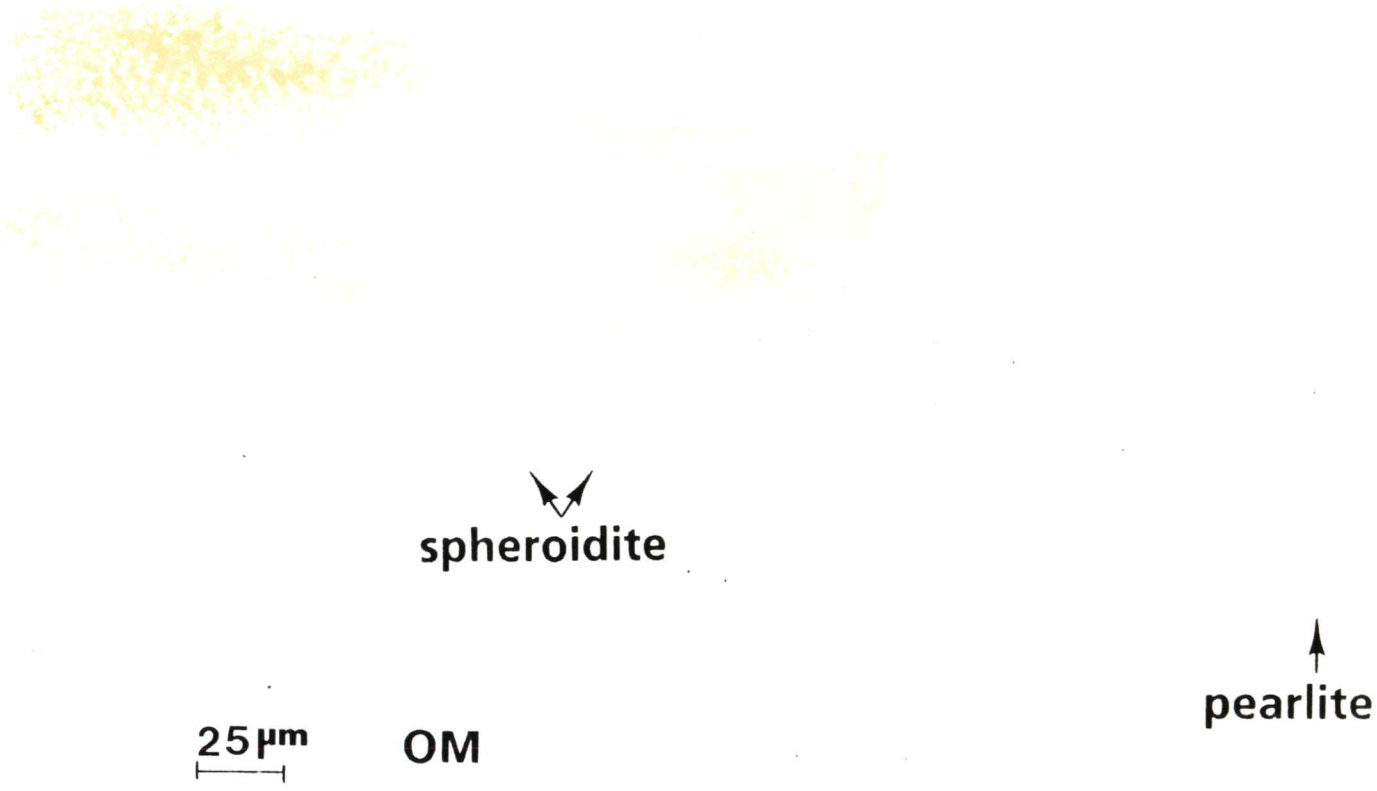

Figure 75. Regions of pearlite and spheroidite from Figure 47 (p. 95).

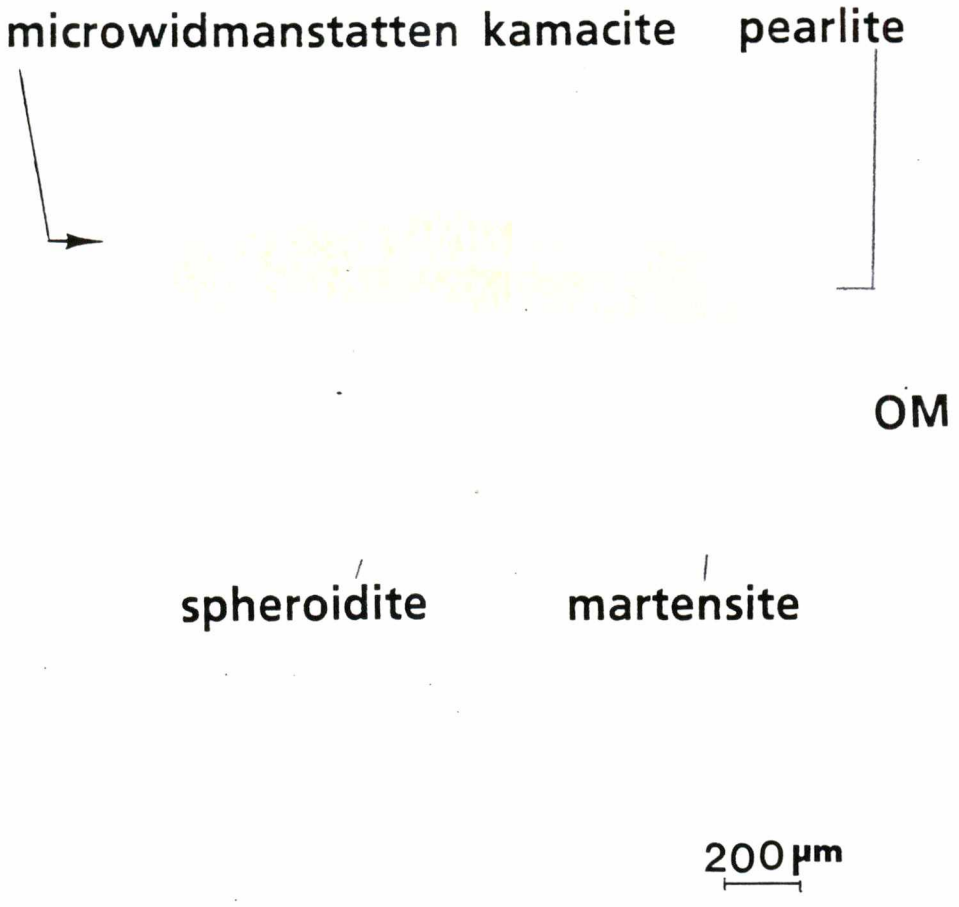

Figure 76. A stringer in sample B showing a wide variety of micro-constituents.

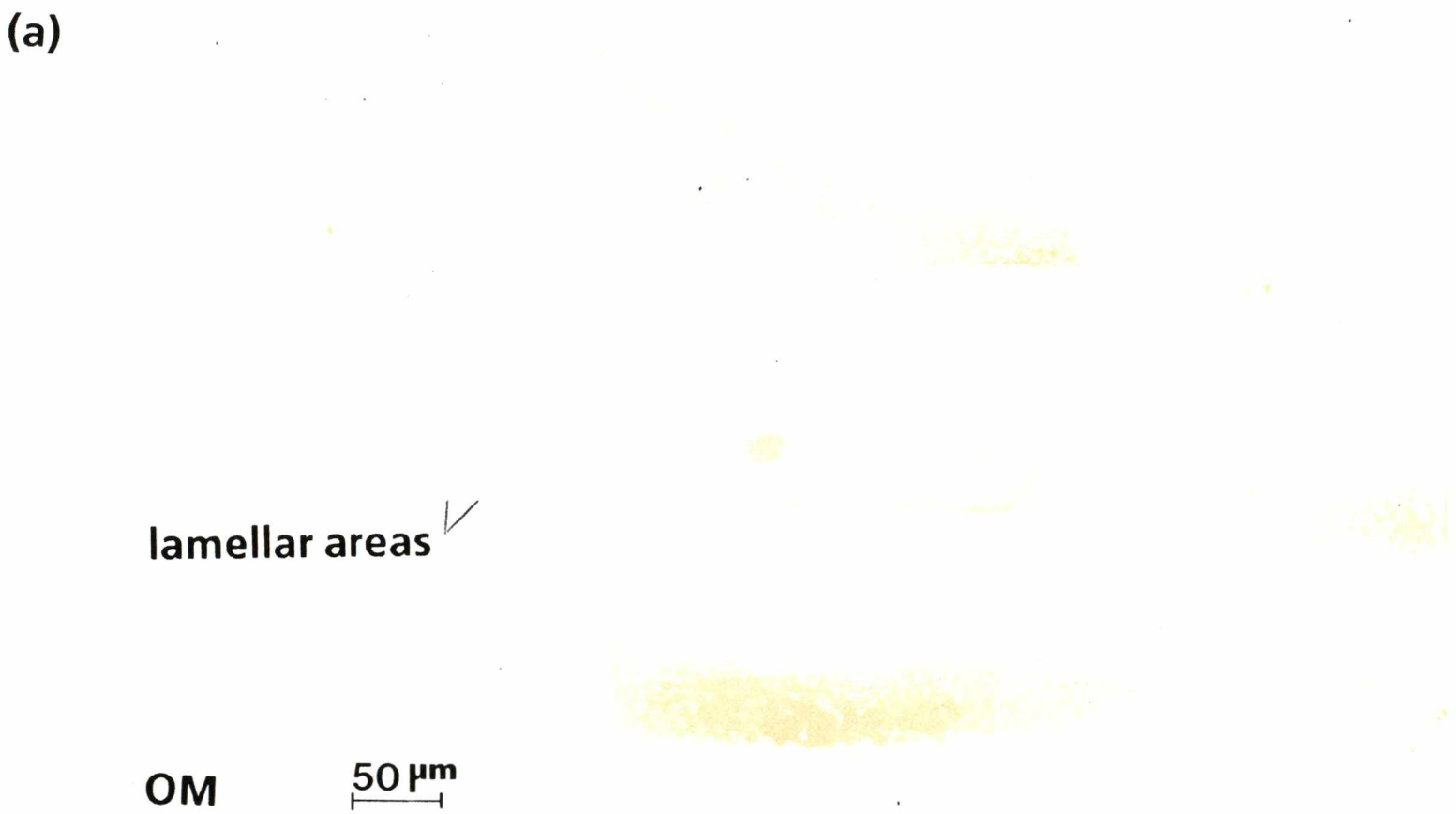

Figure 77. (a) The end of the stringer of Figure 76 closest to the cohenite nest. (b) The interface between the spheroidite and the microwidmanstatten kamacite in this stringer.

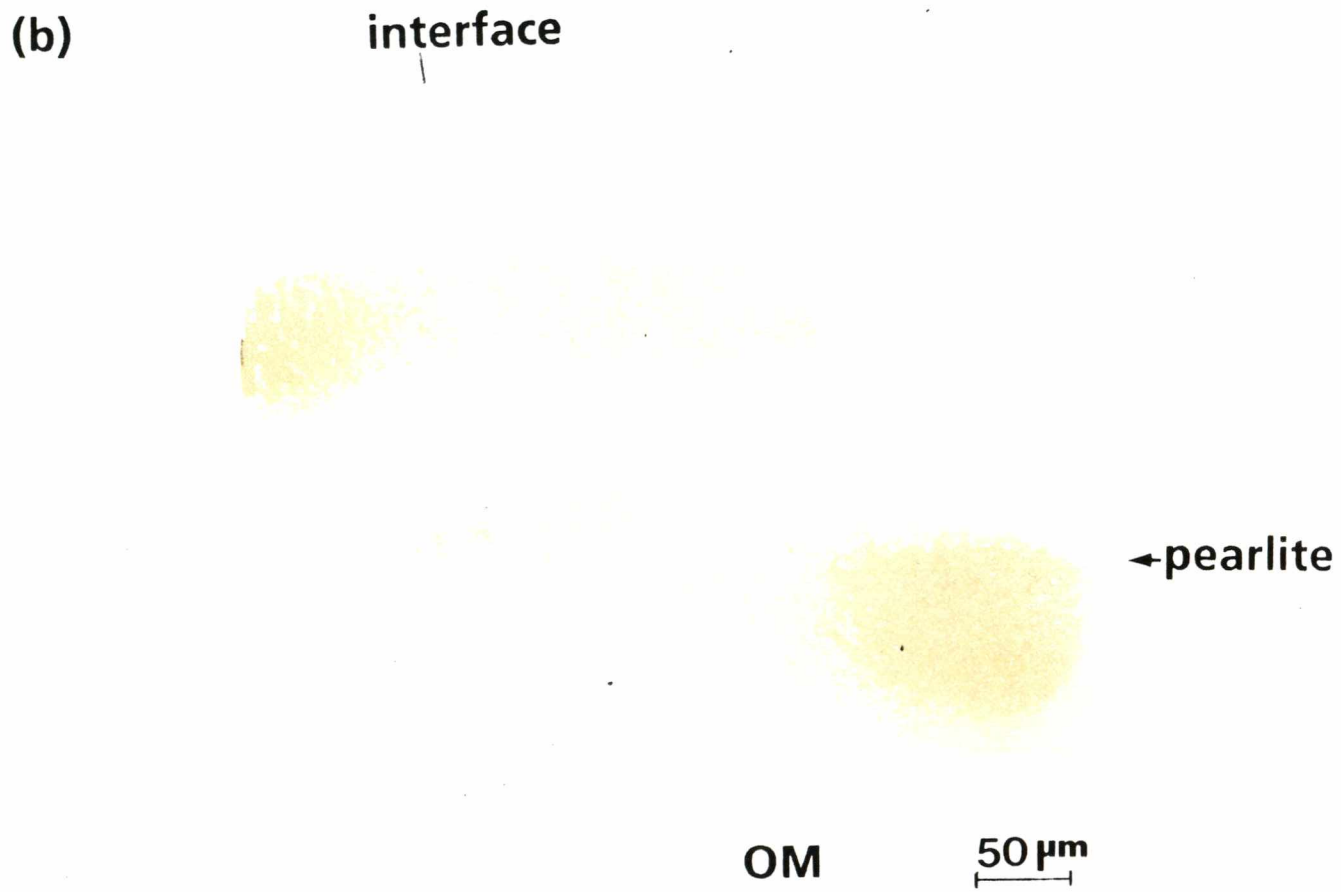

Figure 77 (continued)

entirely clear just what the structure here originally was. Figure 77(a) shows lamellar areas in the center spheroidized area of the stringer, while Figure 77(b) shows remnants of needles or plates (arrow). (Notice in Figure 77(a) that the thick taenite along the edges of the structure has decomposed to pearlite on one side, and to martensite on the other.)

If the structure would form by segmentation, the spheroidite would have the same phases at the same compositions present as the pearlite did, only the morphology would change. However, the transformation from pearlite to spheroidite may represent a phase transformation to FeNi as well as a morphology change (although the spheres do not appear to be FeNi, since it has a tetragonal lattice; and this would cause the spheres to be active under polarized light, but they are not).

E. Phosphides

Schreibersite apparently formed at high temperatures in taenite grains, and served as a nucleation site for the Widmanstatten kamacite plates [57]. In many meteorites, "swathing kamacite" (kamacite not following Widmanstatten orientation) can be seen around schreibersite grains, implying that the schreibersite acted as a nucleus for the kamacite.

Rhabdite probably formed in the kamacite plates either as they grew or after they grew. They appear to have nucleated randomly in the kamacite. The rhabdite crystals formed before the meteorite was

impacted, as Neumann bands that have offset or even shattered rhabdite crystals can be frequently seen (Figures 32 and 31, pp. 76 and 75).

II. INFLUENCE OF COHENITE

No discussion of the Arispe is complete without speculations as to the effect of the cohenite nests on the structure.

The cohenite nests are apparently necessary for the formation of pearlite and spheroidite, as these structures are never seen away from the immediate vicinity of the cohenite nests, implying that carbon (by its absence or presence) is responsible for these structures. For neighboring areas of cohenite and kamacite or taenite to be in local equilibrium, the metallic phases (α and γ) would have to contain the maximum amount of C their structures can hold. (Away from the cohenite, the amount of C in the metallic phases may well rapidly decrease.)

Assuming that a cohenite nest has a "core" from which all of the branches radiate (see Figure 29, arrow, p. 73), the most equilibrated structures in a given stringer tend to occur closest to this core. Where a stringer has pearlite on one end and spheroidite on another, the spheroidite, the more equilibrated structure, is found nearer the cohenite. In structures with pearlite and martensite, the martensite (metastable) generally occurs at the end farther from the cohenite nest core. (The stringer in Figure 76 appears contrary to this—coarse pearlite occurs nearest the cohenite, but this pearlite is somewhat separated from the rest of the stringer, most of which is spheroidite.)

Figure 67 (p. 130) shows a stringer that is pearlite near the cohenite nest core, then suddenly changes to microwidmanstatten kamacite with martensite toward the outer edge of the nest (Figure 60, p. 113), then gradually the amount of martensite decreases until, at the end, little martensite is present (Figure 33, p. 78). One could argue that carbon decreases the M_s, so martensite formation close to the cohenite nest cores is delayed, but this does not explain why martensite is seldom seen in appreciable quantities away from the cohenite nests (in the bulk of the meteorite).

CHAPTER IX

CONCLUSION

The Arispe meteorite was a most puzzling meteorite to study. It displays a perplexing array of microstructures, including areas of pearlite in contact with either martensite or spheroidite, as well as comb plessite, microwidmanstatten plessite, phosphides, and Neumann bands. It also contains large cohenite "nests," a feature unique to the Arispe.

The spheroidite observed was always associated with pearlite, and both were only seen near cohenite nests. The spheroidite appeared to be forming from pearlite by either some boundary migration mechanism, or by segmentation of pearlite lamellae. Although several mechanisms for the formation of this pearlite have been examined, no logical mechanism was isolated.

Martensite was also frequently seen in taenite stringers around the cohenite. Although the martensite appeared similar to those seen in commercial Fe-Ni alloys, several differences were noted (e.g., absence of both midrib and distinct internal striations).

More work needs to be done on this meteorite to understand these structures. Transmission electron microscopy should be done on the pearlite and spheroidite to determine the fine structure morphology and the crystal structure (e.g., FeNi), and also scanning transmission electron microscopy should be used for microchemical analysis of these structures.

REFERENCES

REFERENCES

1. Robert F. Mehl and Gerhard Derge, Iron from heaven, Metal Progress 38:799-804 (1940).

2. Carleton B. Moore, Meteorites (Robert E. Boyer, ed.), Houghton Mifflin, Boston (1971).

3. John A. Wood, Meteorites and the Origin of the Planets, McGraw-Hill Book Company, New York (1968), pp. 10, 11, 16-18.

4. Elbert A. King, The origin of tektites: a brief review, American Scientist 65:212-218 (1977).

5. Max H. Hey, Catalogue of Meteorites, Trustees of the British Museum, London (1966), pp. x-xiii.

6. H. J. Axon, Metallurgy of meteorites, Progress in Materials Science 13:184-228 (1967).

7. John T. Wasson, Meteorites, Springer-Verlag, New York (1974), pp. 54-60.

8. Herbert H. Uhlig, Contribution of metallurgy to the origin of meteorites; Part I - Structure of metallic meteorites, their composition and the effect of pressure, Geochimica et Cosmochimica Acta 6:282-301 (1954).

9. A. E. Ringwood and L. Kaufman, The influence of high pressure on transformation equilibria in iron meteorites, Geochimica et Cosmochimica Acta 26:999-1009 (1962).

10. L. S. Lin, J. I. Goldstein and D. B. Williams, Analytical electron microscopy study of the plessite structure in four IIICD iron meteorites, Geochimica et Cosmochimica Acta 43:725-737 (1979).

11. S. J. B. Reed, Electron-probe microanalysis of schreibersite and rhabdite in iron meteorites, Geochimica et Cosmochimica Acta 29:513-534 (1965).

12. A. S. Doan and J. I. Goldstein, The formation of phosphides in iron meteorites, in Meteorite Research (Peter M. Millman, ed.), D. Reidel Publishing Company, Holland (1968), No. 62, pp. 763-779.

13. A. E. Ringwood, Cohenite as a pressure indicator in iron meteorites, Geochimica et Cosmochimica Acta 20:155-158 (1960).

14. Brian Mason, The minerals of meteorites, in Researches on Meteorites (Carleton B. Moore, ed.), John Wiley & Sons, Inc., New York and London (1962), pp. 145-163.

15. Edward R. D. Scott and John T. Wasson, Classification and properties of iron meteorites, Reviews of Geophysics and Space Physics 13:527-546 (1975).

16. Clark R. Chapman, The nature of asteroids, Scientific American 232:24-33 (1975).

17. D. W. Sears, The Nature and Origin of Meteorites, Oxford University Press, New York (1978), Chap. 6, pp. 159-166.

18. Vagn F. Buchwald, Handbook of Iron Meteorites Vol. 1, University of California Press, Berkeley (1975), Chaps. 10 and 11, pp. 115-136.

19. William K. Hartmann, The smaller bodies of the solar system, Scientific American 233:142-159 (1975).

20. R. A. Fish, G. G. Goles, and E. Anders, The record in Meteorites III. On the development of meteorites in asteroidal bodies, Astrophysical Journal 132:243-258 (1960).

21. Harold C. Urey, Diamonds, meteorites, and the origin of the solar system, Astrophysical Journal 124:623-637 (1956).

22. Joseph I. Goldstein and James M. Short, The iron meteorites, their thermal history and parent bodies, Geochimica et Cosmochimica Acta 31:1733-1770 (1967).

23. John T. Wasson, The chemical classification of iron meteorites; IV. Irons with Ge concentrations greater than 190 ppm and other meteorites associated with group I, Icarus 12:407-423 (1970).

24. F. A. Paneth, The discovery and earliest reproductions of the Widmanstatten figures, Geochimica et Cosmochimica Acta 18:176-182 (1960).

25. H. C. Sorby, On the structure and origin of meteorites, Nature 15:495-498 (1877).

26. N. T. Belaiew, On the genesis of Widmanstatten structure in meteorites and in iron-nickel and iron-carbon alloys, The Mineralogical Magazine and Journal of the Mineralogical Society 20:173-185 (1925).

27. J. P. Joule, Note on the meteor of February 6, 1818, in The Scientific Papers of James Prescott Joule, Phy. Soc., London (1884), pp. 536-539.

28. J. Young, The crystal structure of meteoric iron as determined by x-ray analysis, Proc. Roy. Soc. (London) 112A:630-641 (1926).

29. John A. Wood, The cooling rates and parent planets of several iron meteorites, Icarus 3:429-459 (1964).

30. Joseph I. Goldstein and James M. Short, Cooling rates of 27 iron and stony-iron meteorites, Geochimica et Cosmochimica Acta 31: 1001-1023 (1967).

31. E. Randich and J. I. Goldstein, Cooling rates of seven hexahedrites, Geochimica et Cosmochimica Acta 42:221-233 (1978).

32. K. L. Rasmussen, The cooling rates of iron meteorites—a new approach, Icarus 45:564-576 (1981).

33. C. Narayan and J. I. Goldstein, unpublished.

34. Robert T. Dodd, Meteorites: A petrologic-chemical synthesis, Cambridge University Press, Cambridge (1981), pp. 192-213.

35. J. I. Goldstein and R. E. Ogilvie, The growth of the Widmanstatten pattern in metallic meteorites, Geochimica et Cosmochimica Acta 29:893-920 (1965).

36. Herbert H. Uhlig, Contribution of metallurgy to the origin of meteorites; Part II—The significance of Neumann bands in meteorites, Geochimica et Cosmochimica Acta 7:34-42 (1955).

37. R. A. Jago, A structural investigation of the Cape York meteorite by transmission electron microscopy, Journal of Materials Science 9:564-568 (1974).

38. L. S. Lin, J. I. Goldstein and D. B. Williams, Analytical electron microscopy study of the plessite structure in the Carlton iron meteorite, Geochimica et Cosmochimica Acta 41:1861-1874 (1977).

39. Edward R. D. Scott, The nature of dark-etching rims in meteoritic taenite, Geochimica et Cosmochimica Acta 37:2283-2294 (1973).

40. J. F. Albertsen, J. M. Knudsen, N. O. Roy-Poulsen, L. Vistisen, Meteorites and thermodynamic equilibrium in f.c.c. iron-nickel alloys (25-50% Ni), Physica Scripta 22:171-175 (1980).

41. A. D. Romig, Jr. and J. I. Goldstein, Low temperature phase equilibria in the Fe-Ni and Fe-Ni-P systems: application to the thermal history of metallic phases in meteorites, Geochimica et Cosmochimica Acta 45:1187-1197 (1981).

42. J. F. Albertsen, G. B. Jensen, J. M. Knudsen, J. Danon, On superstructure in meteoritical taenite, Meteoritics 13:379-383 (1978).

43. Edward R. D. Scott and Roy S. Clarke, Jr., Identification of clear taenite in meteorites as ordered FeNi, Nature 281:360-362 (1979).

44. J. F. Albertsen, H. P. Nielsen and V. F. Buchwald, On the fine structure of meteoritical taenite/tetrataenite and its interpretation, Physica Scripta 27:314-320 (1983).

45. S. Mehta, P. M. Novotny, D. B. Williams and J. I. Goldstein, Electron-optical observations of ordered FeNi in the Estherville meteorite, Nature 284:151-153 (1980).

46. J. Danon, R. B. Scorzelli, I. Souza Azevedo, and M. Christophe-Michel-Levy, Iron-nickel superstructure in metal particles of chondrites, Nature 281:469-471 (1979).

47. J. F. Albertsen, Tetragonal lattice of tetrataenite (ordered Fe-Ni, 50-50) from 4 meteorites, Physica Scripta 23:301-306 (1981).

48. Ortrud Kubaschewski, Iron—Binary Phase Diagrams, Springer-Verlag, New York (1982), pp. 73-78.

49. J. I. Goldstein and D. B. Williams, Low temperature phase transformations in the metallic phases of meteorites, in Proc. Inter. Conf. Solid-Solid Phase Transformations (1982), pp. 715-719.

50. A. D. Romig, Jr. and J. I. Goldstein, Determination of the Fe-Ni and Fe-Ni-P phase diagrams at low temperatures (700 to 300°C), Met. Trans. 11A:1151-1159 (1980).

51. A. D. Romig, Jr. and J. I. Goldstein, Determination of the Fe-rich portion of the Fe-Ni-C phase diagram, Met. Trans. 9A:1599-1609 (1978).

52. Vagn F. Buchwald, Handbook of Iron Meteorites Vol. 2, University of California Press, Berkeley (1975), pp. 269-272.

53. C. R. Brooks, unpublished.

54. H. J. Axon and D. Faulkner, Hot-working effects in the parent gamma-phase of iron meteorites, Geochimica et Cosmochimica Acta 31:1539-1542 (1967).

55. J. B. Newkirk, General theory, mechanism and kinetics, in Precipitation from Solid Solution, American Society for Metals (1958), p. 85.

56. G. R. Speich and P. R. Swann, Yield strength and transformation substructure of quenched iron-nickel alloys, Journal of the Iron and Steel Institute 203:480-485 (1965).

57. J. I. Goldstein, Phase transformations in iron meteorites, in Phase Transformations in Ferrous Alloys (A. R. Marder and J. I. Goldstein, eds.), The Metallurgical Society of AIME (1984), pp. 1-10.

58. C. S. Barrett, Crystal structure, in Metals Handbook, Vol. 8, 8th Ed., Metallography, Structures, and Phase Diagrams (Taylor Lyman, ed.), American Society for Metals (1973), pp. 233-240.

APPENDIX

THE $L1_0$ STRUCTURE

The $L1_0$ structure consists of a tetragonal superlattice with atoms in the following positions:

A atoms at 0, 0, 0 and 1/2, 1/2, 0

B atoms at 0, 1/2, 1/2 and 1/2, 0, 1/2

It is also known as the (AuCu I) structure, and has H.M. symbol P4/mmm [58].

VITA

Amy Luckstead DeMint was born in Iowa and grew up in Iowa and Illinois. She graduated from Dubuque Senior High School in 1979, and graduated from Iowa State University in 1983 with a B.S. in Metallurgical Engineering. In 1983, she moved to Tennessee, and in 1985 she graduated from The University of Tennessee in Knoxville with a M.S. in Metallurgical Engineering. Upon graduating, she will be employed by Martin Marietta Energy Systems.